# Neural correlates of human fear conditioning and sources of variability in 2199 individuals

Joaquim Radua<sup>1,2,3</sup>, Hannah S. Savage<sup>4,5,6</sup>, Enric Vilajosana<sup>1,2</sup>, Alec Jamieson<sup>7</sup>, Birgit Abler<sup>8</sup>, Fredrik Åhs<sup>9</sup>, Tom Beckers<sup>10</sup>, Narcís Cardoner<sup>3,11</sup>, Josh Cisler<sup>12</sup>, Juliana B. Diniz<sup>13</sup>, Dominik R. Bach<sup>14,15,16</sup>, Sigrid Elsenbruch<sup>17</sup>, Steve Greening<sup>18</sup>, Daphne J. Holt<sup>19,20,21</sup>, Antonia N. Kaczkurkin<sup>22</sup>, Andreas Keil<sup>23</sup>, Merel Kindt<sup>24</sup>, Kathrin Koch<sup>25,26</sup>, Kevin S. LaBar<sup>27</sup>, Charlene L. Lam<sup>28,29</sup>, Christine Larson<sup>30</sup>, Tina B. Lonsdorf<sup>31,32</sup>, Christian J. Merz<sup>33</sup>, Katie A. McLaughlin<sup>34,35</sup>, Yuval Neria<sup>36</sup>, Daniel Pine<sup>37</sup>, Carien van Reekum<sup>38</sup>, Alexander Shackman<sup>39</sup>, Carles Soriano-Mas<sup>3,40,41</sup>, Victor I. Spoormaker<sup>42</sup>, Daniel M. Stout<sup>43,44,45</sup>, Benjamin Straube<sup>46,47</sup>, Thomas Straube<sup>48</sup>, Lauri Tuominen<sup>49</sup>, Renee M. Visser<sup>24</sup>, Laura Ahumada<sup>23</sup>, Volker Arolt<sup>50,51</sup>, Marcelo C. Batistuzzo<sup>13,52</sup>, Paulo R. Bazán<sup>53</sup>, Emma E. Biggs<sup>10</sup>, Marta Cano<sup>3,54</sup>, Pamela Chavarría-Elizondo<sup>40,55</sup>, Samuel E. Cooper<sup>56</sup>, Udo Dannlowski<sup>50</sup>, Víctor de la Peña-Arteaga<sup>40,57</sup>, Stephanie N. DeCross<sup>34</sup>, Katharina Domschke<sup>58,59</sup>, Mana R. Ehlers<sup>31</sup>, John L. Graner<sup>27</sup>, Alfons O. Hamm<sup>60</sup>, Martin J. Herrmann<sup>61</sup>, Ashley A. Huggins<sup>62</sup>, Adriane Icenhour<sup>17</sup>, Asier Juaneda-Seguí<sup>40</sup>, Markus Junghoefer<sup>51,63</sup>, Tilo Kircher<sup>46,47</sup>, Katja Koelkebeck<sup>64</sup>, Manuel Kuhn<sup>65,66</sup>, Franziska Labrenz<sup>17</sup>, Shmuel M. Lissek<sup>67</sup>, Martin Lotze<sup>68</sup>, Ulrike Lueken<sup>59,69</sup>, Jürgen Margraf<sup>70</sup>, Ignacio Martínez-Zalacaín<sup>40,71</sup>, Robert Moeck<sup>48</sup>, Jayne Morriss<sup>72</sup>, María Ortuño<sup>1</sup>, Andre Pittig<sup>73</sup>, Daniel Porta-Casteras<sup>57</sup>, Jan Richter<sup>74,75</sup>, Isabelle C. Ridderbusch<sup>46,47</sup>, Winfried Rief<sup>76</sup>, Kati Roesmann<sup>63,77</sup>, Jörgen Rosén<sup>78</sup>, Alena N. Rußmann<sup>32,79</sup>, Rachel Sjouwerman<sup>80</sup>, Jennifer Spohrs<sup>81,82</sup>, Andreas Ströhle<sup>83</sup>, Benjamin Suarez-Jimenez<sup>84,85</sup>, Martin Ulrich<sup>8</sup>, Hans-Ulrich Wittchen<sup>86</sup>, Xi Zhu<sup>87,88</sup>, Lea Waller<sup>89</sup>, Henrik Walter<sup>59,90</sup>, Paul M. Thompson<sup>91</sup>, Janna Marie Bas-Hoogendam<sup>92,93,94</sup>, Nynke A. Groenewold<sup>95</sup>, Dan J. Stein<sup>96</sup>, Nic J. Van der Wee<sup>93,94</sup>, Joseph Dunsmoor<sup>97</sup>, Andre F. Marquand<sup>4,5</sup>, Ben J. Harrison<sup>7</sup>, Miquel A. Fullana<sup>1,98</sup> \*

- <sup>1</sup> Institut d'Investigacions Biomèdiques August Pi i Sunyer (IDIBAPS), Barcelona, Spain
- <sup>2</sup> University of Barcelona, Barcelona, Spain
- <sup>3</sup> Centro de Investigación Biomédica en Red de Salud Mental (CIBERSAM), Instituto de Salud Carlos III (ISCIII), Madrid, Spain
- <sup>4</sup> Donders Institute of Brain, Cognition and Behaviour, Radboud University, Nijmegen, The Netherlands
- <sup>5</sup> Department of Cognitive Neuroscience, Radboud University Medical Centre, Nijmegen, The Netherlands
- <sup>6</sup> Institute of Cognitive Neuroscience, UCL, London, UK
- <sup>7</sup> Department of Psychiatry, The University of Melbourne, Victoria, Australia.
- <sup>8</sup> Department of Psychiatry and Psychotherapy III, Ulm University Clinic, Ulm, Germany
- <sup>9</sup> Department of Psychology and Social Work, Mid Sweden University, Östersund, Sweden
- <sup>10</sup> Faculty of Psychology and Educational Sciences and Leuven Brain Institute, KU Leuven, Leuven, Belgium
- <sup>11</sup> Sant Pau Mental Health Group, Institut d'Investigació Biomèdica Sant Pau (IBB-Sant Pau), Hospital de la Sant Creu i Sant Pau, Universitat Autònoma de Barcelona (UAB), Barcelona, Catalonia, Spain
- <sup>12</sup> Department of Psychiatry and Behavioral Sciences, Dell Medical School, University of Texas at Austin, Austin, TX, 78701, USA
- <sup>13</sup> Department of Psychiatry, Faculdade de Medicina, Universidade de São Paulo, São Paulo, Brazil.
- <sup>14</sup> University of Bonn, Transdisciplinary Research Area "Life and Health", Hertz Chair for Artificial Intelligence and Neuroscience, Institute of Computer Science, Medical Faculty, Institute of Experimental Epileptology and Cognition Research
- <sup>15</sup> University Hospital Bonn, Department of Psychiatry and Psychotherapy, Bonn, Germany
- <sup>16</sup> Department for Imaging Neuroscience, UCL Queen Square Institute of Neurology, University College London, UK
- <sup>17</sup> Department of Medical Psychology and Medical Sociology, Medical Faculty, Ruhr University Bochum, Germany
- <sup>18</sup> Brain & Cognitive Sciences, Dept. of Psychology, University of Manitoba, Canada
- <sup>19</sup> Department of Psychiatry, Massachusetts General Hospital, Charlestown, MA, USA
- <sup>20</sup> Harvard Medical School, Boston, MA, USA
- <sup>21</sup> Athinoula A. Martinos Center for Biomedical Imaging, Massachusetts General Hospital, Boston, MA, USA
- <sup>22</sup> Department of Psychology, Vanderbilt University, Nashville, TN 37240, USA
- <sup>23</sup> Department of Psychology, University of Florida, Gainesville FL, 32611, USA
- <sup>24</sup> University of Amsterdam, Amsterdam, The Netherlands
- <sup>25</sup> School of Medicine and Health, Department of Diagnostic and Interventional Neuroradiology, Technical University of Munich, Munich, Germany
- <sup>26</sup> School of Medicine and Health, TUM-NIC Neuroimaging Center, Technical University of Munich, Munich, Germany
- <sup>27</sup> Center for Cognitive Neuroscience, Duke University, Durham, NC USA
- <sup>28</sup> Laboratory of Clinical Psychology & Affective Neuroscience, Department of Psychology, University of Hong Kong, Hong Kong, China
- <sup>29</sup> State Key Laboratory of Brain and Cognitive Sciences, Hong Kong, China
- 30 University of Wisconsin-Milwaukee, Department of Psychology
- <sup>31</sup> Biological Psychology and Cognitive Neuroscience, Bielefeld University, Bielefeld, Germany
- 32 Institute for Systems Neuroscience, University Medical Center Hamburg Eppendorf, Hamburg, Germany
- 33 Department of Cognitive Psychology, Institute of Cognitive Neuroscience, Ruhr University Bochum, Bochum, Germany
- <sup>34</sup> Department of Psychology, Harvard University, Cambridge, MA USA
- 35 Ballmer Institute for Children's Behavioral Health, University of Oregon

- <sup>36</sup> Columbia University Irving Medical Center
- <sup>37</sup> Section on Development and Affective Neuroscience, National Institute of Mental Health
- 38 School of Psychology and Clinical Language Sciences, University of Reading, Reading, UK
- <sup>39</sup> Department of Psychology, Neuroscience and Cognitive Science Program, and Maryland Neuroimaging Center, University of Maryland, College Park, MD 20742 USA
- <sup>40</sup> Psychiatry and Mental Health Group, Neuroscience Program, Institut d'Investigació Biomèdica de Bellvitge IDIBELL, L'Hospitalet de Llobregat, Spain
- 41 Department of Social Psychology and Quantitative Psychology, Institute of Neurosciences, University of Barcelona, Barcelona, Spain
- <sup>42</sup> Max Planck Institute of Psychiatry
- <sup>43</sup> University of California, San Diego
- 44 VA San Diego Healthcare System
- <sup>45</sup> Center of Excellence for Stress and Mental Health
- <sup>46</sup> Department of Psychiatry and Psychotherapy, University of Marburg, Marburg, Germany
- <sup>47</sup> Center for Mind, Brain and Behavior (CMBB), University of Marburg, Marburg, Germany.
- <sup>48</sup> Institute of Medical Psychology and Systems Neuroscience, University of Muenster, Germany
- <sup>49</sup> University of Ottawa Institute of Mental Health Research at the Royal
- 50 Institute for Translational Psychiatry, University of Münster, Germany
- <sup>51</sup> Otto-Creutzfeld-Center of Cognitive Neuroscience, University of Münster, Germany
- <sup>52</sup> Department of Methods and Techniques in Psychology, Pontifical Catholic University, São Paulo, SP, Brazil.
- <sup>53</sup> Radiology Institute, Faculdade de Medicina, Universidade de São Paulo, Rua Dr Ovídio Pires de Campos, 75, 05403-010, São Paulo, SP, Brazil;
- 54 Sant Pau Mental Health Research Group, Institut de Recerca Sant Pau (IR SANT PAU), Barcelona, Spain,
- 55 Department of Clinical Sciences, School of Medicine, Universitat de Barcelona UB, L'Hospitalet de Llobregat, Spain
- <sup>56</sup> Department of Psychiatry and Behavioral Sciences, University of Texas at Austin
- <sup>57</sup> Sant Pau Mental Health Research Group, Institut de Recerca Sant Pau (IR SANT PAU), Barcelona, Spain
- <sup>58</sup> Department of Psychiatry and Psychotherapy, Medical Center University of Freiburg, Faculty of Medicine, University of Freiburg, Freiburg, Germany
- <sup>59</sup> German Center of Mental Health (DZPG), partner site Berlin/Potsdam, 10177 Berlin, Germany
- <sup>60</sup> Department of Psychology, University of Greifswald, Greifswald, Germany.
- <sup>61</sup> Department of Psychiatry, Psychosomatics and Psychotherapy, University of Würzburg, Germany
- <sup>62</sup> Department of Psychology, University of Arizona, Tucson, AZ, USA
- <sup>63</sup> Institute for Biomagnetism and Biosignalanalysis, University of Münster, Germany
- <sup>64</sup> Bielefeld University, Medical School and University Medical Center OWL, Protestant Hospital of the Bethel Foundation, Department of Psychiatry and Psychotherapy
- 65 Center for Depression, Anxiety, and Stress Research, McLean Hospital, Belmont, MA, USA
- 66 Department of Psychiatry, Harvard Medical School, Cambridge, MA, USA
- <sup>67</sup> Department of Psychology, University of Minnesota, 55455, Minneapolis, MN, USA
- 68 Diagnostic Radiology, University Medicine Greifswald, Gernany
- <sup>69</sup> Department of Psychology, Humboldt-Universität zu Berlin, Berlin, Germany
- <sup>70</sup> Mental Health Researcch and Treatment Center, Ruhr-UNiversity Bochum (FBZ) and German Center for Mental Health (DZPG), partner site Bochum/Marburg
- <sup>71</sup> Radiology Department, Hospital Universitari de Bellvitge, L'Hospitalet de Llobregat, Carrer de Feixa Llarga SN, Barcelona, 08907, Spain.
- <sup>72</sup> School of Psychology, Faculty of Environmental and Life Sciences, University of Southampton, Southampton, UK
- <sup>73</sup> Translational Psychotherapy, Institute for Psychology, University of Göttingen, Göttingen, Germany.
- <sup>74</sup> Department of Experimental Psychopathology, University of Hildesheim, Hildesheim, Germany
- 75 Network Center for Biomedical Research on Mental Health (CIBERSAM), Instituto de Salud Carlos III (ISCIII), Madrid, Spain.
- <sup>76</sup> Div. of Clinical Psychology and Psychotherapy, University of Marburg, Germany
- <sup>77</sup> Institute of Psychology, Clinical Psychology in Childhood and Adolescence, University of Osnabrück, Germany
- <sup>78</sup> Department of Clinical Neuroscience, Karolinska Institutet, Stockholm, Sweden
- <sup>79</sup> Department of Psychology, Clinical Psychology and Neuroscience, University of Hamburg, Hamburg, Germany
- <sup>80</sup> Experimental Health Psychology, Maastricht University, Maastricht, The Netherlands
- 81 Department of Child and Adolescent Psychiatry and Psychotherapy, Ulm University Medical Centre, Ulm, Germany
- 82 Department of Psychiatry, Psychotherapy and Psychotraumatology Military Medical Centre, Ulm, Germany
- 83 Department of Psychiatry and Psychotherapy, Charité Universitätsmedizin Berlin, Campus Charité Mitte, Berlin Germany
- 84 Department of Neuroscience, University of Rochester Medical Center, NY, USA.
- 85 Center for Visual Sciences, University of Rochester, NY, USA
- <sup>86</sup> Psychiatric University Hospital, Ludwig-Maximilians-University München, Germany
- <sup>87</sup> Department of Psychiatry, Columbia University Irving Medical Center, New York, NY, USA
- 88 New York State Psychiatric Institute, New York, NY, USA
- 89 Research Division of Mind and Brain, Department of Psychiatry and Neurosciences CCM, Charité-Universitätsmedizin Berlin, Corporate Member of Freie Universität Berlin, Humboldt-Universität zu Berlin, and Berlin Institute of Health, Charitéplatz 1, 10117 Berlin, Germany
- <sup>90</sup> Department of Psychiatry and Psychotherapy, Charité-Universitätsmedizin Berlin, corporate member of Freie Universität Berlin and Humboldt-Universität zu Berlin, 10177 Berlin, Germany.
- <sup>91</sup> Imaging Genetics Center, Stevens Neuroimaging & Informatics Institute, Keck School of Medicine, University of Southern California, Los Angeles, CA, USA
- <sup>92</sup> Developmental and Educational Psychology, Institute of Psychology, Leiden University, Leiden, THe Netherlands
- 93 Leiden Insitute for Brain and Cognition, Leiden University Medical Center, The Netherlands
- 94 Department of Psychiatry, Leiden University Medical Center, Leiden, The Netherlands
- 95 Department of Psychiatry & Mental Health, Neuroscience Institute, University of Cape Town, Cape Town, South Africa
- 96 SAMRC Unit on Risk & Resilience in Mental Disorders, Dept of Psychiatry & Mental Health, Neuroscience Institute, University of Cape Town, Cape Town, South Africa
- <sup>97</sup> Department of Neuroscience, University of Texas at Austin
- 98 Adult Psychiatry and Psychology Department, Institute of Neurosciences, Hospital Clinic, Barcelona, Spain.

These authors contributed equally: Joaquim Radua, Hannah S. Savage. These authors jointly supervised this work: Joseph Dunsmoor, Andre F. Marquand, Ben J. Harrison, Miquel A. Fullana. Correspondence and requests for materials should be addressed to M.A.F. (email: mafullana@clinic.cat).

#### **ABSTRACT**

Pavlovian fear conditioning is a fundamental process in both health and disease. We investigated its neural correlates and sources of variability using harmonized functional magnetic resonance imaging data from 2,199 individuals across nine countries, including 1,888 healthy individuals and 311 with anxiety-related or depressive disorders. Using mega-analysis and normative modeling, we show that fear conditioning consistently engages brain regions within the "central autonomic—interoceptive" or "salience" network. Several task variables strongly modulate activity in these regions, contributing to variability in neural responses. Additionally, brain activation patterns differ between healthy individuals and those with anxiety-related or depressive disorders, with distinct profiles characterizing specific disorders such as post-traumatic stress disorder and obsessive-compulsive disorder. While the neural correlates of fear conditioning are highly generalizable at the population level, variability arises from differences in task design and clinical status, highlighting the importance of methodological diversity in capturing fear learning mechanisms.

#### INTRODUCTION

Fear conditioning, also known as threat conditioning, is a psychological paradigm developed over a century ago to study associative learning mechanisms. It remains one of the most widely used and productive experimental models for investigating both normal and pathological fear and anxiety in humans<sup>1</sup>. Fear conditioning models how the association between an initially neutral stimulus (conditioned stimulus, CS) and an innately aversive stimulus (unconditioned stimulus, US) is learned. The success of learning in fear conditioning is typically assessed by comparing responses to the fear cue (CS+, paired with the US) and the safety cue (CS-, not paired with the US) across subjective, autonomic, or neural domains. Successful conditioning is indicated by greater responses to the CS+ than to the CS-2. In the brain, this involves activity changes within a "central autonomicinteroceptive" or "salience" network, which in humans includes functionally and anatomically connected regions like the dorsal anterior cingulate cortex (dACC) and the anterior insular cortex (AIC)<sup>3</sup>. Additionally, fear conditioning has been linked to decreased activity in regions like the ventromedial prefrontal cortex (vmPFC), although such decreases have been less extensively studied<sup>3</sup>. Although the amygdala plays a crucial role in fear conditioning in rodents<sup>4–6</sup>, and classical lesion studies have implicated the amygdala in human fear conditioning<sup>7</sup>, this relationship has not been consistently identified in human fMRI studies <sup>3,8–12</sup>.

Limitations in prior research on the neural correlates of human fear conditioning include the use of small sample sizes (typically n<30) and the reliance on heterogeneous neuroimaging processing and analytical methods <sup>3,13</sup>. While group-level meta-analyses can partially address the sample size issue<sup>3</sup>, individual-level *mega-analyses* offer additional advantages. These include enhanced statistical power, more precise effect size estimation, standardized preprocessing and analysis techniques, and substantially improved power to detect whether activation is modulated by individual variability -one of the primary goals of the current study<sup>14–16</sup>.

Individual differences, such as sociodemographic factors (e.g., age) and trait variables (e.g., trait anxiety), are likely to modulate the neural correlates of fear conditioning, potentially affecting the generalizability of findings across groups, such as younger versus older adults or individuals with high versus low anxiety<sup>13</sup>. However, existing research on individual differences has been inconsistent and often hampered by limited sample sizes (n<50<sup>13</sup>) or sampling biases<sup>17</sup>. Moreover, task-specific variables, such as task instructions or characteristics of the US, may also influence conditioning at the behavioral or neural level <sup>2,13,18,19</sup>. For example, compared to other USs, a tactile electric shock may elicit greater activation in the dACC and the ventral supplementary motor area<sup>3</sup>. A primary challenge in this field is integrating prior data to accurately assess how individual differences and task variables affect neural outcomes. This complexity arises from variations in adjustable factors and sampling across studies and participants, highlighting the need for methods that can account for and isolate

specific sources of variation—such as the normative modeling approach used here. Normative modeling allows us to integrate multiple smaller-scale studies into a common reference space—a standardised baseline against which to statistically quantify individual variations. This approach allows for meaningful comparisons across diverse studies by controlling for multiple sources of variation As a result, the variance associated with specific variables and individuals can be isolated, quantified, and systematically analysed<sup>20</sup>. (For details on the underlying mathematics, see references <sup>21–23</sup>; for applications, see <sup>24–29</sup>).

Fear conditioning has also been used to study the development and persistence of mental health disorders marked by pathological fear, such as anxiety-related disorders 1,30–33, which are highly prevalent and rank among the leading causes of disability worldwide<sup>33</sup>. However, there is ongoing debate over whether anxiety-related disorders consistently show abnormal fear conditioning at behavioral or neural levels<sup>34,35</sup> or if these abnormalities are specific to certain clinical groups—such as post-traumatic stress disorder (PTSD<sup>36</sup>) but not others, like social anxiety disorder (SAD)<sup>37</sup>. Inconsistencies maybe due in part to small sample sizes (ns<100 for anxiety-related disorders as a group, ns<25 for comparisons among clinical groups). Furthermore, most research in this area has relied on case-control designs and traditional analysis techniques, both of which have limitations that could be addressed through normative modeling. This framework enables statistical inference for individual subjects relative to an expected population pattern, providing a more detailed examination of the heterogeneity underlying group-level analyses<sup>20</sup>.

In this study with pre-registered hypotheses and analyses (cf. Materials and Methods), we used both mega-analysis and normative modelling to analyse individual-level, harmonized fMRI data acquired during fear-conditioning from 43 samples from 21 laboratories across 9 countries (total n=2199), including both healthy participants and individuals diagnosed with anxiety-related and depressive disorders. First, we assessed the overall neural correlates of fear conditioning in healthy participants to provide a comprehensive delineation of the brain regions underlying human fear conditioning. Based on previous studies, we hypothesized that during fear conditioning, the CS+>CScontrast would be associated with robust activations in regions such as the dACC, AIC, pre/supplementary motor areas, and dorsolateral prefrontal cortex (dlPFC), whereas the CS+<CScontrast would be associated with deactivations in the vmPFC and hippocampus. We expected the mega-analysis to be more sensitive than previous studies in detecting subtle effects in other brain regions not previously (or not consistently) identified. Second, we assessed variation among healthy participants. Given their role in mediating subjective arousal and autonomic expression of fear<sup>38</sup>, we hypothesised that regions including the vmPFC and the anterior-to-mid cingulate cortex would show the greatest between-subject heterogeneity. Third, we examined how individual differences (e.g., age, trait anxiety) and task variables (e.g., task instructions) influenced this variation. Finally, we explored differences in the neural correlates of fear conditioning between individuals with anxiety-related and

depressive disorders and healthy controls, as well as among clinical subgroups (e.g., PTSD, SAD). We show that fear conditioning is consistently associated with brain activation in regions of the central autonomic-interoceptive network, despite methodological variations. However, specific task variables also influence the responses of these regions during conditioning. Additionally, brain activation patterns during conditioning differ between healthy individuals and those with anxiety-related or depressive disorders, with certain groups displaying distinct activation profiles.

# **RESULTS**

All results -including effect sizes for the linear models- are available in a free open-access repository (see **Data availability statement**).

# Conditioning is associated with extensive brain (de)activations

In the mega-analysis (**Fig. 1a**), we included data from 1888 healthy individuals (42 experiment samples) and used linear mixed-effect models (LMMs) to perform a mega-analysis of whole-brain activation during fear conditioning (CS+>CS- contrast). We observed significant activation encompassing clusters within the bilateral anterior and mid insular cortices; the secondary somatosensory cortices (SII); the dlPFC; the lateral premotor cortices; and the dorsal and lateral cerebellum (**Fig. 1b**). Significant activation was also observed in multiple regions across the cortical midline, including the dACC extending to the pre-supplementary and supplementary motor areas (SMA), ventral posterior cingulate cortex, and dorsal precuneus (dPrec).

Additionally, the CS+>CS- mega-analysis revealed the broad activation of subcortical regions, particularly the thalamus and basal ganglia. The largest of these activation patterns were observed in the dorsal striatum, specifically the caudate nucleus (CN); the globus pallidus extending to the striatum; the ventral tegmental area extending to the habenula; the mediodorsal thalamus (Thal); and the midbrain tegmentum. Activation of the midbrain was noted generally across the dorsal midbrain (~substantia nigra/red nucleus and pretectal nuclei) (**Supplementary Fig. S1**). To specifically assess the role of the amygdala, we conducted a Region of Interest (ROI) mega-analysis focusing on this region (see **Materials and Methods**), which indicated that neither the left (Cohen's d = 0.13, 95% CI [-0.029, 0.624]) nor the right amygdala (Cohen's d = 0.12, 95% CI [-0.002, 0.260]) showed significant activation during fear conditioning (both p-values > 0.05).

We also observed significant deactivations (CS+<CS- contrast) during fear conditioning, predominantly in regions of the default mode network (**Fig. 1c**). This included the posterior cingulate cortex (PCC) and precuneus; the vmPFC extending to the mPFC and subgenual cingulate cortex medially, as well as the left dorsal prefrontal cortex (dPFC); the bilateral angular gyri; and the parahippocampi and hippocampi (Hipp). Additional deactivation was observed in the lateral orbitofrontal cortex; the primary somatosensory cortex (SI); as well as the left temporal (TG) and

fusiform gyri (see **Supplementary Fig. S2** for detailed activation and deactivation across axial, sagittal, and coronal slices).

# Heterogeneity in the neural correlates of conditioning

We estimated voxel-wise normative models of fear-conditioning related activation using the CS+>CScontrast from 894 controls (training sample), and specifying age, biological sex, sample, and task variables as covariates (see Materials and Methods for all variables. The normative modeling sample is smaller than the mega-analysis due to the requirement for participants to have data on all covariates used in model construction). Testing these models with a held-out test sample (n=646) showed good model fit with explained variance reaching 0.3 in regions that showed activation during fear conditioning (Fig. 1b), and skew and kurtosis within acceptable limits (Supplementary Fig. S3). For each participant in our held-out test sample, we then calculated a deviation score (z-score) within each voxel. In other words, for each participant, we quantified the distance from the predicted mean activation of each voxel, relative to the normative reference distribution for that voxel (Fig. 1d). While almost every voxel had at least 5 participants with large deviations (deviations  $>\pm 2.6$ ), including areas such as the bilateral insula and expanses of the cingulate cortex extending to the medial prefrontal cortex (Supplementary Fig. S4), controls most frequently had large deviations (both positive and negative) within the most ventral region of the vmPFC and inferior temporal pole. As this ventral region is notoriously prone to signal drop out, we interpret this result as most likely reflecting varying signal intensity rather than individual differences, and thus chose to interpret deviations within this region with caution (Fig. 1e).

# Individual differences have small associations with conditioning

We examined the role of the following individual differences variables using LMMs and normative models (**Fig 1a**): age, biological sex, and self-reported trait anxiety and depressive symptoms. In normative models, we analyzed both regression coefficients, reflecting each variable's contribution to the regression equation, and structure coefficients, indicating the direct bivariate relationship between a variable and brain activity without accounting for other predictors.

In LMMs, age (n=1884 controls) and biological sex (n=1888 controls) showed a significant association with brain activation or deactivation during fear conditioning (**Supplementary Fig. S5**). However, the effect sizes were small (**Supplementary Discussion**). Additionally, the age range was restricted (see **Table 1**). Regression and structure coefficients also showed minimal effects of age and biological sex (n=646 controls) (**Supplementary Fig. S5**). Neither trait anxiety (n=1402 controls), using either harmonised or non-harmonised scores (**Supplementary Methods**), nor depressive symptoms (n=213 controls) were significantly associated with brain activation or deactivation during fear conditioning in LMMs. Similarly, elastic net regressions showed that whole-brain deviation

scores derived from normative models could not explain the variance in individual levels of trait anxiety (n = 751 controls and cases;  $r^2 = -0.095$ , p = 0.459), nor depressive symptoms (n = 152 controls and cases;  $r^2 = -0.257$ , p = 0.605). See **Methods** for a note on negative  $r^2$  values and **Supplementary Table S1** for trait anxiety and depressive symptoms scores.

# Task variables have a robust effect on conditioning

The influence of task variables on brain activation during fear conditioning was also examined using LMMs and structure coefficients from normative models in healthy controls. Several task variables were associated with robust effects across individuals, showing at least moderate effect sizes in LMMs and reaching significance in normative modeling analyses. These included instructions given to the participant about contingency prior to the task, the type of US, the use of a paradigm with multiple CSs (i.e., more than one CS+ or CS-), the pairing rate (i.e., percentage of CS+ followed by a US), and potential US confounding (i.e. whether trials followed by the US were included in the CS+ vs CS- contrast, and therefore the effects of the US may confound the effects of the CS+).

Partial instructions about CS-US contingency (n=1388) were associated with significantly increased activation in the supplementary motor area and superior parietal lobule compared to no instructions about contingency (n=500) in LMMs. Structure coefficients from the normative models (n=646) showed that partial instructions (as compared to no instructions) produced a model predicting more activation in the bilateral anterior insula, the thalamus, the left caudate, clusters within the dorsomedial prefrontal cortex, the dorsolateral precuneus, and in the posterior region of the vmPFC. The model also predicted less activation within the bilateral visual cortex, the anterior medial temporal gyrus, and in the anterior vmPFC with the use of partial instructions (**Figure 2a**). Note that we excluded instructed conditioning studies (**Materials and Methods**).

Compared with an auditory US (n=337), a tactile electric shock US (n=1472) produced significantly greater activation in bilateral dorsal mid-insula, dorsal medial thalamus, and presupplementary motor area, extending to the dACC (n=337) in LMMs. In normative modelling analyses, a tactile electric shock US predicted increased activation within the dACC extending to the pre-supplementary motor area, the dorsal precuneus, secondary somatosensory cortex, the bilateral dorsal mid- to- posterior insula, the midbrain and pons, and the superior cerebellum, and less activation (i.e., more deactivation) within an expanse of the vmPFC, and SI. Moreover, the use of an auditory US was significantly associated with increased activation in the left auditory cortex and was predictive of increased activation in the bilateral auditory cortex (superior temporal lobe) and less deactivation (i.e., more differential activation) within an expanse of the vmPFC extending to the dorsomedial prefrontal cortex, posterior cingulate cortex, angular gyrus, and SI (**Figure 2b**).

In LMMs, compared to paradigms with a single CS+ (n=1283), paradigms with multiple CS+ (n=605) produced increased activation in the left supplementary motor area (SMA) and left dorsal precuneus and widespread increased deactivation in regions including the bilateral temporal poles, the

right parahippocampal gyrus extending to the fusiform gyrus, the left visual association cortex extending to the angular gyrus, and the right primary motor and somatosensory cortex. Comparing paradigms with multiple CS- (n=302) and those with a single CS- (n=1586) revealed identical regions with increased activation to paradigms with multiple CS+. Conversely, increased deactivation was shown in the bilateral anterior hippocampus, ventral PCC, primary motor and somatosensory cortex, precuneus, and right mid-insula. In normative models, this was modelled using two variables (multiple CS+ and multiple CS-). Multiple CS+ predicted less activation within the bilateral amygdala, a bilateral expanse of SI the angular gyrus, the posterior cingulate cortex, the bilateral putamen and caudate, and the lingual gyrus. Similarly, multiple CS- predicted decreased activation within a bilateral expanse of SI and the lingual gyrus (**Figure 2c**).

Pairing rate, treated as a continuous variable, did not relate to brain activation during conditioning in LMMs. However, due to the non-normal distribution of pairing rates across studies and individuals, we categorized pairing rates (e.g., 30%, 50%, and 100%) and conducted ANOVA-like LLMs followed by pairwise comparisons with Holm-Bonferroni correction, which revealed significant effects (**Figure 2d**). In particular, the comparisons involving the 50% pairing rate category was the category where significant differences between categories occurred most frequently. The significant differences between the pairing rate categories occurred both with (**Supplementary Fig. S6**) and without (**Supplementary Fig. S7**) US confounding. The structure coefficients for pairing rate (as a linear association), showed that a higher pairing rate predicted greater activation within visual regions (calcarine, lingual gyrus and cuneus), the precuneus, the left dorsolateral prefrontal cortex, the superior gyrus of the temporal lobe, and (less deactivation of) an anterior region of the vmPFC. Conversely, a higher pairing rate predicted less activation within the mid-cingulate cortex, the bilateral anterior insula, a posterior region of the vmPFC as well as the thalamus and caudate (**Figure 2d**).

Finally, potential US confounding (n = 997), compared to no confounding (n = 891), was associated with significantly increased widespread activation during fear conditioning (CS+ > CS-contrast). This activation was observed across the bilateral fusiform and lingual gyri, temporal poles, angular gyri, posterior insula, primary motor cortex, retrosplenial cortex (extending to the posterior hippocampus), and right amygdala, predominantly in the superficial amygdala, in linear mixed models (LMMs). Similarly, structure coefficients from the normative models showed that the model predicted greater activation within the bilateral mid-cingulate cortex extending to the dorsomedial prefrontal cortex and pre-supplementary motor area, angular gyri, mid-to-posterior insula, superior temporal gyrus and temporal poles, fusiform gyri and lateral mid-occipital gyrus, amygdala, caudate, dorsal thalamus, and dorsolateral cerebellum with potential US confounding (**Figure 2e**).

None of the above results were affected by excessive multicollinearity, except for the association between pairing rate and the potential US confound (**Supplementary Tables S2-S5**). We

identified six small clusters where the effects of both variables overlapped. To further disentangle their contributions, we conducted mixed-effects models within these clusters, including both variables as predictors. Results indicated that both variables exerted statistically significant effects in all clusters except for one small cluster in the right middle occipital region, where the effect of the US confound was no longer significant. Given the absence of multicollinearity (Variance Inflation Factor= 1.8), we concluded that activation in this region is specifically modulated by the pairing rate, rather than by the US confound.

The remaining task variables (for example, the number of trials during preconditioning) showed weaker effects or were not significantly associated with brain (de)activation during conditioning in the mega-analysis or normative modelling analyses (**Supplementary Figs. S8** and **S9** and **Supplementary Discussion**).

# Cases and controls show differences in conditioning

In the mega-analysis, individuals with anxiety-related and depressive disorders (cases, n=311) showed significantly increased activation in the right ventrolateral prefrontal cortex (anterior pars orbitalis), dorsal frontal pole, posterior cingulate cortex, left temporal pole, and bilateral primary motor areas compared to controls (n=1888) (**Fig. 3a**). Similar results were found when comparing individuals with anxiety-related disorders (i.e., excluding major depressive disorder; remaining n=297) and controls, with additional clusters observed in the dorsal prefrontal cortex, visual association cortex, and primary somatosensory cortex (**Supplementary Fig. S10**). After excluding individuals who were taking medication at the time of the scan (**Supplementary Table S6**), those with anxiety-related and depressive disorders (n=221) still showed significantly increased activation in the dorsal medial prefrontal cortex, dorsal PCC extending to the superior parietal lobule, left medial TG and bilateral ventrolateral prefrontal cortex compared to controls (**Supplementary Fig. S11**).

In normative modelling, we tested our clinical test sample (260 controls  $\pm$  222 cases) against our reference normative models. This analysis compared the individuals' deviation scores (z-score) within each voxel, and quantified, as a percentage of the sample, the frequency of participants with large positive or large negative deviations (**Fig. 3b**). We compared the frequency of extreme deviations throughout the whole brain (Normative Probability Maps thresholded at  $\pm$  2.6), and found that cases had, on average, a greater frequency of extreme deviations than controls (Mann Whitney Utest = 111167.5, p= 0.014; **Fig. 3c**). Qualitatively, cases showed a different pattern of deviation frequency than controls. Large deviations (i.e., more activity than would be predicted by the model) were common across cases within the dorsomedial prefrontal cortex, the primary somatomotor cortex, precuneus, the bilateral primary visual cortex (medial occipital lobe extending to the inferior medial and inferior lateral lobe) extending to the lingual and fusiform gyrus. As with controls, cases frequently had large negative deviations within the most ventral region of the vmPFC.

#### PTSD and OCD show distinct activation patterns and deviations

We divided our patient sample by primary diagnosis (PTSD, n=141; OCD, n=68; GAD, n=48; and SAD, n=31; other diagnoses were not included due to small sample size). ANOVA-like LMMs indicated that there were significant differences in brain activation during conditioning among patient groups. Post-hoc pairwise comparisons corrected for multiple comparisons showed that the most significant differences occurred between individuals with PTSD and OCD with respect to individuals with GAD and SAD (Supplementary Fig. S12).

Similarly, normative modelling analyses identified a significant difference in the frequency of large deviations among patient groups (Kruskal-Wallis H-test = 71.529, p=1.984^-13; **Fig. 3c**). Follow-up Mann Whitney U-test's (FDR corrected for multiple comparisons) clarified, for example, that extreme deviations occurred most frequently in individuals with PTSD, as compared to other disorders, followed by OCD. We then illustrated the location of these extreme deviations at the voxel level to determine whether they were spatially overlapping within and between patient groups (**Fig. 3d** and **Supplementary Fig. S13**). Individuals with PTSD showed frequent large positive deviations within the bilateral medial occipital lobe extending to the inferior temporal lobe and lingual gyrus, bilateral vlPFC, an expanse of the dmPFC, precuneus, and bilateral amygdala. They also showed frequent large negative deviations within an expanse of the vmPFC (posterior vmPFC focus), precuneus, and a focus of the lingual gyrus and fusiform gyrus. There were very few regions wherein individuals with GAD showed overlapping large deviations, and similarly for SAD except for a small region of the bilateral lingual gyrus frequently found to have large positive deviations. Individuals with OCD showed frequent large deviations within the inferior parietal cortex, and temporal pole.

A support vector machine could not classify cases from controls better than chance using whole-brain deviation maps (mean AUC = 0.44 +/- 0.07, p = 1.0). However, a multi-class support vector classifier confirmed a unique pattern of deviations among cases (**Fig. 3e**). More specifically, PTSD, on average, was accurately classified 54.55% of the time (mean F1 score = 0.58; p= 2.06x10-23, balanced accuracy = 0.43 where chance level across 4 classes = 0.25). Interestingly, despite fewer overlapping extreme deviations within the OCD group, the classifier was able to accurately label individuals with OCD 73.74% of the time (mean F1 score: 0.57; p =1.71x10-7). GAD and SAD were only accurately classified 31.78% (mean F1 score: 0.35) and 13.33% (mean F1 score: 0.17) of the time, respectively, and were often misclassified as OCD. The mean voxel-wise coefficient weights and frequency of contribution (in penalised permutations) to this classification are displayed in **Supplementary Fig. S14**.

# Sample size for future studies

We conducted a series of sample size analyses to guide the design of future fMRI fear-conditioning studies (**Supplementary Methods**). To detect activation or deactivation in 50% of the brain regions identified in the mega-analysis (based on the AAL atlas<sup>39</sup>), a sample size of 122 was required, while detecting 80% of these regions required 243 participants (**Supplementary Figure S15**). When considering activations only, the required sample sizes were slightly smaller: 100 participants to detect 50% and 199 participants to detect 80% of the mega-analytical findings. In contrast, substantially larger samples were needed to detect deactivations.263 for 50% detection and 522 for 80%. The overall false positive rate was 9%, and 8% and 3% when activations and deactivations were assessed separately, averaging 5%. Additional sample sizes results are presented in **Supplementary Figures S16-S18**.

# Early and late conditioning

Given the importance of accounting for temporal dynamics in brain activity during human fear conditioning<sup>8</sup>, we compared neural activation during the early and late phases of conditioning in a subset of participants (n = 634 controls; **Supplementary Table S8**). Consistent with the effects observed across the entire task, both phases showed significant activation in the CS+>CS- contrast across several brain regions. These included the insular cortices, SII, dlPFC, lateral premotor cortices, dorsal and lateral cerebellum, dACC extending to the pre-supplementary motor area and SMA, and the dPrec (**Supplementary Figure S19**). Notably, there were several significant differences between the phases. The early phase showed greater activation in the bilateral fusiform gyrus, SMA, right amygdala, left frontal eye fields, and left motor cortex compared to the late phase (**Supplementary Figure S19**). Additionally, significant differences were also observed in the left angular gyrus; dorsal, medial, and ventral anterior prefrontal cortices; and lateral orbitofrontal cortex. However, as these regions were implicated in the CS+<CS- contrast, this suggests that they exhibited reduced deactivation during the late phase.

# **DISCUSSION**

We compiled the largest (n=2199) sample of individual-level fear conditioning fMRI data to date to comprehensively delineate the neural correlates of human fear conditioning, to assess the influence of several relevant sources of variation - including individual differences and task variables- and to evaluate potential differences in fear conditioning at the neural level between individuals with anxiety-related and depressive disorders and controls.

Our individual-level mega-analysis mapped fear conditioning activation to the "central autonomic—interoceptive" or "salience" network. As hypothesised, fear conditioning was associated with robust activations in the anterior insula, ventral striatum, pre-supplementary /supplementary motor areas, dorsal anterior cingulate cortex, and dorsolateral prefrontal cortex. It was also associated with activation in several subcortical regions, particularly the thalamus and basal ganglia. While many of the observed effects replicated previous findings³, the increased statistical power provided by our analyses suggests that peak effects in the dorsal midbrain may originate in the substantia nigra/red nucleus and pretectal nuclei. Future work with a specific focus on these nuclei may aid in disentangling their specific contributions to fear conditioning. Also as hypothesised, fear conditioning was associated with robust deactivations in the ventromedial prefrontal cortex and hippocampus. Other brain regions that were deactivated during conditioning included primarily regions of the default mode network (e.g., posterior cingulate cortex and precuneus).

By incorporating a large sample from multiple laboratories worldwide, our study underscores the generalizability of the neural correlates of conditioning at the population level. At the same time, the methodological diversity across laboratories and studies suggests that our findings extend beyond specific experimental conditions, reinforcing their relevance to the broader fear conditioning process. Notably, at a time when neuroimaging research is increasingly emphasizing sample sizes in the thousands<sup>40</sup>, our analyses show that studies with 100 participants can still reliably detect the neural correlates of fear conditioning, at least when considering activations only. Furthermore, our findings highlight that a significant source of variability in neural responses during fear conditioning stems from differences in task design. This insight is crucial for future human fMRI studies, as it enables researchers to anticipate the expected effects of various task and contrast design choices, along with their magnitudes, at the neural level. By making these adjustments in advance, researchers can strike a balance between the advantages of large, standardized studies and those of smaller studies with greater methodological diversity. Moreover, our normative modeling results underscore the potential of fear conditioning paradigms for informing the development of targeted interventions. Specifically, normative models can identify brain regions with atypical activation during conditioning, providing valuable guidance for interventions such as neuromodulatory treatments aimed at these regions<sup>41</sup>. Additionally, by pinpointing abnormal activation patterns, normative models enable clinicians to tailor treatments more precisely to address these specific neural deviations.

The amygdala was not robustly activated during fear conditioning in either our mega-analysis or ROI-based mega-analysis for the contrast averaging across all trials, consistent with our previous group-level meta-analysis<sup>3</sup>. However, and in line with a recent study by Wen and colleagues<sup>8</sup> (n = 601, including individuals with anxiety-related disorders and controls), our analysis of early versus

late trials in a large subsample of participants (n=634 controls) revealed significantly greater activation in the right amygdala during early compared to late trials.

Inconsistencies regarding amygdala involvement in human fMRI conditioning studies have been attributed to several factors, including small sample sizes and limited anatomical specificity. The amygdala consists of distinct subregions, such as the basolateral (BLA) and centromedial (CMA) amygdala, and averaging responses may mask specific activations<sup>8,10</sup>. Moreover, the amygdala's subcortical and ventral location, its small size, and the susceptibility artifacts and low signal-to-noise ratio associated with traditional imaging techniques can further hinder detection of significant effects<sup>44</sup>. Ultra-high field imaging has been shown to reduce these limitations and allows for more precise investigation of amygdala subnuclei<sup>45,46</sup>, making it a valuable tool for future human fear conditioning studies.

Taken together with the findings of Wen and colleagues, our results highlight the importance of considering temporal dynamics when assessing amygdala activity during fear conditioning<sup>8</sup>. Specifically, they confirm that amygdala activation is strongest during early trials and habituates thereafter<sup>42</sup>,<sup>43</sup>, suggesting that averaging across all conditioning trials may obscure these effects. In the current study, we also identified specific task features- such as the use of paradigms with multiple CS+ stimuli or US-related confounds- and diagnostic categories (e.g., PTSD; see also<sup>36</sup>) that modulate amygdala activity during conditioning. These findings underscore that both clinical and task-related variables may also contribute to the inconsistencies observed in the literature.

Biological sex had only minor effects, suggesting that fear conditioning mechanisms are relatively stable at the neural level between sexes. Additionally, none of our analyses found significant associations between brain activation during conditioning and levels of trait anxiety or depressive symptoms. While some mental health frameworks suggest that dimensional constructs of psychopathology, like trait anxiety, may better reflect neural activation patterns<sup>47</sup>, the variability and complexity in the neural states underlying these constructs and their lack of direct mapping to neural processes makes it challenging to identify clear linear relationships<sup>48,49</sup>.

The brain activation differences during conditioning between individuals with anxiety-related and depressive disorders and healthy controls, observed in the mega-analysis, aligned with normative modeling results, showing a higher frequency of large deviations in cases. Importantly, these differences remained significant even after excluding medicated cases, suggesting that the observed effects are not due to medication. This is crucial, as commonly used treatments like selective serotonin reuptake inhibitors (SSRIs) can influence brain activation patterns observed with fMRI<sup>50</sup>. When the analysis was limited to anxiety-related disorders, significant differences in brain activation persisted, indicating that individuals with pathological anxiety are characterized by abnormal neural

responses during fear conditioning. These findings suggest that such abnormalities could eventually serve as neural markers for anxiety-related disorders<sup>51,52</sup>.

Among individuals with anxiety-related disorders, those with PTSD and OCD showed distinct patterns of brain activation and had distinct patterns of voxel-wise deviations that can be used to distinguish them from other anxiety-related disorders. This provides neurobiological support for the decision of current diagnostic classifications to separate these conditions<sup>53</sup>. In addition, it may provide new insights into the underlying mechanisms of psychopathology. The sample of individuals with PTSD was still relatively heterogeneous, with data from three independent samples, and yet there were often overlapping extreme positive deviations. Furthermore, using the derived deviation scores we were able to differentiate and classify individuals with PTSD and OCD with striking precision, compared to GAD and SAD. This is consistent with the previous literature that used mean averaging methods and reported differences in activation levels between groups of individuals with PTSD, compared to controls<sup>36,54</sup>. Taken together, this suggests that the neural mechanisms engaged during a fear conditioning paradigm are specifically relevant to the psychopathology of, and to some extent, similarly altered across individuals with PTSD; reinforcing the notion that fear conditioning is a foundational process in PTSD psychopathology, and as such, related tasks are a useful clinical model<sup>31</sup>. The accurate differentiation of OCD, despite few regions of overlapping large deviations, appeared to be driven by consistent coefficient weights with a region of the bilateral superior temporal gyrus and right vlPFC. Combined with no strong behavioural evidence<sup>55</sup>, mixed imaging evidence of differences in fear conditioning tasks in this population<sup>56–59</sup>, and evidence of altered baseline activity within the superior temporal region<sup>60</sup>, this finding may be interpreted as capturing compensatory mechanisms that individuals with OCD engage to overcome obsessions and achieve the same behavioural output<sup>55,60,61</sup>. Despite significant differences in the frequency of extreme deviations between individuals with GAD and SAD compared to controls, their limited spatial overlap and less accurate classifications, suggest that there is significant heterogeneity in fear conditioning among individuals with these diagnoses. Thus, while we suggest that the psychopathology of PTSD is uniquely related to fear or threat processing as captured by fear conditioning tasks, we propose that other anxiety-related disorders, particularly GAD and SAD are less so.

Our study has several limitations. First, despite using harmonized pre-processing pipelines and statistical models to account for site differences, variations in diagnostic routines and imaging acquisition contributed to sample heterogeneity, particularly among individuals with anxiety and depressive disorders (a label that includes already heterogenous disorders). Second, mega-analyses may have limited power to detect effects in small subgroups (e.g., SAD patients). Third, for participants with a mental health diagnosis, we focused on primary diagnoses and we could not assess (or control for) comorbidity. Fourth, while our normative models adjusted for site, age, biological sex,

and task influences on brain activity, future studies should explore the impact of adding more variables in the model construction. It is possible that alternative model structures could have increased the explained variance in the relatively noisy BOLD activation (where other literature has explained up to 51.3% of the variance<sup>25</sup>). However, care must be taken not to overfit or reduce the generalisability of models to ensure their wider utility. Fifth, we were unable to include other individual-level measures of conditioning (e.g., psychophysiological data) in our analyses, as this would have required separate collection and harmonization procedures. Finally, cross-sectional data on brain activation during fear conditioning raises concerns about the reliability of outcome measures. Although fMRI-based fear conditioning shows limited test-retest reliability at the whole-brain level, significant within-subject similarity across repeated time points has been observed<sup>62</sup>, suggesting that large test-retest samples could help further validate the normative modeling approach, as demonstrated in other tasks<sup>25</sup>.

With this work, we provide the largest analysis of the neural correlates of human fear conditioning and potential sources of variation to date. Our results confirm that human fear conditioning is a robust phenomenon at the neural level, consistently engaging multiple brain regions within the central autonomic-interoceptive or salience network. Our comprehensive review of the influence of task design choices on elicited and predicted brain activation can be used to help interpret differences in the previous literature and should remind researchers of the potentially significant influence of task design choices. Finally, we found that there are overall differences in fear conditioning at the neural level between individuals with anxiety-related and depressive disorders and controls, and that a unique mechanism of PTSD psychopathology is well captured by fear conditioning paradigms, supporting the use of these models to study this disorder.

#### **METHODS**

The current manuscript combines two pre-registered analyses of individual-level fear conditioning fMRI data (https://osf.io/7n953; https://osf.io/w74bt). Data were collated from 43 samples originating from 23 sites in 9 countries. Collation was coordinated by the lead group (IDIBAPS Barcelona). ENIGMA Fear Conditioning is part of the larger ENIGMA-Anxiety Working Group<sup>63</sup>. **Table 1** and **Table 3** summarize the descriptive information on the samples. Informed consent was obtained from all participants by the sites providing their data. Some site-specific data have been reported previously, but no reports have examined all individual data together.

# Fear conditioning task

We included data from participants who completed a fear conditioning experiment during an fMRI scan. There are several human fear conditioning paradigms, which vary based on the time elapsed between the CS and the US (e.g., delay, trace, simultaneous, or backward conditioning), the use of one (single-cue) versus two or more (differential-cue) CSs, and the instructions given to participants<sup>2</sup>: 1) *No instructions*: For example, "During this experiment, you will see various images and might experience mild electric shocks at certain times"; 2) *Partial instructions*: For example, "During this experiment, you may see a particular image sometimes followed by a mild electric shock. However, the shock won't happen every time you see the image, and sometimes it might not appear at all. Pay attention to the images, as they might give you some indication of when the shock could occur"; 3) *Full instructions* (instructed conditioning): For example, "During this experiment, you will see the image X, which is always followed by a mild electric shock. Whenever this image appears, it will be followed by the shock shortly afterward. No other images will be associated with the shock".

We focused on delay differential cue-conditioning paradigms with no or partial instructions (i.e., excluded instructed conditioning studies), and focused our analysis on comparing the response to a CS+ compared to a CS-. **Table 2** summarises information on the fear conditioning tasks included in this manuscript.

# Non-imaging data: sociodemographics and individual differences

All sites were asked to provide information regarding sociodemographics (age, biological sex) and individual differences: trait anxiety, assessed with the Trait subscale of the State-Trait Anxiety Inventory (STAI-T)<sup>64</sup>; and depressive symptoms, assessed with the Beck Depression Inventory (BDI)<sup>65</sup> (**Supplementary Table S1**). For individuals with anxiety-related and depressive disorders, sites were asked about principal mental health diagnosis and psychotropic medication use at the time of the scan (**Supplementary Table S6**. Previous normative studies of trait anxiety (STAI-T) have shown additive and multiplicative differences across countries, for which we harmonised trait anxiety

scores across countries using ComBat<sup>14</sup> (**Supplementary Methods**) and conducted subsequent analyses twice: once with the raw scores and once with the country-harmonised scores.

# Non-imaging data: task-related variables

We collected information about the following task variables: instructions given to the participant about contingency prior to the task (partial versus no information); type of US (e.g., electric shock versus aversive sound); number of trials during pre-conditioning; use of a paradigm with multiple CSs (i.e., more than one CS+ or CS-) during conditioning; type of CS (e.g. geometrical figures, faces, etc); number of CS+ and CS- trials during conditioning; average ITI (inter-trial interval); average ISI (inter-stimulus interval, i.e., between the CS+ and the US); pairing rate (percentage of CS+ followed by a US); potential US confounding; and the number of CS+ trials and CS- trials included in the fMRI contrast. For studies assessing awareness (conscious recognition of the association between the CS+ and the US, after the task), we also asked about participant's contingency awareness (yes vs. no). Task variables were not explicitly listed in the pre-registration. The decision to include these variables was based on previous research<sup>2,13</sup>.

# Processing of neuroimaging data

We included only neuroimaging data acquired with whole-brain coverage. Individual-level raw task-based fMRI data were processed using the Harmonized Analysis of Functional MRI pipeline (HALFpipe, version 1.2.2)<sup>66</sup>, a tool developed within the ENIGMA consortium to harmonise fMRI analyses across sites and facilitate reproducible analyses. HALFpipe provides a standardised workflow that extends fMRIprep<sup>67</sup> with several additional preprocessing steps, including spatial smoothing, grand mean scaling, temporal filtering, and confound regression. Moreover, HALFpipe generates a standardised quality assessment of the preprocessing outputs and imaging raw data (**Supplementary Table S7**). We used HALFPIPE default parameters (smoothing using 6mm FWHM; confound removals using ICA-AROMA; and a high-pass filter of 125 s).

For the current study, each site was provided with a comprehensive manual to perform image pre-processing and quality control with HALFpipe in a fully harmonised manner, and each group shared the HALFPIPE output files for each individual along with the non-imaging data for each individual. The lead group (IDIBAPS-Barcelona) processed 5 sites, aggregated all the data, and carried out additional quality control procedures and measures to ensure the comparability of the data, as described in the **Supplementary Methods**).

# Statistical analyses

We conducted two types of statistical analyses: mega-analyses and normative modelling analyses.

# Mega-analyses

#### **Participants**

We included data from 2199 participants (M\_Age=25.26, SD=5.47; 57.2% female), comprising 1888 healthy controls (M\_Age=25.85, SD=8.51; 51.53 % female) and 311 individuals with a primary diagnosis of an anxiety-related or depressive disorder (M\_Age=29.91, SD=10.75; 58.84 % female) (**Table 1** and **Table 3**). Diagnoses were established with structured clinical interviews.

# **Pre-scaling**

Although we used the exact same processing protocol and conducted extensive quality control (see above), we observed differences in the BOLD response between samples, most likely due to varying units of measurement (note that MRI scans are acquired in arbitrary units<sup>68</sup>. To address these differences, we pre-scaled the images for healthy controls so that, for each sample, the voxel-wise-median standard deviation (after removing the effects of covariates) was 1 (see **Supplementary Methods**). We then applied the pre-scaling parameters obtained from the healthy controls to the cases (individuals with a primary diagnosis of an anxiety-related or depressive disorder). This approach differs from using the individual z-statistic images (i.e., dividing the BOLD response by its standard error), which we did not adopt for the mega-analysis. The reason is that the standard error may differ between cases and controls, and thus, differences in z-statistics between groups could reflect differences in the standard error rather than in the BOLD response (for more details, see **Supplementary Methods**).

# **Analyses**

Differences in brain coverage across sites prevented us from using the standard ComBat method, which determines the harmonisation parameters using all voxels<sup>14</sup>. Additionally, there was no need to remove differences in scaling because we had already pre-scaled the images as described above. Thus, we used LMMs (with the sample as a random intercept) to investigate: 1st the pattern of brain activation during fear conditioning in healthy controls and in cases (individuals with anxiety-related and depressive disorders), which tested whether the mean activation in each voxel was non-null; 2nd the pattern of differences in brain activation during fear conditioning between cases and controls, which tested whether activation in each voxel was different between cases and controls; 3rd the pattern of differences in brain activation during fear conditioning among patient groups (PTSD, OCD, GAD, SAD), testing whether activation in each voxel differed among patient groups; 4th the potential influence of individual differences and task variables (see above) on brain activation during fear conditioning in healthy controls, which tested whether activation in each voxel was significantly associated with each task variable. In all models, we incorporated age and sex as covariates.

Significant LMMs comparing three or more groups (analog to ANOVAs) were followed by pairwise comparisons with Holm-Bonferroni correction.

We also conducted an ROI mega-analysis focusing on the amygdala. For this analysis, we extracted the pre-scaled BOLD response in the left and right amygdala based on the Automated Anatomical Labeling atlas<sup>39</sup>. We used an LMM, with age and sex as covariates, to test whether the mean activation significantly differed from zero. Potential differences between early and late conditioning were also analyzed using a LMM, with age and sex as covariates in a subsample of controls (n=679; **Supplementary Table S8**).

We fitted the LMMs using custom functions (included in 'combat.enigma' R package) that call the 'nlme' R package voxel-wise and address voxel-specific details (e.g., varying collinearity due to differing brain coverage; see **Supplementary Methods**). FSL was then used to derive cluster-based corrected p-values using Gaussian Random Field (GRF) theory.

# **Analyses of multicollinearity**

Given the diverse range of variables examined in this study—many of which may be influenced by methodological factors (e.g., pairing rate, type of conditioned stimuli) or sample characteristics (e.g., patient vs. control group)—there is a potential risk of confounding. That is, the observed effects attributed to one task variable may partially or wholly reflect the influence of another. To address this possibility, we systematically assessed interrelationships among all methodological and clinical variables using correlation analysis and evaluated multicollinearity using variance inflation factors (VIF). For pairs of variables with correlation coefficients exceeding 0.5 (or eta and Cramér's V when involving categorical variables), we further examined whether their associated activation maps exhibited spatial overlap. Overlap was defined as clusters of at least 10 contiguous voxels showing significant activation for both task contrasts. This approach was guided by the rationale that classical confounding requires both variables to be associated with activation in the same brain region. For any pair of correlated variables with overlapping activation, we re-estimated the mixed-effects linear models within the overlapping clusters, this time including both variables as predictors, to determine whether their effects remained statistically significant. A reduction to non-significance upon joint inclusion could indicate either collinearity (as suggested by the VIF) or potential confounding.

# **Effect sizes**

To compare the effect sizes of different variables and to exclude findings with negligible or very small effects, we converted the regression coefficients of the peaks into correlation coefficients (Pearson r). For variables comparing two groups (e.g., cases vs. controls), we also calculated the corresponding standardised mean differences (Cohen's d). We considered effects with r<0.2 (roughly equivalent to d<0.4 for balanced binary variables) to be small, and only highlighted larger effects (i.e.,

r>0.2, i.e., at least moderate) in the main text. It is important to note that peak effect sizes should be interpreted with caution, as they correspond to the peaks of clusters of statistical significance and are, therefore, larger than those obtained by other methods. Effect sizes for all the LMMs can be found at <a href="https://figshare.com/s/d44cc1390711bad3c147">https://figshare.com/s/d44cc1390711bad3c147</a>

# Normative modelling analyses

# **Participants**

We included data from 2022 participants; 1800 healthy controls (age range 8-66 years, mean age:  $25.66 \pm 8.4$ , 53.05% female) and 222 individuals with anxiety-related and depressive disorders (age range 9-63, mean age:  $28.27 \pm 11.06$ , 54.95% female) to build and test the normative models. See **Table 1** note to explain discrepancy in participant numbers from mega-analysis.

# Generating Normative Models of Activation to the CS+ > CS- contrast

The z-statistic maps (files) from the CS+ > CS- contrast for each participant were used as inputs (response variables) for the normative models. We created a normative model of fear-related activation per voxel, as a function of age, sex, and task variables (the same reported in the **Non-imaging data: task-related variables** section, except contingency awareness) by training a Gaussian Bayesian Linear Regression (BLR) model to predict activation for the CS+ > CS- contrast<sup>22</sup>. We included dummy coded site-related variables (sample, and MR strength) and a b-spline basis expansion as additional covariates of no-interest. This was performed in the Predictive Clinical Neuroscience toolkit (PCNtoolkit) software v0.26 (https://pcntoolkit.readthedocs.io/en/latest) implemented in python 3.8. Generalisability was assessed by using a stratified train-test sample (train: 894, control test sample: 646).

#### Quantifying voxel-wise deviations from the normative model

To estimate a pattern of regional deviations from typical brain function for each participant in the control test sample (n = 646, mean age:  $25.45 \pm 7.19$  years, 52.16% female), we derived a normative probability map (NPM) that quantifies the voxel-wise deviation from the normative model. The subject-specific Z-score indicates the difference between the predicted activation and true activation scaled by the prediction variance. This was repeated for the clinical test sample (n = 482, 260 controls + 222 cases, mean age:  $26.76 \pm 10.94$  years, 54.97% female). We thresholded participant's NPM at Z =  $\pm 2.6$  (i.e., p < .005) as in previous work<sup>69-71</sup> and summed the number of significantly deviating voxels for each participant. Kruskal-Wallis H-tests were used to test for group (cases or controls) and

diagnosis effects and, when applicable, follow-up Mann Whitney U-tests were False Discovery Rate  $(FDR)^{72}$  corrected at  $\alpha = 0.05$ .

# Normative models: individual differences and task variables

*Model Coefficients:* To probe the magnitude of the influence of individual differences (sociodemographics) and task variables on the predicted brain activation, we examined both the regression coefficients and the structure coefficients (correlation coefficients) of all sociodemographic and task variables input variables. Structure coefficients are preferable to regression coefficients when variables are collinear<sup>73</sup>. Note that negative R^2 values ("negative" explained variance) is a possible outcome when the model fails to generalize effectively to new data, despite in-sample performance yielding non-negative explained variance (which is always positive or zero by construction). This phenomenon is not uncommon and arises when the model's predictions result in a residual sum of squares that exceeds the variance of the true values.

Linear Regression (Elastic Net) and Support Vector Classification (SVC): We applied an elastic net linear regression as implemented in the scikit-learn package (version 1.0.2)<sup>74</sup> with 10 repeats of nested 5-fold cross validation [alphas = 0.0001, 0.001, 0.01, 0.1, 0.3, 0.5, 0.7, 1; 90% train, 10% test split] to predict trait anxiety as measured by the STAI-T (n = 751), or depressive symptoms as measured by the BDI (n = 440) from participants' whole brain (unthresholded) deviation maps. The mean coefficient values and the frequency of the voxel's contribution (in other words, how many of the cross-folds split found this voxel to be important) indicate which voxel contributed to the prediction. The statistical significance of these results was tested against a 1000-fold nested 5-fold test for each variable. To classify participants (n = 703) who were contingency aware from those who were not based on their unthresholded whole-brain deviation maps, we used an SVC model with a linear kernel, regularisation parameter set to 1.0, and balanced class weights as implemented in the scikit-learn package (version 1.0.2).

#### Quantifying patterns of deviations between cases and controls

To classify individuals with anxiety-related or mood disorders and controls based on their whole brain unthresholded deviation maps, we used a SVC model with a linear kernel, regularisation parameter set to 1.0, as is common in neuroimaging, and balanced class weights (i.e. adjusted inversely proportional to class frequencies in the input data) as implemented in the scikit-learn package (version 1.0.2)<sup>74</sup>. The evaluation metric for the classification is area under the receiving operator curve (AUC) averaged across all folds within a 10-fold cross validation framework.

# Quantifying patterns of deviations among patient groups

We used a one versus rest support vector classifier (SVC OvR) model as implemented in the scikit-learn package (sklearn.multiclass.OneVsRestClassifier version 1.0.2) to determine if there were quantifiably differentiable patterns within the whole brain unthresholded deviation maps among patient groups. Due to the small number of individuals with major depressive disorder (n = 11), specific phobia (n=7) and panic disorder (n=2), this analysis only included individuals with a diagnosis of PTSD (n=55), OCD (n=68), GAD (n=48) and SAD (n=31) (total n = 202). The model classes were the participants' diagnosis. The evaluation metric for the classification was the F1-metric (the harmonic mean of precision and recall, also known as the balanced F-score, where values closer to 1 indicate greater classification success) per class within a 5-fold cross-validation framework, and the statistical significance was tested against a 1000-fold nested 5-fold test.

#### Data availability statement

All results from this manuscript can be found at <a href="https://figshare.com/s/d44cc1390711bad3c147">https://figshare.com/s/d44cc1390711bad3c147</a>

The ENIGMA-Fear Conditioning Group (part of the ENIGMA-Anxiety Working Group<sup>63</sup> is open to sharing the individual-level data (HALFIPE results files) from this investigation to researchers for secondary data analysis. To request access to data, an analysis plan can be submitted to the ENIGMA-Anxiety Working Group (<a href="http://enigma.ini.usc.edu/ongoing/enigma-anxiety/">http://enigma.ini.usc.edu/ongoing/enigma-anxiety/</a>). Data access is contingent on approval by PIs from contributing samples.

# Code availability statement

All code to reproduce the analyses in this manuscript is available at: <a href="https://figshare.com/s/d44cc1390711bad3c147">https://figshare.com/s/d44cc1390711bad3c147</a>. The functions needed to conduct the mega-analysis are also included in the 'combat.enigma' R package.

**Table 1.** Descriptive statistics for all samples (N=43) included in the analyses.

Sample	Country	N	Sex (%females)	Healthy Controls (n)	Patients (n)	Age M (SD)   Range (min-max)	Years of education M (SD)   Range (min-max)
Amsterdam_Visser/Kindtsample_1	NL	18	72	18	0	22.06 (3.35)   18-31	not available
Amsterdam_Visser/Kindtsample_2	NL	41	73	41	0	20.56 (1.79)   18-24	not available
Amsterdam_Visser/Kindtsample_3	NL	12	75	12	0	21 (1.35)   19-23	not available
Amsterdam_Visser/Kindtsample_4	NL	10	80	10	0	22.8 (2.04)   20-26	not available
Amsterdam_Visser/Kindtsample_5	NL	13	85	13	0	22.23 (4.07)   19-35	not available
Amsterdam_Visser/Kindtsample_6	NL	14	79	14	0	23.43 (2.71)   18-29	not available
Amsterdam_Visser/Kindtsample_7	NL	16	44	16	0	24.06 (3.36)   18-29	not available
Amsterdam_Visser/Kindtsample_8	NL	9	100	9	0	20.33 (1.41)   18-22	not available
Amsterdam_Visser/Kindtsample_9	NL	38	58	38	0	23.66 (3.78)   18-33	not available
Austin_Cisler	US	61	100	0	61	33.72 (8.48)   21-50	15.46 (2.64)   10-22
Barcelona_Cardoner	SP	71	66	45	26	22.66 (4.67)   18-40	14.49 (2.15)   12-20
Barcelona_Soriano_sample_1	SP	35	51	17	18	37.43 (10.54)   19-58	14.69 (3.72)   6-18
Barcelona_Soriano_sample_2	SP	147	50	122	25	24.76 (4.22)   19-36	18.63 (3.95)   13-26
Bielefeld_Lonsdorf_sample_1	GE	116	66	116	0	24.61 (3.61)   18-34	15.26 (2.14)   1-16
Bielefeld_Lonsdorf_sample_2	GE	80	56	80	0	24.88 (3.51)   19-34	not available
Bielefeld_Lonsdorf_sample_3	GE	28	64	28	0	24.68 (4.95)   18-39	13.36 (1.75)   11-20
Bochum_Elsenbruch	GE	29	48	29	0	26.45 (3.59)   19-33	17.45 (4.02)   3-23

Bochum_Merz_sample_1	GE	59	49	59	0	23.88 (4.17)   18-34	16.07 (3.4)   9-26	
Bochum_Merz_sample_2	GE	59	47	59	0	24.39 (3.83)   18-35	15.86 (3.72)   5-23	
Bochum_Merz_sample_3	GE	47	49	47	0	22.87 (2.61)   19-30	not available	
Bochum_Merz_sample_4	GE	29	0	29	0	24.21 (3.62)   19-33	not available	
Bochum_Merz_sample_5	GE	31	0	31	0	24.71 (3.87)   20-34	not available	
Bochum_Merz_sample_6	GE	60	50	60	0	23.57 (2.95)   18-33	not available	
Columbia_Neria	US	95	46	65	30	35.65 (12.26)   18-60	15.11 (2.45)   10-24	
Duke_LaBar_sample_1	US	38	47	38	0	24.68 (4.2)   19-35	not available	
Duke_LaBar_sample_2	US	37	49	37	0	29.16 (11.07)   19-66	not available	
Florida_Keil	US	14	36	14	0	19.79 (2.08)   18-26	14 (0)   14-14	
Harvard_McLaughlin	US	89	55	75	14	13.06 (2.6)   8-17	7.04 (2.32)   2-10	
Manitoba_Greening_sample_1	CA	13	38	13	0	24 (5.07)   19-36	17.15 (3.02)   14-23	
Manitoba_Greening_sample_2	CA	31	55	31	0	24.23 (4.56)   17-33	not available	
Melbourne_Harrison	AU	112	61	75	37	20.88 (2.34)   16-25	15.02 (2.21)   11-21	
Munich_Koch	GE	45	56	23	22	34.47 (12.39)   20-63	not available	
Munster_Moeck_sample_1	GE	42	69	42	0	26.02 (6.22)   19-51	12.33 (1.37)   7-15	
Munster_Moeck_sample_2	GE	29	52	29	0	15.79 (0.98)   14-17	10.64 (0.99)   8-12	
Reading_Reekum_sample_1	UK	21	57	21	0	24 (2.59)   21-31	not available	
Reading_Reekum_sample_2	UK	50	60	50	0	17.8 (3.46)   12-25	11.34 (1.82)   8-14	
MGH_Tuominen_sample_1	US	14	0	14	0	36.36 (9.61)   22-49	15.69 (1.84)   12-19	

MGH_Tuominen_sample_2	US	37	43	37	0	28.51 (5.81)   19-42	17.08 (2.27)   12-23
USP_Diniz	BR	55	58	27	28	35.56 (10.97)   19-63	13.13 (4.1)   1-17
Texas_Dunsmoor	US	45	64	23	22	23.47 (4.51)   18-37	NA
Ulm_Abler	GE	50	0	50	0	22.6 (2.92)   18-29	NA
Uppsala_Ahs	SW	278	58	278	0	33.87 (10)   20-58	14.16 (1.65)   9-15
Vanderbilt_Kaczkurkin	US	81	0	53	28	33.47 (9.7)   19-61	15.74 (2.18)   13-20
Total n/Mean (SD)/Range		2199	52.69	1888	311	25.26 (5.47)   8-66	14.53 (2.56)   1-26

AU, Australia; BR, Brazil; CA, Canada; GE, Germany; NA, Not available; NL, The Netherlands; SP, Spain; SW, Sweden; UK, United Kingdom, US, United States. Note: To be included in the normative modelling analysis each participant had to have all essential data (age, sex) available, samples had to have control participants and larger samples required both genders available. These reasons lead to the exclusion of the entire Austin\_Cisler and Vanderbilt\_Kaczkurkin datasets, as well as 7 additional participants. The Bielefeld\_Lonsdorf\_sample\_3 was not approved for inclusion in the normative modelling analysis. Thus, a total of 177 fewer participants were included in the normative modelling analysis.

**Table 2.** Characteristics of the fear conditioning tasks for each sample.

Sample	CS+/CS- (n/n)	CS+ trials (n)	CS- trials (n)	Average ITI (ms)	Average ISI (ms)	Pairing rate (%)	CS type	Type of US	US confound	Assessment of awareness	Preconditi oning phase
Amsterdam_Visser/Kindtsample_1	2/2	22	22	22000	6000	55	Neutral faces & pictures	Electric shock	no	yes	yes
Amsterdam_Visser/Kindtsample_2	2/2	22	22	20000	4000	55	Neutral faces & pictures	Electric shock	no	yes	yes
Amsterdam_Visser/Kindtsample_3	2/2	18	18	17500	4000	56	Neutral faces & pictures	Electric shock	no	yes	yes
Amsterdam_Visser/Kindtsample_4	2/2	18	18	17500	4000	56	Neutral faces & pictures	Electric shock	no	yes	yes
Amsterdam_Visser/Kindtsample_5	2/2	18	18	10350	4000	56	Neutral faces & pictures	Electric shock	no	yes	yes
Amsterdam_Visser/Kindtsample_6	2/2	18	18	10350	4000	56	Neutral faces & pictures	Electric shock	no	yes	yes
Amsterdam_Visser/Kindtsample_7	2/2	18	18	4650	4000	56	Neutral faces & pictures	Electric shock	no	yes	yes
Amsterdam_Visser/Kindtsample_8	2/2	18	18	17500	4000	56	Neutral faces & pictures	Electric shock	no	yes	yes
Amsterdam_Visser/Kindtsample_9	2/2	22	22	20000	4000	55	Neutral faces & pictures	Electric shock	no	yes	yes
Austin_Cisler	1/1	18	18	4000	2500	50	Neutral pictures	Electric shock	no	yes	yes

Barcelona_Cardoner	1/1	32	32	5891	1900	50	Neutral pictures	Auditory stimulus	no	yes	yes
Barcelona_Soriano_sample_1	2/1	16	16	15000	5800	62.5	Neutral pictures	Electric shock	yes	yes	yes
Barcelona_Soriano_sample_2	1/1	15	10	12000	1750	33	Neutral pictures	Electric shock	no	yes	yes
Bielefeld_Lonsdorf_sample_1	1/1	14	14	13000	6800	100	Neutral pictures	Electric shock	yes	yes	yes
Bielefeld_Lonsdorf_sample_2	1/1	14	14	13000	7000	100	Neutral pictures	Electric shock	yes	no	yes
Bielefeld_Lonsdorf_sample_3	2/2	18	18	10000	7000	100	Grey fractals	Electric shock	yes	yes	yes
Bochum_Elsenbruch	1/1	8	8	25000	9000	100	Neutral pictures	Other*	yes	yes	no
Bochum_Merz_sample_1	2/1	16	8	10750	8000	62.5	Neutral pictures	Electric shock	no	yes	no
Bochum_Merz_sample_2	2/1	16	8	10750	8000	62.5	Neutral pictures	Electric shock	no	yes	no
Bochum_Merz_sample_3	1/1	21	21	12000	8000	100	Neutral pictures	Electric shock	yes	yes	no
Bochum_Merz_sample_4	2/1	16	8	10062	6000	62.5	Neutral pictures	Electric shock	no	yes	no
Bochum_Merz_sample_5	1/1	16	16	10750	8000	62.5	Neutral pictures	Electric shock	no	yes	no

Bochum_Merz_sample_6	2/1	16	8	10062	6000	62.5	Neutral pictures	Electric shock	no	yes	no
Columbia_Neria	1/2	15	30	3600	4000	80	Neutral pictures	Electric shock	yes	no	yes
Duke_LaBar_sample_1	2/2	20	20	5750	6000	50	Avatars with neutral faces	Electric shock	yes	no	yes
Duke_LaBar_sample_2	1/1	16	16	15900	4000	31	VR affective pictures	Electric shock	yes	no	yes
Florida_Keil	1/1	29	20	7000	5100	25	Gabor patches	Electric shock	yes	yes	yes
Harvard_McLaughlin	1/1	8	4	20000	1500	40	Neutral pictures	Auditory stimulus	no	no	no
Manitoba_Greening_sample_1	1/1	24	24	12000	6000	50	Gabor patches	Electric shock	no	no	yes
Manitoba_Greening_sample_2	1/1	24	24	12000	3995	50	Gabor patches	Electric shock	no	no	yes
Melbourne_Harrison	1/1	15	10	12000	1950	33	Neutral pictures	Auditory stimulus	no	yes	yes
Munich_Koch	1/1	8	8	12000	12000	50	Affective faces and pictures	Electric shock	yes	no	no
Munster_Moeck_sample_1	1/1	27	27	5750	300	33	Neutral faces	Auditory stimulus	no	yes	yes

Munster_Moeck_sample_2	1/1	27	27	5750	300	33	Neutral faces	Auditory stimulus	no	yes	yes
Reading_Reekum_sample_1	1/1	12	12	10530	500	100	Neutral pictures	Auditory stimulus	yes	no	no
Reading_Reekum_sample_2	1/1	12	12	10530	500	100	Neutral pictures	Auditory stimulus	yes	no	no
MGH_Tuominen_sample_1	2/1	16	16	15000	6000	62.5	Neutral pictures	Electric shock	yes	no	no
MGH_Tuominen_sample_2	1/1	8	8	15000	6000	62.5	Neutral faces	Electric shock	yes	no	no
USP_Diniz	2/1	16	16	15000	3000	62.5	Neutral pictures	Electric shock	yes	yes	no
Texas_Dunsmoor	1/1	24	24	6000	5000	50	Other**	Electric shock	yes	no	no
Ulm_Abler	2/1	80	20	variable	2500	50	Neutral pictures	Thermal stimulus	no	no	no
Uppshala_Ahs	1/1	16	16	14000	6000	50	Humanoi d characters	Electric shock	yes	yes	yes
Vanderbilt_Kaczkurkin	2/1	15	30	3600	3900	80	Neutral pictures	Electric shock	yes	yes	yes

CS, conditioned stimulus; CS+, CS followed by unconditioned stimulus; CS –, CS not followed by unconditioned stimulus; CS+/CS-, Number of different CS+ and CS-; ITI, intertrial interval; ISI, inter-stimulus interval; US=Unconditioned stimulus. All samples used visual conditioned stimuli. All samples included an independent assessment of conditioning (e.g., skin conductance responses) except Amsterdam\_Visser/Kindt\_\_1. For all samples, the fMRI contrast (CS+ > CS-) included either all CS+ trials (with US present) or all CS+ trials without the US, along with all CS- trials. Exceptions included

Barcelona\_Cardoner, Duke\_LaBar\_sample\_1, and Duke\_LaBar\_sample\_2, which only included trials from an early conditioning phase (n = 4CS + /4CS - 5CS + /5CS - 3CS + /5CS - 3CS - 3CS + /5CS - 3CS + /5CS - 3CS - 3CS + /5CS - 3CS -

**Table 3.** Characteristics of individuals with anxiety-related and depressive disorders included in the analyses.

Sample	N	Age M (SD)	Females	Medicatio	Comorbidity	GAD	MDD	OCD	PTSD	SAD	PD	SP
		<i>E</i> ( )	(%)	n (%)	(%)	(n)	(n)	(n)	(n)	(n)	(n)	(n)
Austin_Cisler	61	33.72 (8.48)	100	59.02	67.21	0	0	0	61	0	0	0
Barcelona_Cardoner	26	23.88 (4.78)	61.54	3.85	11.54	26	0	0	0	0	0	0
Barcelona_Soriano_sample_1	18	40.56 (11.91)	61.11	88.89	50	0	0	18	0	0	0	0
Barcelona_Soriano_sample_2	25	25.56 (3.68)	64	0	16	21	0	0	0	4	0	0
Columbia_Neria	30	35.07 (13.82)	33.33	0	80	0	0	0	30	0	0	0
Harvard_McLaughlin	14	14.57 (2.14)	50	0	0	1	0	0	3	1	2	7
Melbourne_Harrison	37	19.89 (2.31)	51.35	0	56.76	0	11	0	0	26	0	0
Munich_Koch	22	33.55 (13.59)	59.09	54.55	27.27	0	0	22	0	0	0	0
USP_Diniz	28	33.68 (8.09)	53.57	0	71.43	0	0	28	0	0	0	0
Texas_Dunsmoor	22	25.95 (5.04)	68.18	NA	0	0	0	0	22	0	0	0
Vanderbilt_Kaczkurkin	28	34.57 (9.36)	0	3.57	32.14	0	3	0	25	0	0	0
Total n/M	31 1	29.91 (10.75)	58.84	21.22	44.05	48	14	68	141	31	2	7

Data refer to primary mental health diagnoses. "'Comorbidity' refers to the presence of at least one additional mental disorder. Data on comorbidity were not included in the analyses. GAD=Generalized Anxiety Disorder, MDD=Major Depressive Disorder, NA=Not available, OCD=Obsessive-Compulsive Disorder, PD=Panic Disorder; PTSD=Post-traumatic Stress Disorder, SAD=Social Anxiety Disorder; SP=Specific Phobia.

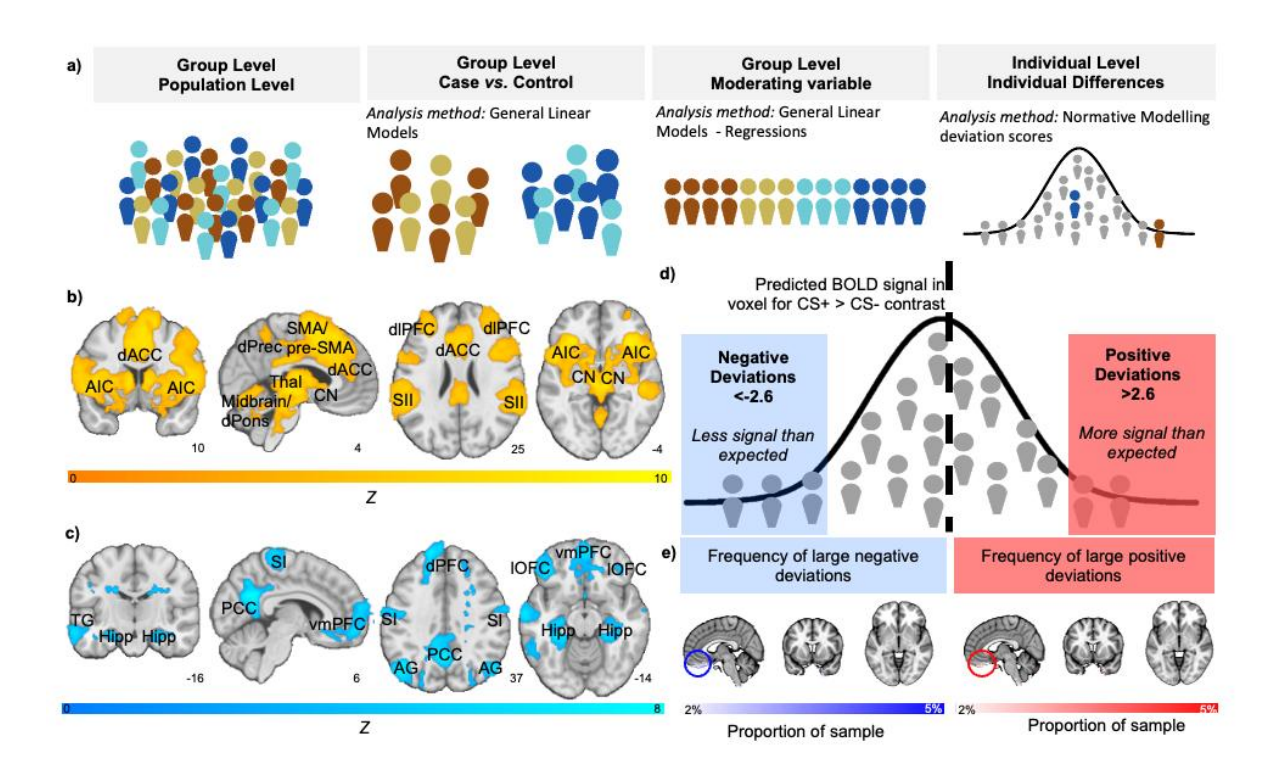


Figure 1. Neural correlates and individual-level heterogeneity in human fear conditioning. Schematic indicating the levels of analysis (a). Significant brain functional activation (b) and deactivation (c) to the CS+ versus CS- determined by mega-analysis (n=1888 healthy controls). Schematic of normative modelling framework (d). Normative probability maps illustrate the percentage of participants in the healthy control test sample who had positive (hot colours -right) or negative deviations (cool colours - left) >±2.6 within each voxel. Circle highlights frequent large deviations (both positive and negative) within the most ventral region of the vmPFC (e). Abbreviations: AIC, anterior insular cortex; AG, angular gyrus; CN, caudate nucleus; dACC, dorsal anterior cingulate cortex; dlPFC, dorsolateral prefrontal cortex; dPFC, dorsal prefrontal cortex; dPons, dorsal pons; dPrec, dorsal precuneus; Hipp, hippocampus; HYP, hypothalamus; lOFC, lateral orbitofrontal cortex; PCC, posterior cingulate cortex; SI, primary somatosensory cortex; SII, secondary somatosensory cortex; SMA, supplementary motor area; TG, temporal gyrus; Thal, thalamus; vmPFC, ventromedial prefrontal cortex.

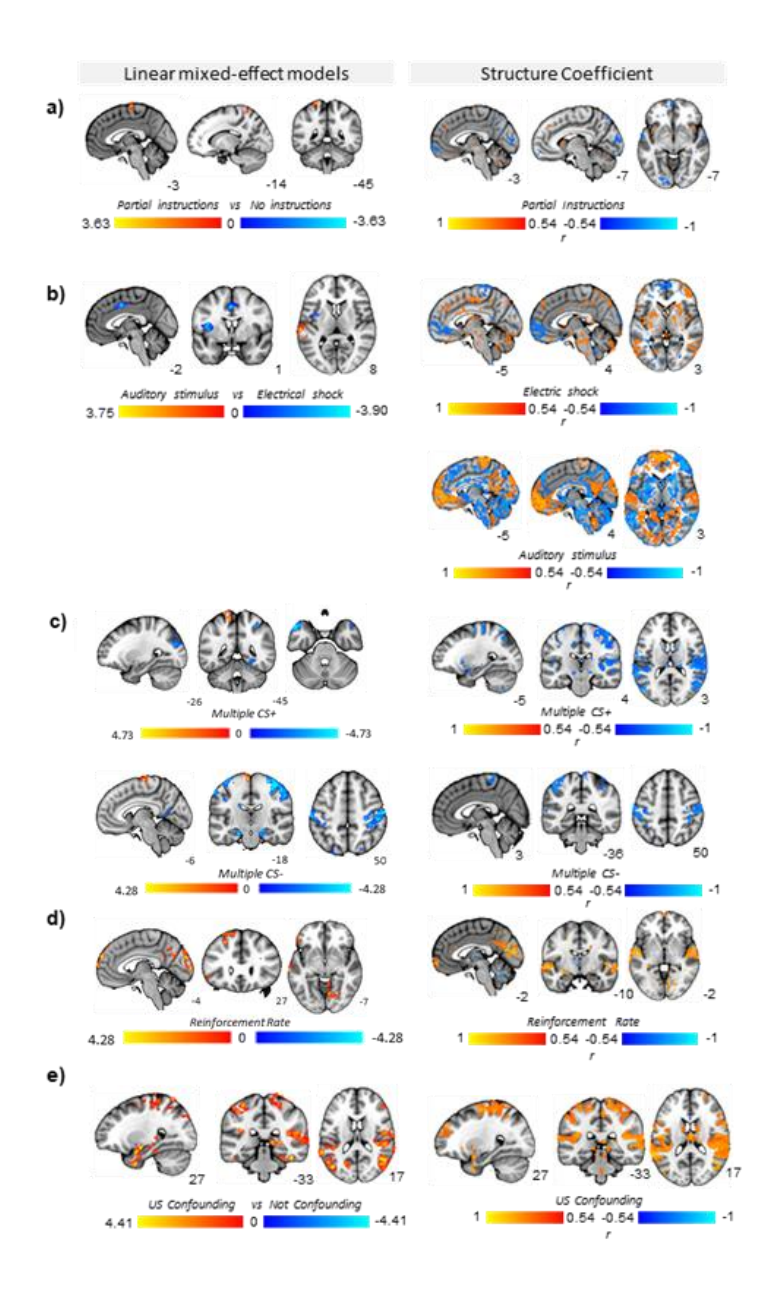


Figure 2. Robust influence of task variables on brain activation during fear conditioning. Maps show the influence of pre-task instructions about CS-US contingency (a), type of US (b), number of CS used in paradigm (i.e. multiple CS+ or CS- or single CS+ or CS-) (c), pairing rate (d), and potential US confounding in CS+ > CS- contrast (e) on mean activation (left; mega-analysis linear mixed-effects models) and relation to predicted activation (right; normative model structure coefficients). Structure coefficient maps show the correlation coefficients (rho) thresholded by their respective coefficients of determination (rho2 > 0.3) of selected task variables. This can be interpreted as showing how predicted activation to the CS+ > CS- contrast relates to the task variables included in the building of the normative models. Positive correlations (warm colours) indicate greater activation for higher values of the input variable and negative correlations (cool colours) greater activation for lower values of the input variables are dummy coded, e.g. pre-task instructions, type of US).CS=Conditioned Stimulus; US=Unconditioned Stimulus. For Pairing Rate (RR) in linear mixed-effects models, the figure shows significant results in the ANOVA comparing four categories (RR30, RR50, RR62, RR100). For the results of post-hoc tests, see Supplementary Figures S5 and S6.

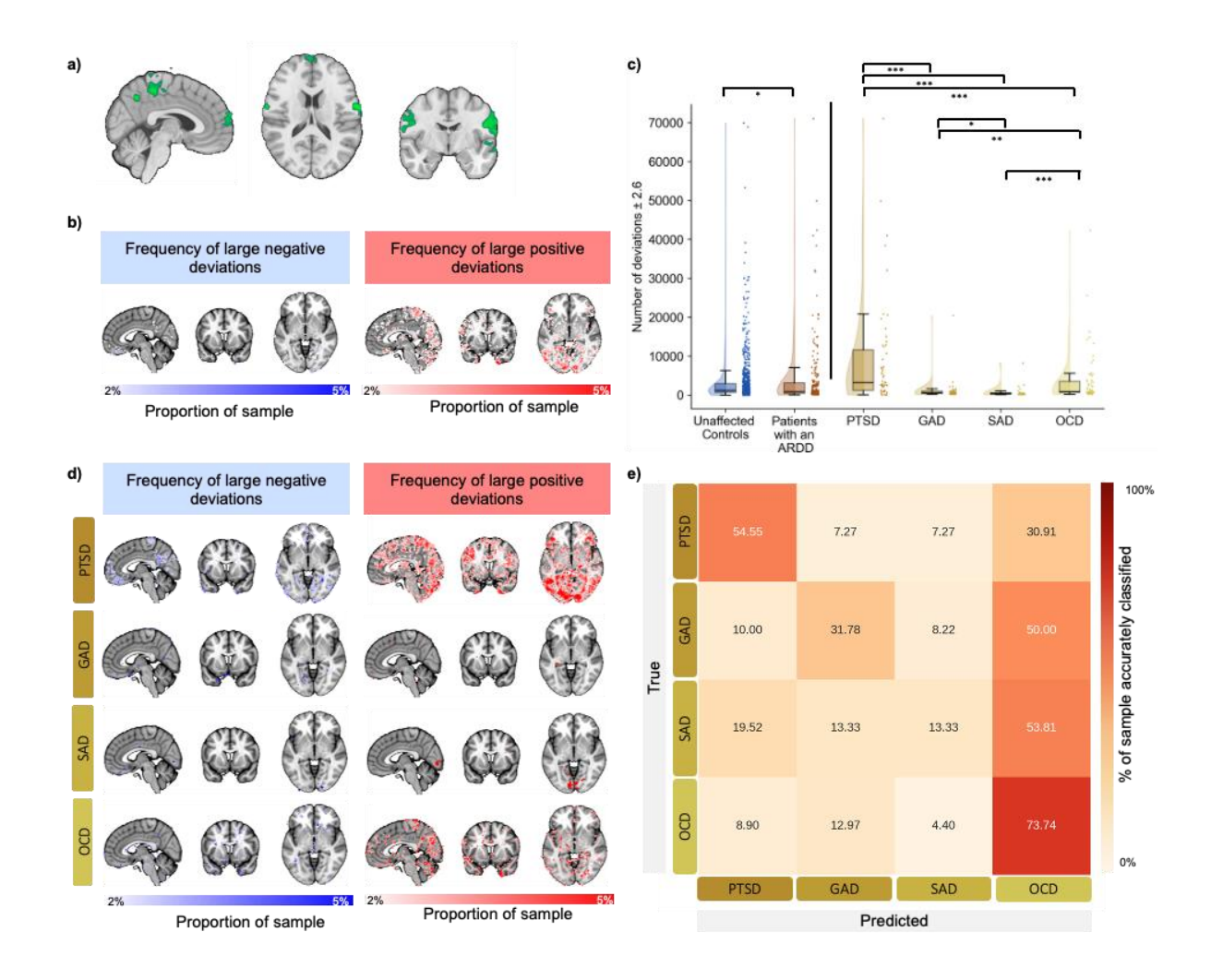


Figure 3. Differences between individuals with anxiety-related and depressive disorders and healthy controls in human fear conditioning. Regions wherein individuals with anxiety-related and depressive disorders (n=311) (a) showed significantly increased functional activation to the CS+ versus CS-, as compared to healthy controls. Normative probability maps illustrate the percentage of participants of the sample (test controls - top; individuals with anxiety-related and depressive disorders - bottom) who had positive (hot colours - right) or negative deviations (cool colours - left) >±2.6 within each voxel (b). Box plots show frequency (median line) of the total number of large deviations (>±2.6) per clinical group. Whiskers show ±1.5 times interquartile range (c). Normative probability maps illustrate the percentage of each clinical group who had positive (hot colours - right) or negative deviations (cool colours - left) >±2.6 within each voxel (d). Confusion matrix for multi-class support vector differentiating patterns of deviations among clinical groups (e).

Abbreviations: GAD, Generalised Anxiety Disorder; OCD, Obsessive Compulsive Disorder; PTSD, Post-traumatic Stress Disorder; SAD, Social Anxiety Disorder.

### References

- 1. Beckers, T. *et al.* Understanding clinical fear and anxiety through the lens of human fear conditioning. *Nature Reviews Psychology* **2**, 233–245 (2023).
- 2. Lonsdorf, T. B. *et al.* Don't fear 'fear conditioning': Methodological considerations for the design and analysis of studies on human fear acquisition, extinction, and return of fear. *Neurosci Biobehav Rev* 77, 247–285 (2017).
- 3. Fullana, M. A. et al. Neural signatures of human fear conditioning: an updated and extended meta-analysis of fMRI studies. Mol Psychiatry 21, 500–508 (2016).
- 4. Tovote, P., Fadok, J. P. & Lüthi, A. Neuronal circuits for fear and anxiety. Nat Rev Neurosci 16, 317–331 (2015).
- 5. LeDoux, J. The amygdala. Current Biology 17, R868–R874 (2007).
- 6. Johansen, J. P., Cain, C. K., Ostroff, L. E. & LeDoux, J. E. Molecular mechanisms of fear learning and memory. Cell 147, 509–524 (2011).
- 7. Bechara, A. et al. Double dissociation of conditioning and declarative knowledge relative to the amygdala and hippocampus in humans. Science 269, 1115–1118 (1995).
- 8. Wen, Z. et al. Temporally and anatomically specific contributions of the human amygdala to threat and safety learning. Proc Natl Acad Sci U S A 119, e2204066119 (2022).
- 9. Visser, R. M., Bathelt, J., Scholte, H. S. & Kindt, M. Robust BOLD responses to faces but not to conditioned threat: challenging the amygdala's reputation in human fear and extinction learning. J Neurosci 41, 10278–10292 (2021).
- 10. Bach, D. R., Weiskopf, N. & Dolan, R. J. A stable sparse fear memory trace in human amygdala. Journal of Neuroscience 31, 9383–9389 (2011).
- 11. Fullana, M. A. et al. Amygdala where art thou? Neurosci Biobehav Rev 102, 430–431 (2019).
- 12. Morriss, J., Hoare, S. & van Reekum, C. M. It's time: A commentary on fear extinction in the human brain using fMRI. Neurosci Biobehav Rev 94, 321–322 (2018).
- 13. Lonsdorf, T. B. & Merz, C. J. More than just noise: Inter-individual differences in fear acquisition, extinction and return of fear in humans Biological, experiential, temperamental factors, and methodological pitfalls. Neurosci Biobehav Rev 80, 703–728 (2017).
- 14. Radua, J. et al. Increased power by harmonizing structural MRI site differences with the ComBat batch adjustment method in ENIGMA. Neuroimage 218, 116956 (2020).
- 15. Müller, V. I. et al. Ten simple rules for neuroimaging meta-analysis. Neurosci Biobehav Rev 84, 151–161 (2018).
- 16. Thompson, P. M. et al. ENIGMA and the individual: Predicting factors that affect the brain in 35 countries worldwide. Neuroimage 145, 389–408 (2017).
- 17. Sjouwerman, R., Scharfenort, R. & Lonsdorf, T. B. Individual differences in fear acquisition: multivariate analyses of different emotional negativity scales, physiological responding, subjective measures, and neural activation. Sci Rep 10, 15283 (2020).
- 18. Smith, M. C. CS-US interval and US intensity in classical conditioning of the rabbit's nictitating membrane response. J Comp Physiol Psychol 66, 679–687 (1968).
- 19. Garcia, J. & Koelling, R. A. Relation of cue to consequence avoidance learning. Psychon Sci 4, 123–124 (1966).
- 20. Segal, A. et al. Embracing variability in the search for biological mechanisms of psychiatric illness. Trends Cogn Sci 85–99 (2025).
- 21. Marquand, A. F. et al. Conceptualizing mental disorders as deviations from normative functioning. Mol Psychiatry 24, 1415–1424 (2019).
- 22. Fraza, C. J., Dinga, R., Beckmann, C. F. & Marquand, A. F. Warped Bayesian linear regression for normative modelling of big data. Neuroimage 245, 118715 (2021).

- 23. Marquand, A. F., Rezek, I., Buitelaar, J. & Beckmann, C. F. Understanding heterogeneity in clinical cohorts using normative models: beyond case-control studies. Biol Psychiatry 80, 552–561 (2016).
- 24. Rutherford, S. et al. Evidence for embracing normative modeling. Elife 12, e85082 (2023).
- 25. Savage, H. S. et al. Dissecting task-based fMRI activity using normative modelling: an application to the Emotional Face Matching Task. Commun Biol 7, 814–888 (2024).
- Wolfers, T. et al. Individual differences v. the average patient: mapping the heterogeneity in ADHD using normative models. Psychol Med 50, 314–323 (2020).
- 27. Zabihi, M. et al. Fractionating autism based on neuroanatomical normative modeling. Transl Psychiatry 10, 384 (2020).
- 28. Tian, Y. E., Cole, J. H., Bullmore, E. T. & Zalesky, A. Brain, lifestyle and environmental pathways linking physical and mental health. Nature Mental Health 2, 1250–1261 (2024).
- 29. Kjelkenes, R. et al. Deviations from normative brain white and gray matter structure are associated with psychopathology in youth. Dev Cogn Neurosci 58, 101173 (2022).
- 30. Pittig, A., Treanor, M., LeBeau, R. T. & Craske, M. G. The role of associative fear and avoidance learning in anxiety disorders: Gaps and directions for future research. Neurosci Biobehav Rev 88, 117–140 (2018).
- 31. Fullana, M. A. et al. Human fear conditioning: From neuroscience to the clinic. Behav Res Ther 124, 103528 (2020).
- 32. Greco, J. A. & Liberzon, I. Neuroimaging of Fear-Associated Learning. Neuropsychopharmacology 41, 320–334 (2016).
- 33. Craske, M. G. et al. Anxiety disorders. Nat Rev Dis Primers 3, 17024 (2017).
- 34. Marin, M.-F., Hammoud, M. Z., Klumpp, H., Simon, N. M. & Milad, M. R. Multimodal categorical and dimensional approaches to understanding threat conditioning and its extinction in individuals with anxiety disorders. JAMA Psychiatry 77, 618–627 (2020).
- 35. Kausche, F. M., Carsten, H. P., Sobania, K. M. & Riesel, A. Fear and safety learning in anxiety- and stress-related disorders: An updated meta-analysis. Neurosci Biobehav Rev 105983 (2024).
- 36. Suarez-Jimenez, B. et al. Neural signatures of conditioning, extinction learning, and extinction recall in posttraumatic stress disorder: a meta-analysis of functional magnetic resonance imaging studies. Psychol Med 50, 1442–1451 (2020).
- 37. Savage, H. S., Davey, C. G., Fullana, M. A. & Harrison, B. J. Threat and safety reversal learning in social anxiety disorder an fMRI study. J Anxiety Disord 76, 102321 (2020).
- 38. Savage, H. S. et al. Neural mediators of subjective and autonomic responding during threat learning and regulation. Neuroimage 245, 118643 (2021).
- 39. Tzourio-Mazoyer, N. et al. Automated Anatomical Labeling of Activations in SPM Using a Macroscopic Anatomical Parcellation of the MNI MRI Single-Subject Brain. NeuroImage 15, 273–289 (2002).
- 40. Marek, S. et al. Reproducible brain-wide association studies require thousands of individuals. Nature 603, 654–660 (2022).
- 41. Likhtik, E. & Johansen, J. P. Neuromodulation in circuits of aversive emotional learning. Nat Neurosci 22, 1586–1597 (2019).
- 42. Blackford, J. U., Allen, A. H., Cowan, R. L. & Avery, S. N. Amygdala and hippocampus fail to habituate to faces in individuals with an inhibited temperament. Soc Cogn Affect Neurosci 8, 143–150 (2013).
- 43. Bas-Hoogendam, J. M. et al. Impaired neural habituation to neutral faces in families genetically enriched for social anxiety disorder. Depress Anxiety 36, 1143–1153 (2019).

- 44. Boubela, R. N. et al. fMRI measurements of amygdala activation are confounded by stimulus correlated signal fluctuation in nearby veins draining distant brain regions. Sci Rep 5, 10499 (2015).
- 45. Sladky, R. et al. High-resolution functional MRI of the human amygdala at 7 T. Eur J Radiol 82, 728–733 (2013).
- 46. Kirstein, C. F., Güntürkün, O. & Ocklenburg, S. Ultra-high field imaging of the amygdala A narrative review. Neurosci Biobehav Rev 152, 105245 (2023).
- 47. Morris, S. E. et al. Revisiting the seven pillars of RDoC. BMC Med 20, 220 (2022).
- 48. Pessoa, L. How many brain regions are needed to elucidate the neural bases of fear and anxiety? Neurosci Biobehav Rev 146, 105039 (2023).
- 49. Poldrack, R. A. Inferring mental states from neuroimaging data: from reverse inference to large-scale decoding. Neuron 72, 692–697 (2011).
- 50. Armand, S. et al. Functional brain responses to emotional faces after three to five weeks of intake of escitalopram in healthy individuals: a double-blind, placebo-controlled randomised study. Sci Rep 14, 3149 (2024).
- 51. Shackman, A. J. & Fox, A. S. Two decades of anxiety neuroimaging research: New insights and a look to the future. Am J Psychiatry 178, 106–109 (2021).
- 52. Wen, Z., Marin, M.-F., Blackford, J. U., Chen, Z. S. & Milad, M. R. Fear-induced brain activations distinguish anxious and trauma-exposed brains. Transl Psychiatry 11, 46 (2021).
- 53. American Psychiatric Association. Diagnostic and Statistical Manual of Mental Disorders. American Psychiatric Association, 2013.
- 54. Kaczkurkin, A. N. et al. Neural substrates of overgeneralized conditioned fear in PTSD. American Journal of Psychiatry 174, 125–134 (2017).
- 55. Cooper, S. E. & Dunsmoor, J. E. Fear conditioning and extinction in obsessive-compulsive disorder: A systematic review. Neurosci Biobehav Rev 129, 75–94 (2021).
- 56. Milad, M. R. et al. Deficits in conditioned fear extinction in obsessive-compulsive disorder and neurobiological changes in the fear circuit. JAMA Psychiatry 70, 608–554 (2013).
- 57. Apergis-Schoute, A. M. et al. Neural basis of impaired safety signaling in Obsessive Compulsive Disorder. Proc Natl Acad Sci U S A 114, 3216–3221 (2017).
- 58. Cano, M. et al. Neural correlates of fear conditioning and fear extinction and its association with cognitive-behavioral therapy outcome in adults with obsessive-compulsive disorder. Behav Res Ther 144, 103927 (2021).
- 59. Hearne, L. J. et al. Revisiting deficits in threat and safety appraisal in obsessive-compulsive disorder. Hum Brain Mapp 44, 6418–6428 (2023).
- 60. Fan, J. et al. Spontaneous neural activity in the right superior temporal gyrus and left middle temporal gyrus is associated with insight level in obsessive-compulsive disorder. J Affect Disord 207, 203–211 (2017).
- 61. Westlin, C. et al. Improving the study of brain-behavior relationships by revisiting basic assumptions. Trends Cogn Sci 27, 246–257 (2023).
- 62. Klingelhöfer-Jens, M., Ehlers, M. R., Kuhn, M., Keyaniyan, V. & Lonsdorf, T. B. Robust group- but limited individual-level (longitudinal) reliability and insights into cross-phases response prediction of conditioned fear. Elife 11, e78717 (2022).
- 63. Bas-Hoogendam, J. M. et al. ENIGMA-anxiety working group: Rationale for and organization of large-scale neuroimaging studies of anxiety disorders. Hum Brain Mapp 43, 83–112 (2022).
- 64. Spielberger, C. D., Gorsuch, R. L., Lushene, R., Vagg, P. R. & Jacobs, G. A. Manual for the State-Trait Anxiety Inventory. (Consulting Psychologists Press, Palo Alto, CA, 1983).
- 65. Beck, A. T., Ward, C. H., Mendelson, M., Mock, J. & Erbaugh, J. An inventory for measuring depression. Arch Gen Psychiatry 4, 561–571 (1961).

- 66. Waller, L. et al. ENIGMA HALFpipe: Interactive, reproducible, and efficient analysis for resting-state and task-based fMRI data. Hum Brain Mapp 43, 2727–2742 (2022).
- 67. Gorgolewski, K. et al. Nipype: A flexible, lightweight and extensible neuroimaging data processing framework in python. Front Neuroinform 5, (2011).
- 68. Shinohara, R. T. et al. Statistical normalization techniques for magnetic resonance imaging. Neuroimage Clin 6, 9–19 (2014).
- 69. Wolfers, T. et al. Mapping the heterogeneous phenotype of schizophrenia and bipolar disorder using normative models. JAMA Psychiatry 75, 1146–1155 (2018).
- 70. Holz, N. E. et al. A stable and replicable neural signature of lifespan adversity in the adult brain. Nat Neurosci 26, 1603–1612 (2023).
- 71. Floris, D. L. et al. Atypical brain asymmetry in autism—a candidate for clinically meaningful stratification. Biol Psychiatry Cogn Neurosci Neuroimaging 6, 802–812 (2021).
- 72. Benjamini, Y. & Hochberg, Y. Controlling the false discovery rate: A practical and powerful approach to multiple testing. J R Stat Soc Series B Stat Methodol 57, 289–300 (1995).
- 73. Kraha, A., Turner, H., Nimon, K., Zientek, L. R. & Henson, R. K. Tools to support interpreting multiple regression in the face of multicollinearity. Front Psychol 3, 44 (2012).
- 74. Pedregosa, F. et al. Scikit-learn: Machine Learning in Python. (2012).

### **ACKNOWLEDGEMENTS**

The research was supported by Secretaria d'Universitats i Recerca del Departament d'Economia i Coneixement de la Generalitat de Catalunya (No. 2021 SGR 1128, J.R.: M.A.F.), the Swedish Research Council (No. 2014-01160, F.Å.), the European Research Council (No. 648176, T.B.; ERC-2018 CoG-816564, D.B.; 101001118, A.F.M.), the National Institute of Mental Health (No. R01MH119132 and MH108753, J.C.; R01MH095904 and K23MH076054, D.J.H.; R01MH125615, A.K.; R01-MH103291, K.A.M.; 1R61MH129559-02, Y.N.; R01-AA031261, A.S.; K01MH122774, X.Z.; R01MH131532, B.S.J; R01MH125615, L.A.), the German Research Foundation (No. 316803389 - SFB 1280, S.E., C.J.M. and A.I.; LO 1980/1-1 and SFB TRR 58 subproject B07, T.B.L.; LO 1980/4-1, T.B.L. and M.R.E.; 521379614 – TRR393, B.S., U.D. and T.K.; 44541416 CRC-TRR58 T.S., K.R., K.D. and M.J.; 442075332 (RU 5187) and 461947532 (RU 5389), U.L.; WA 1539/11-1, H.W.;), the Economic and Social Research Council UK (No. ES/W000776/1, D.B.), the NSERC Discovery (No. RGPIN-2021-02906, S.G.), the National Institute of Health (No. R01 MH106574, C.L.; R01 MH122387, J.D.), the United states-israel binational science foundation and NIA (No. 2P30AG064198, Y.N.), the National Institute of Mental Health Intramural Research (No. ZIA-MH-002781, D.P.), the Biotechnology and Biological Sciences Research Council (No. BB/L02697X/1, C.vR.), NIAAA (No. R01-AA030042, A.S.), the Instituto de Salud Carlos III (ISCIII) (No. PI16/00889 and PI19/01171, C.S.M.; FI22/00219, M.O.), Fundació Marató de TV3 (No. 202201-31, C.S.M.), Agència de Gestió d'Ajuts Universitaris i de Recerca (No. 2021SGR01017, C.S.M.), the Ministerio de Ciencia, Innovación y Universidades, Spain (No. PID2022-139081OB-C22, C.S.M.), the Department of Veteran Affairs (No. I01-CX002760, D.M.S.), the German Federal Ministry of Education and Research (No. 01EE1402E, B.S., T.K., A.P., U.D., K.D. and H-U.W.; 01EE2101, U.L.), Brain and Behavior Research Foundation NARSAD Young Investigator Award (X.Z.), "la Caixa" Foundation (No. LCF/BO/IN17/11620071, V.P.A.), Spanish Ministry of Science, Innovation and Universities (No. JDC2022-048445-I, V.P.A), the National Eye Institute Core Grant (No. P30 EY001319, B.S.J.), the Medical Research Council (No. MR/J003980/1, J.M.), National Science Foundation Graduate Research Fellowship (No. DGE1745303, S.N.D.), the South African Medical Research Council (D.J.S.), the EU Innovative Medicines Initiative (IMI) 2 Joint Undertaking (IMI2 JU) (No. 101034377, N.JA.VdW), the Dutch Research Agenda (NeuroLabNL-Small Projects for NWA routes 21/22) (No. NWA.1418.22.025, JM.B-H.), the Talent Acceleration grant (Medical Delta) (JM.B-H.), the NIH Big Data to Knowledge (BD2K) award (No. U54 EB020403 and R01MH131806, P.M.T.), the National Health and Medical Research Council of Australia (NHMRC) Project Grants (No. 1161897 and 1145010, B.J.H.).

### **AUTHOR CONTRIBUTIONS**

J.R., H.S., E.V., and M.A.F. designed and performed analyses. J.R., H.S., A.J., and M.A.F. wrote the manuscript. J.M.B-H., N.A.G., D.J.S., N.J.W., J.D., A.F.M., and B.J.H. discussed the results. M.A.F. supervised research. All authors commented on the manuscript.

### **COMPETING INTERESTS**

Dr Stein has received consultancy honoraria from Discovery Vitality, Johnson & Johnson, Kanna, L'Oreal, Lundbeck, Orion, Sanofi, Servier, Takeda and Vistagen. The other authors declare no competing interests.

### INCLUSION AND ETHICS STATEMENT

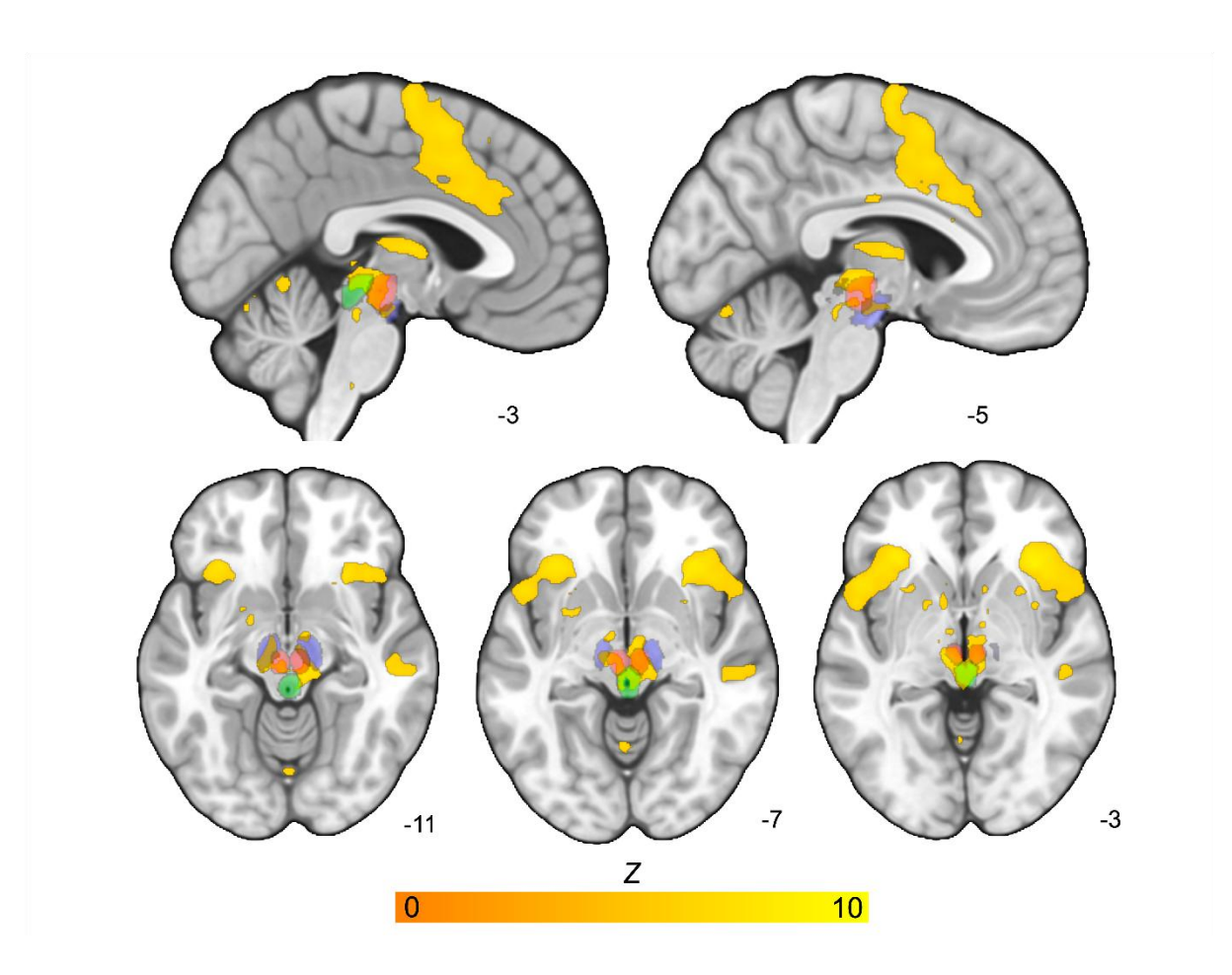
This study involved a mega-analysis of previously collected human neuroimaging datasets. All original studies received approval from their respective institutional ethics committees and were conducted in accordance with the Declaration of Helsinki. Informed consent was obtained from all participants in the original studies. Inclusion and exclusion criteria were prespecified in each dataset and applied consistently during data aggregation. Both male and female participants were included across datasets, and efforts were made to account for demographic diversity (e.g., age, sex) in the analysis. No new data were collected specifically for this study.

# Neural correlates of human fear conditioning and sources of variability in 2199 individuals

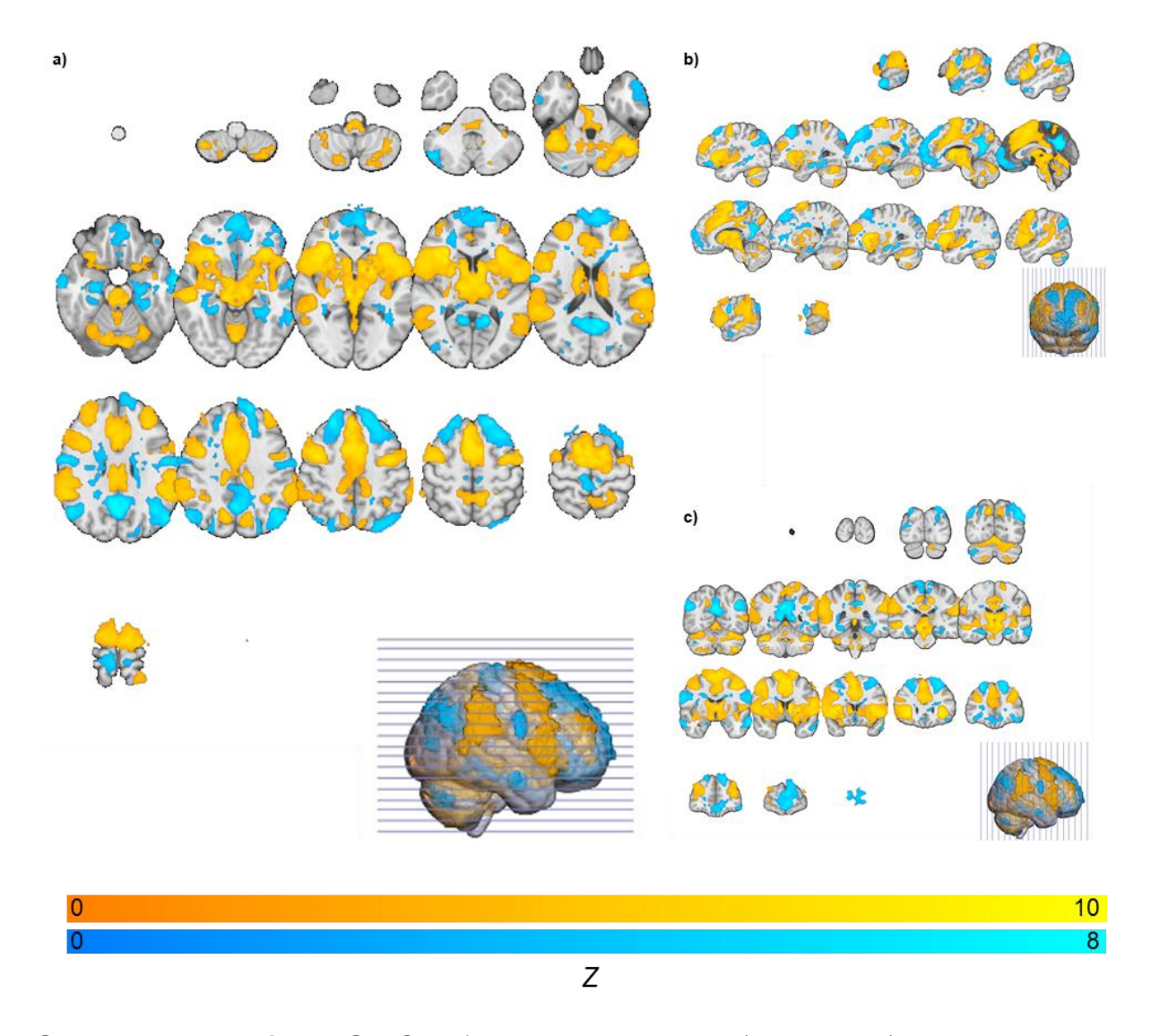
# SUPPLEMENTARY INFORMATION

	Page
Supplementary Figures	1
Supplementary Tables	21
Supplementary Methods	32
Changes with respect to pre-registration	
Variables collected and not included in analyses	
Non-imaging data	
Neuroimaging data	
Statistical analyses	
Supplementary Discussion	40
Supplementary References	43

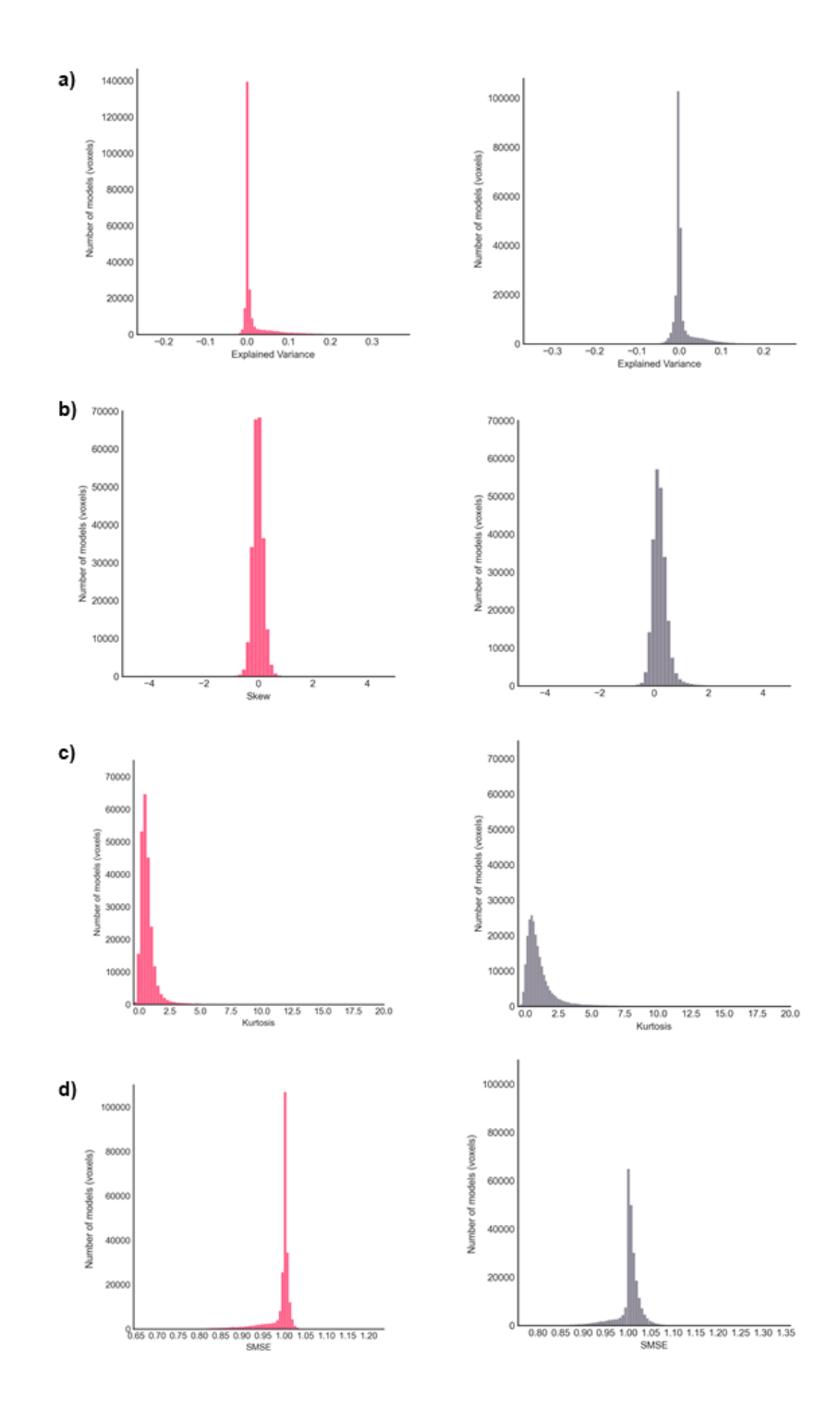
## **Supplementary Figures**



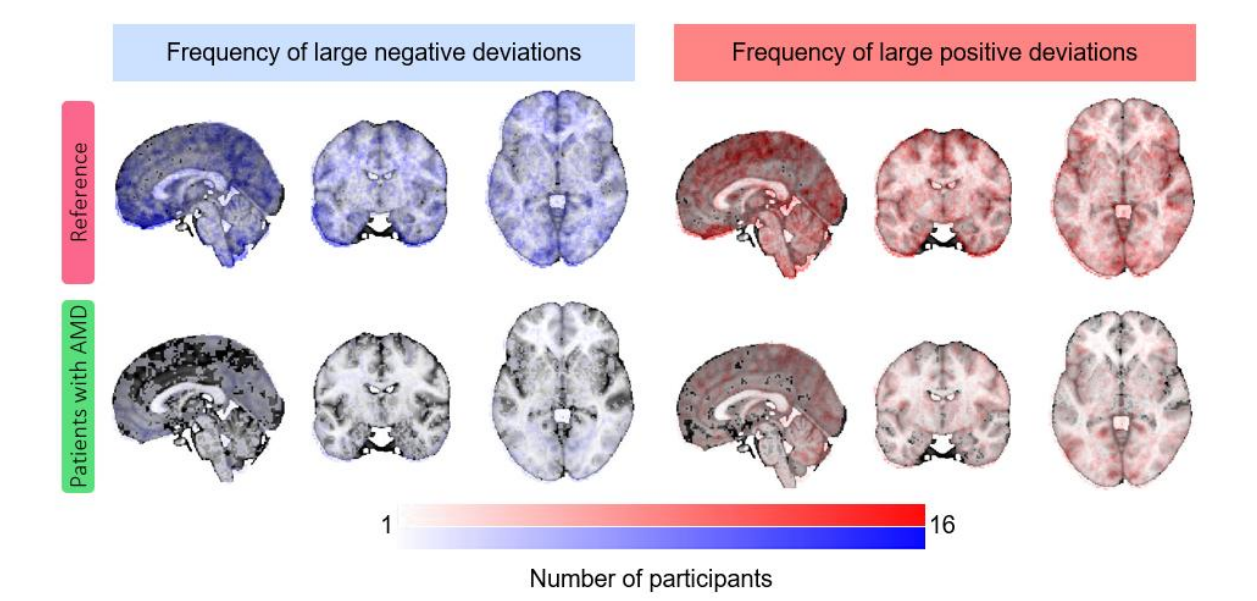
**Supplementary Figure S1**. CS+ versus CS- contrast thresholded to the top 1% of activated voxels (Z > 6.06) to highlight specific subcortical regions. Masks for the substantia nigra (blue), red nucleus (red), and periaqueductal grey area (green) are shown to aid in the localization of effects.



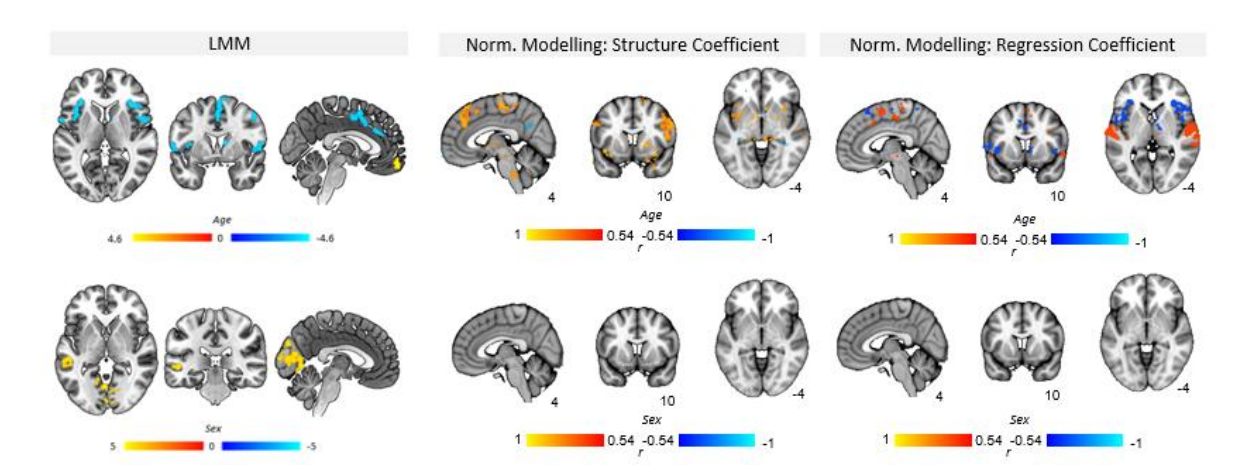
**Supplementary Figure S2**. Significant brain activation (hot colours) and deactivation (cool colours) to the CS+ versus CS- across axial ( $\mathbf{a}$ ; Z = -68 to 106), sagittal ( $\mathbf{b}$ ; X = -86 to 88) and coronal ( $\mathbf{c}$ ; Y = -120 to 86) slices (n=1888 controls).



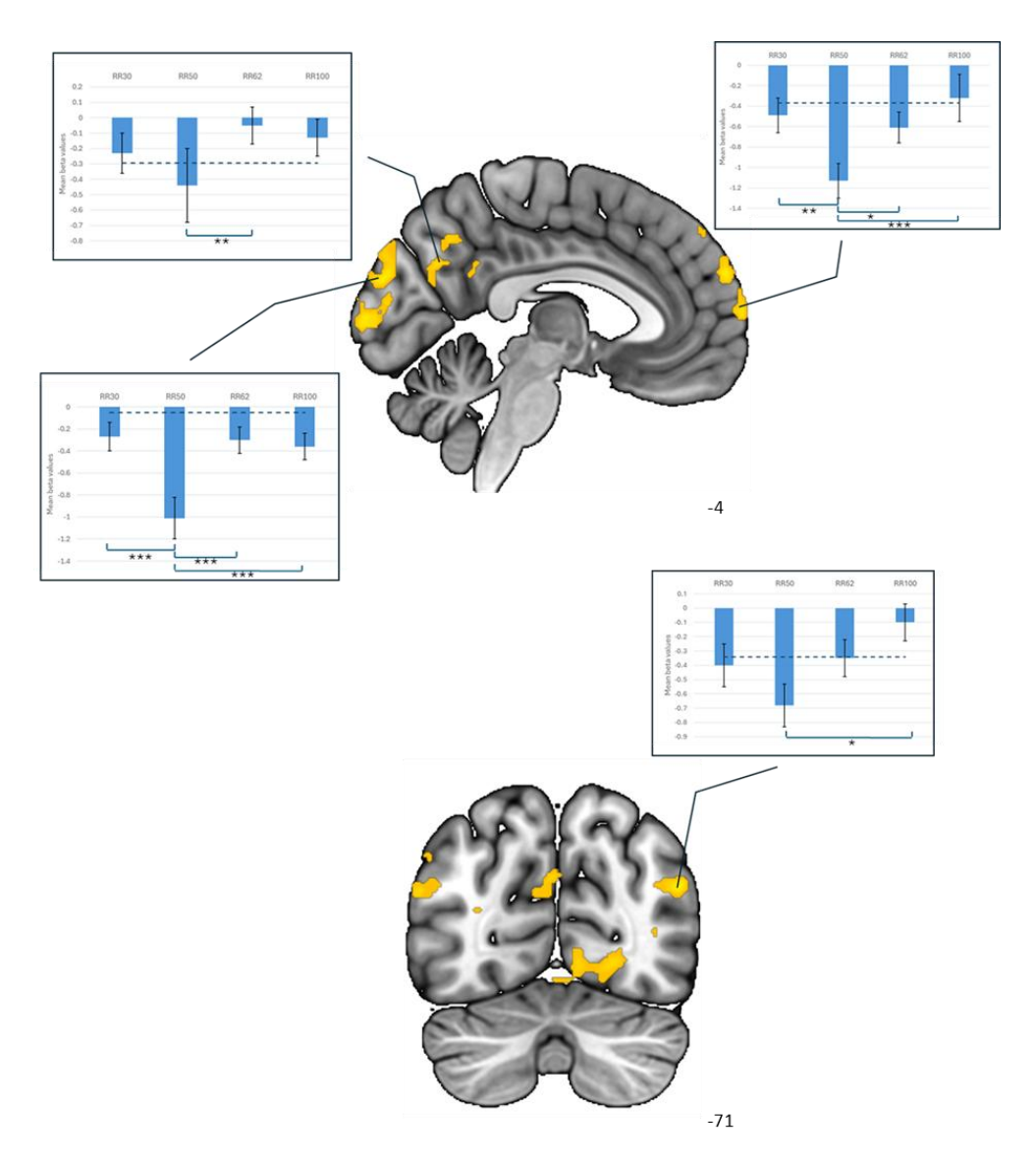
**Supplementary Figure S3.** Evaluation metrics of normative models. Explained variance (a), skew (b), kurtosis (c), and Standardized Mean Squared Error (SMSE) (d) for control test (n = 646 controls - left, pink) and clinical test (n = 260 controls + 222 individuals with anxiety-related or depressive disorders).



**Supplementary Figure S4.** Normative probability maps illustrate the number of participants in the sample (test controls - top; individuals with anxiety-related or depressive disorders (AMD) - bottom) who had positive (hot colours - right) or negative deviations (cool colours - left) >±2.6 within each voxel.

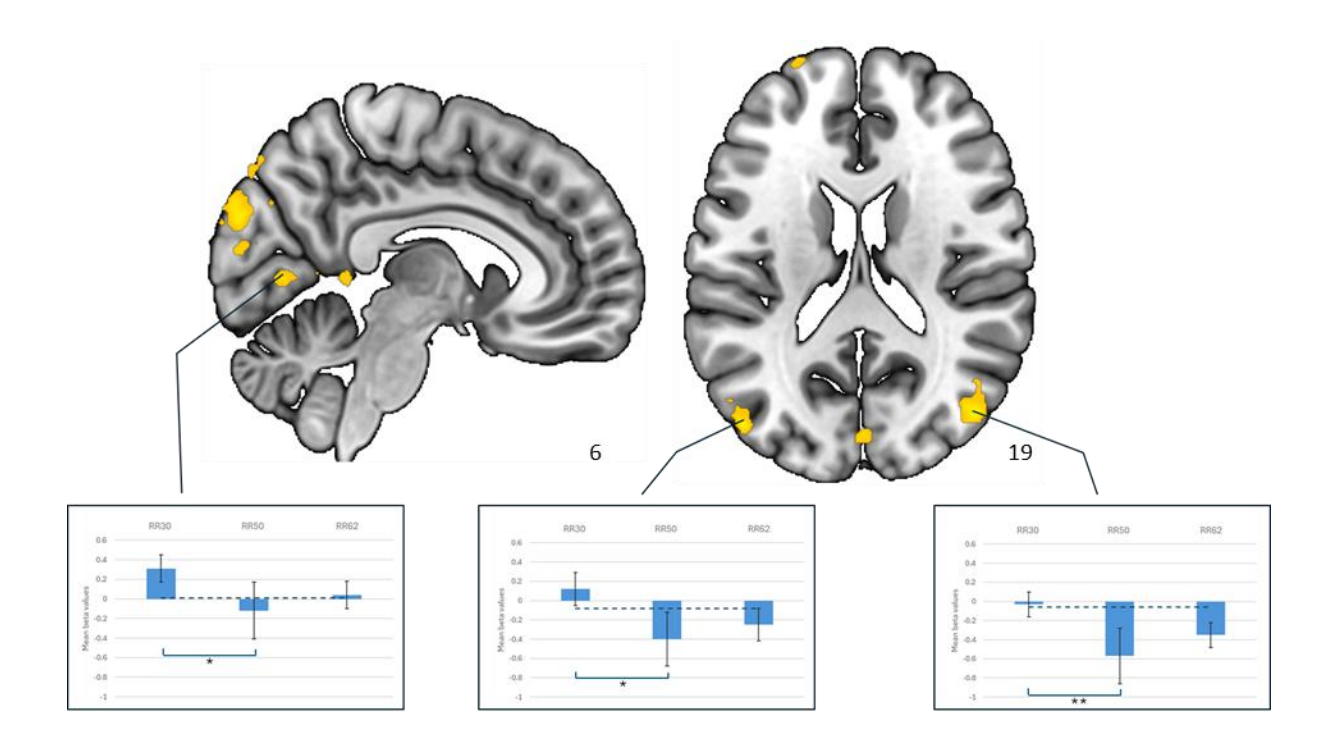


**Supplementary Figure S5.** Association of age and sex with brain (de)activation during fear conditioning. Results from linear mixed-effect models and normative modeling. For normative modeling, maps show the regression coefficient or structure coefficients (rho) from normative models for each task variable, thresholded by their respective coefficients of determination (rho^2 > 0.3). Positive correlations (warm colours) indicate greater activation for higher values of the input variable and negative correlations (cool colours) greater activation for lower values of the input variable.

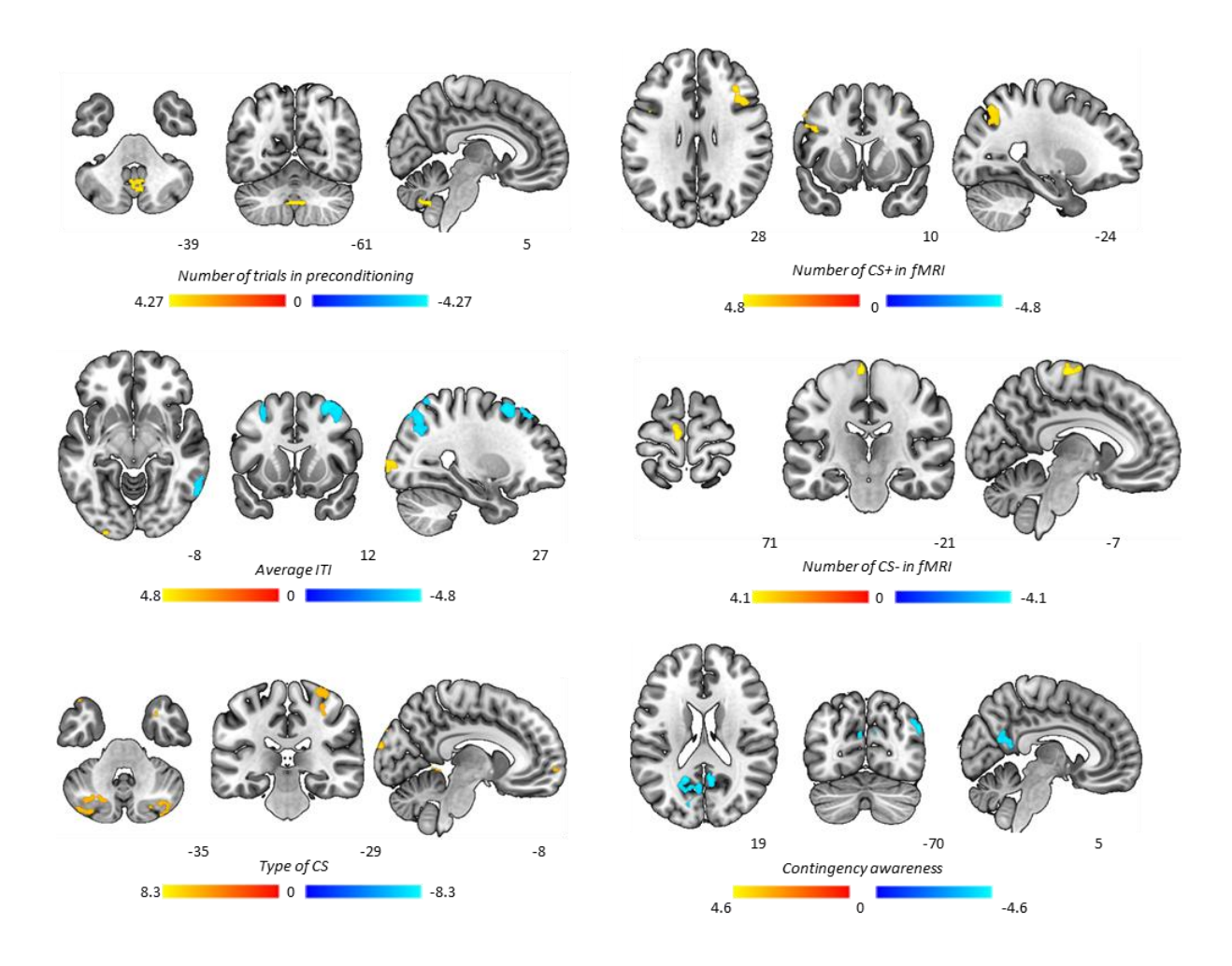


Supplementary Figure S6. Differences in brain activation between different reinforcement rates (including participants with potential US confounding effect). RR30 (n=268); RR50 (n=501); RR62 (n=333); RR100 (n=371).

RR=reinforcement rate. Results of pairwise comparisons after significant ANOVAs. Asterisks indicate significant differences between groups with Bonferroni correction (\*p<.05, \*\*p<.01; \*\*\*p<.001). Dashed blue lines indicate mean brain activation for healthy controls. Error bars represent standard errors



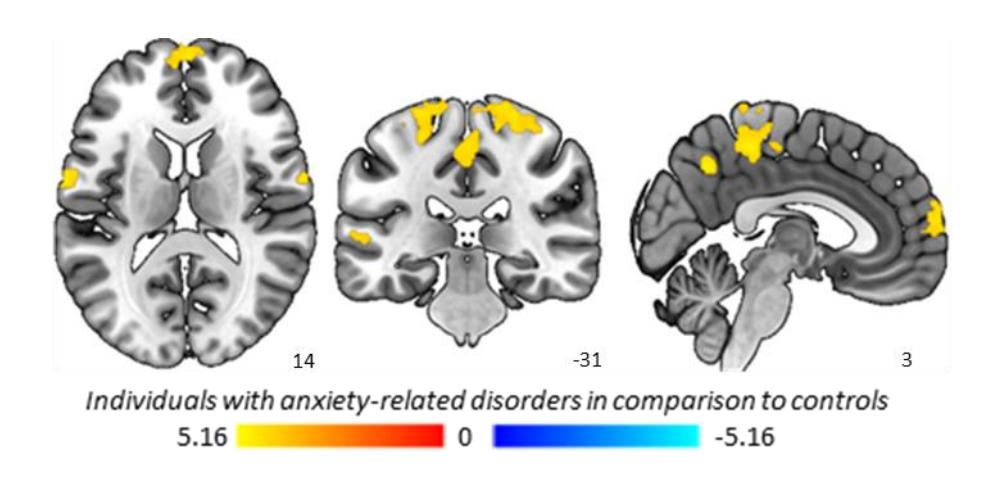
Supplementary Figure S7. Differences in brain activation between different reinforcement rates (excluding participants with potential US confounding effect). RR30 (n=268); RR50 (n=139); RR62 (n=238). RR=reinforcement rate. Results of pairwise comparisons after significant ANOVAs. Asterisks indicate significant differences between groups with Bonferroni correction (\*p<.05, \*\*p<.01; \*\*\*p<.001). Dashed blue lines indicate mean brain activation for healthy controls. Error bars represent standard errors.



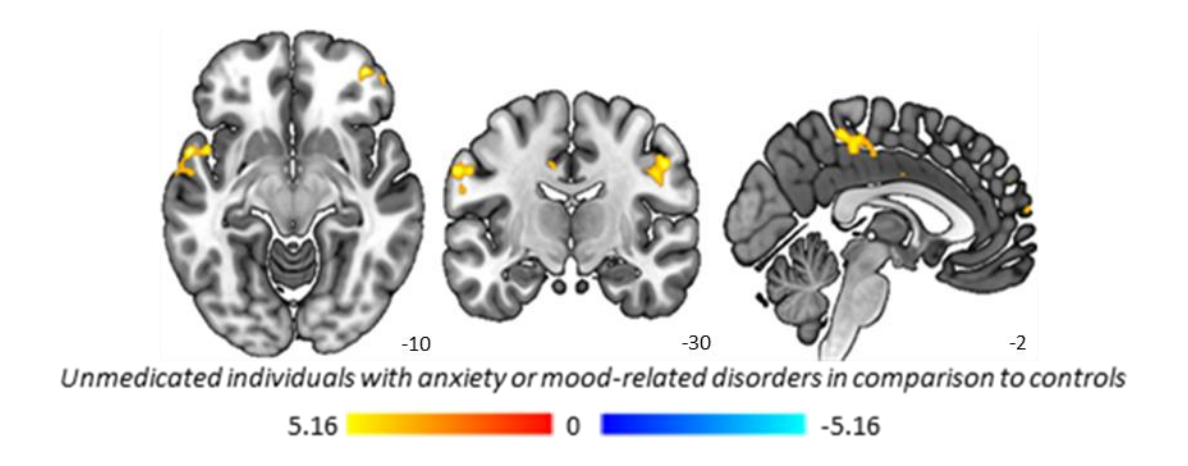
Supplementary Figure S8. Influence of task variables on brain activation during fear conditioning. Results from linear mixed-effect models for task variables not presented in the main text. CS+=Conditioned Stimulus followed by the Unconditioned Stimulus. ITI= Intertrial Interval. Number of CS+ in fMRI=Number of CS+ included in fMRI contrast. For type of CS, the figure shows significant results in the ANOVA comparing three categories (humanoid, affective pictures, and neutral faces).



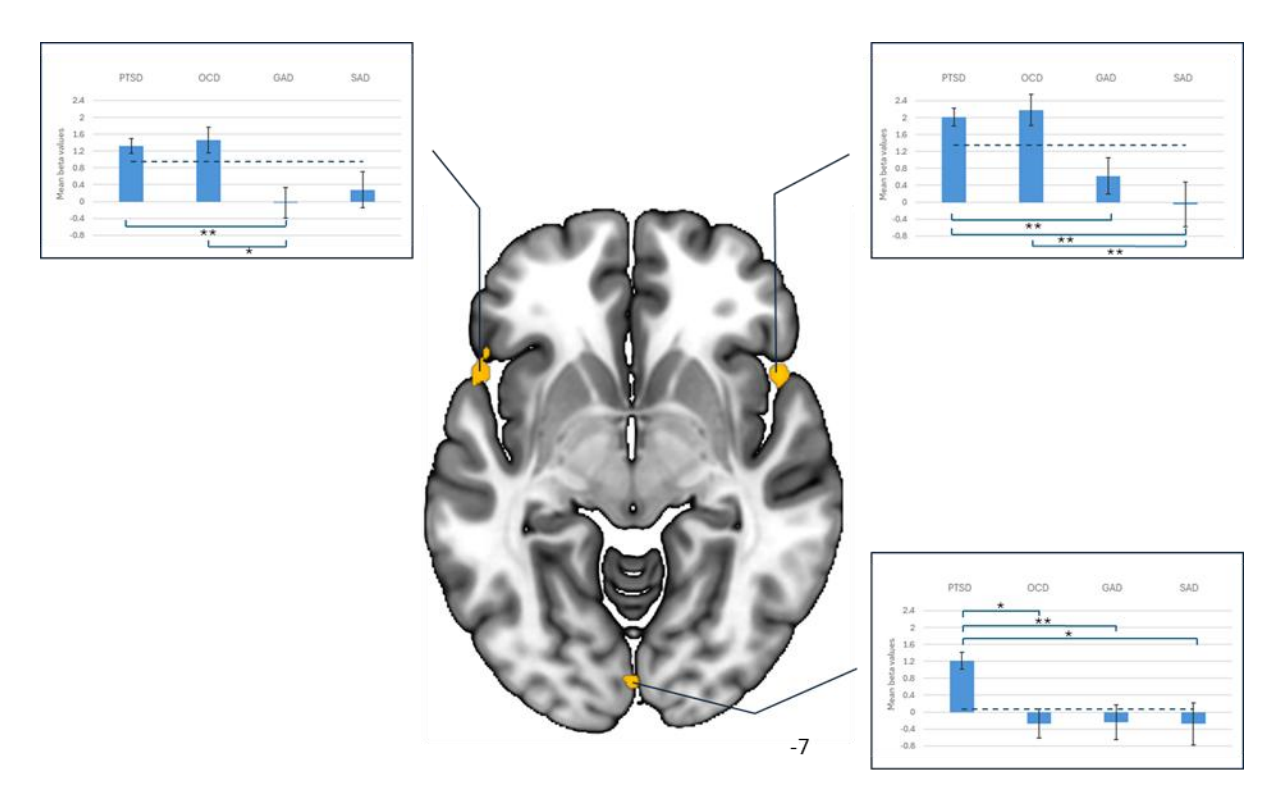
**Supplementary Figure S9.** Influence of task variables on brain activation during fear conditioning. Results from normative models. Maps show the regression coefficient or structure coefficients (rho) from normative models for each task variable, thresholded by their respective coefficients of determination (rho^2 > 0.3). Positive correlations (warm colours) indicate greater activation for higher values of the input variable and negative correlations (cool colours) greater activation for lower values of the input variable (note that some variables are dummy coded, e.g., instructions, type of US stimuli). CS=Conditioned Stimulus; US=Unconditioned Stimulus. Any task-related variable maps not shown in the main text or in this table did not contain any voxels exceeding the threshold (i.e., they were empty maps).



**Supplementary Figure S10.** Differences in brain activation between individuals with anxiety-related disorders (n=297) and healthy controls (n=1888).

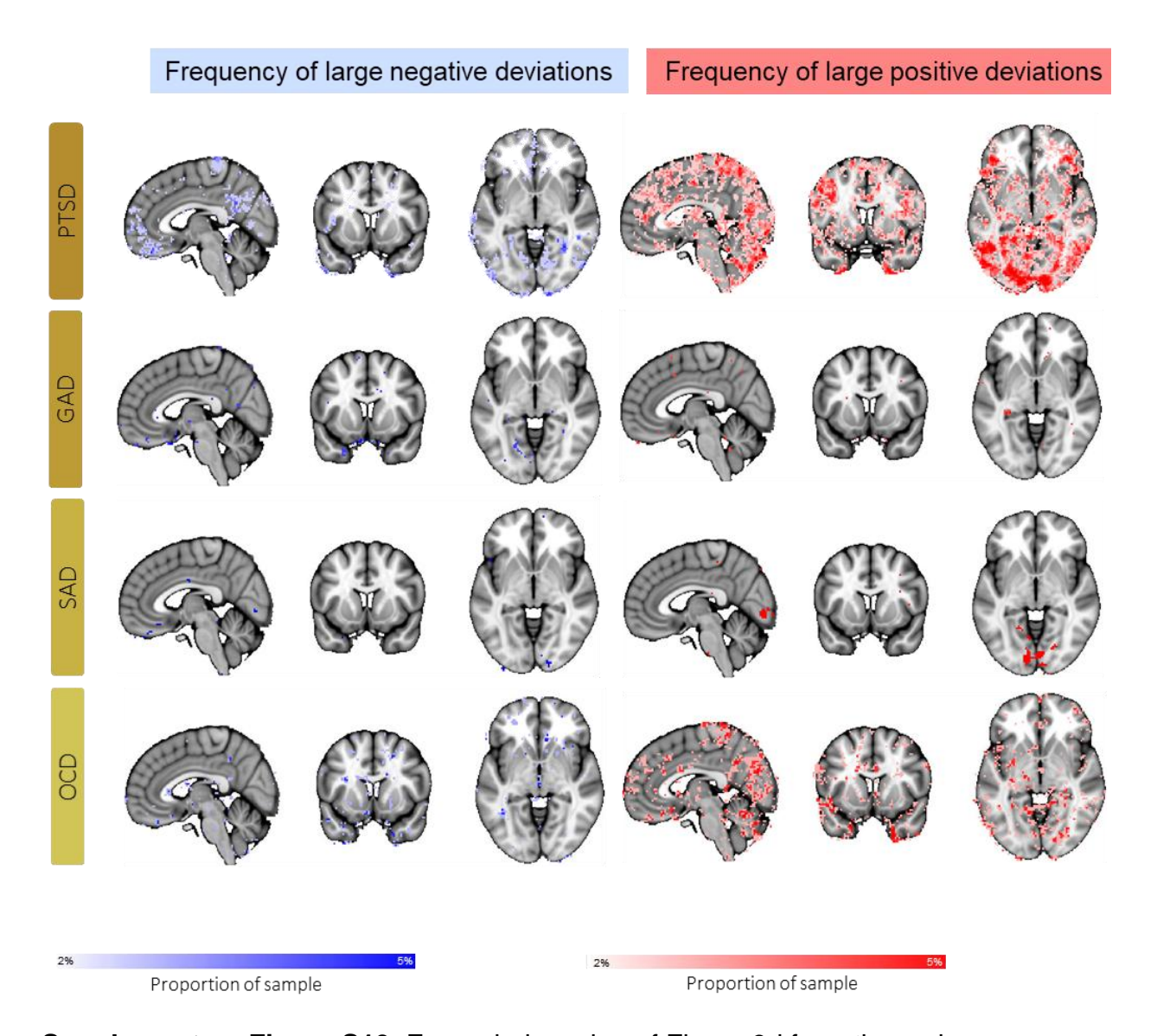


**Supplementary Figure S11.** Differences in brain activation between unmedicated individuals with anxiety or mood-related disorders (n=221) and healthy controls (n=1859).

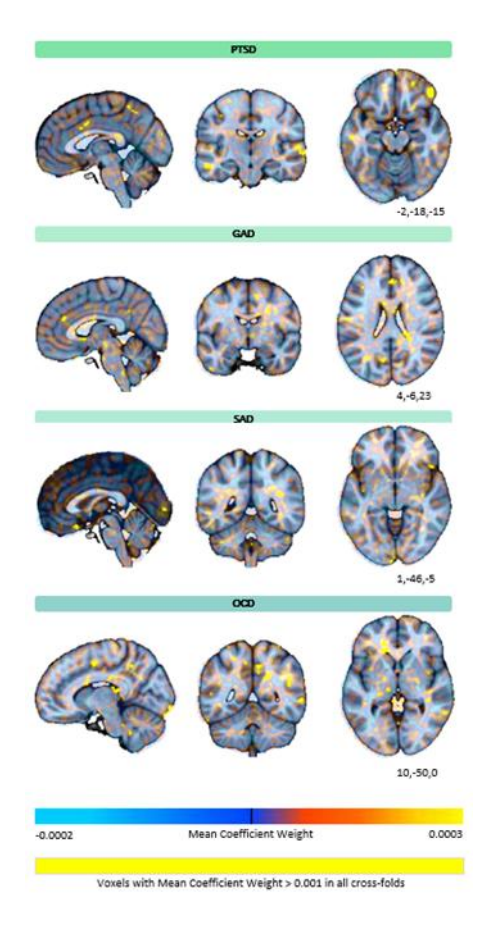


### Supplementary Figure S12 Differences in brain activation between patient

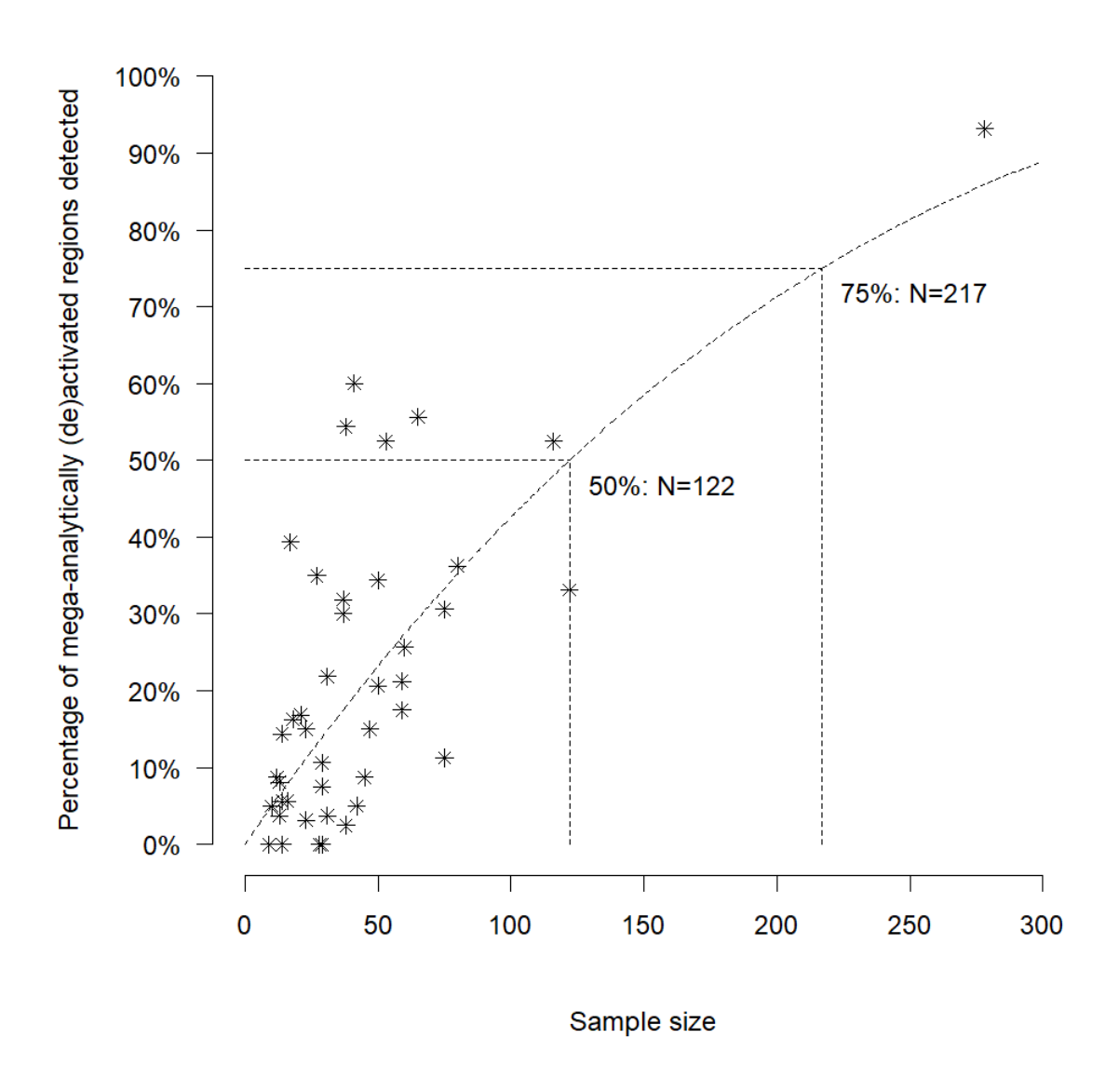
**groups.** PTSD=post-traumatic stress disorder; OCD=obsessive-compulsive disorder; GAD=generalized anxiety disorder; SAD=social anxiety disorder. Results of pairwise comparisons after significant ANOVAs. Asterisks indicate significant differences between groups with Bonferroni correction (\*p<.05, \*\*p<.01; \*\*\*p<.001). Dashed blue lines indicate mean brain activation for healthy controls. Dashed blue lines indicate mean brain activation for healthy controls. Error bars represent standard errors.



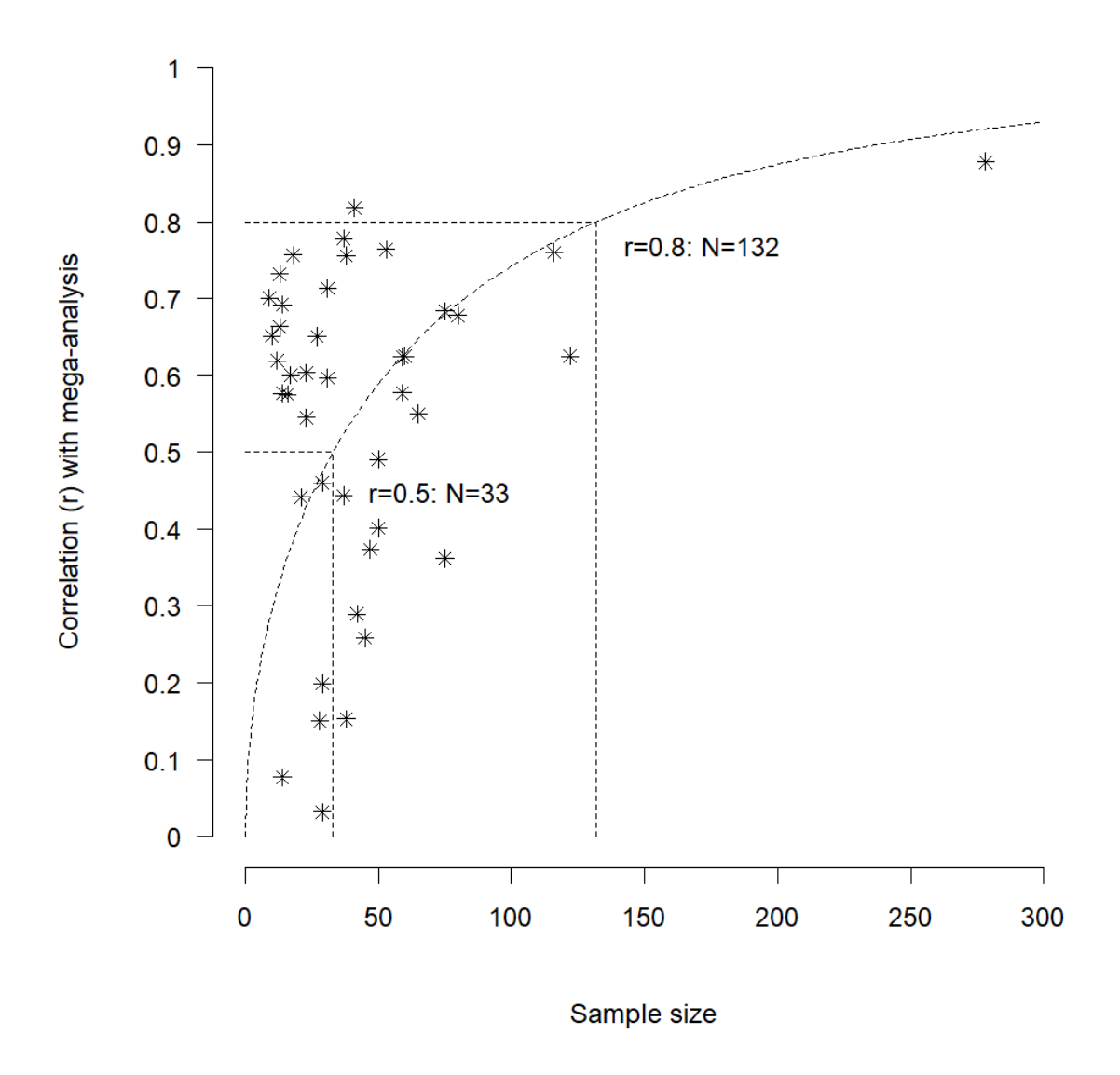
**Supplementary Figure S13**. Expanded version of Figure 3d from the main manuscript with enhanced visualization for improved clarity and detail.



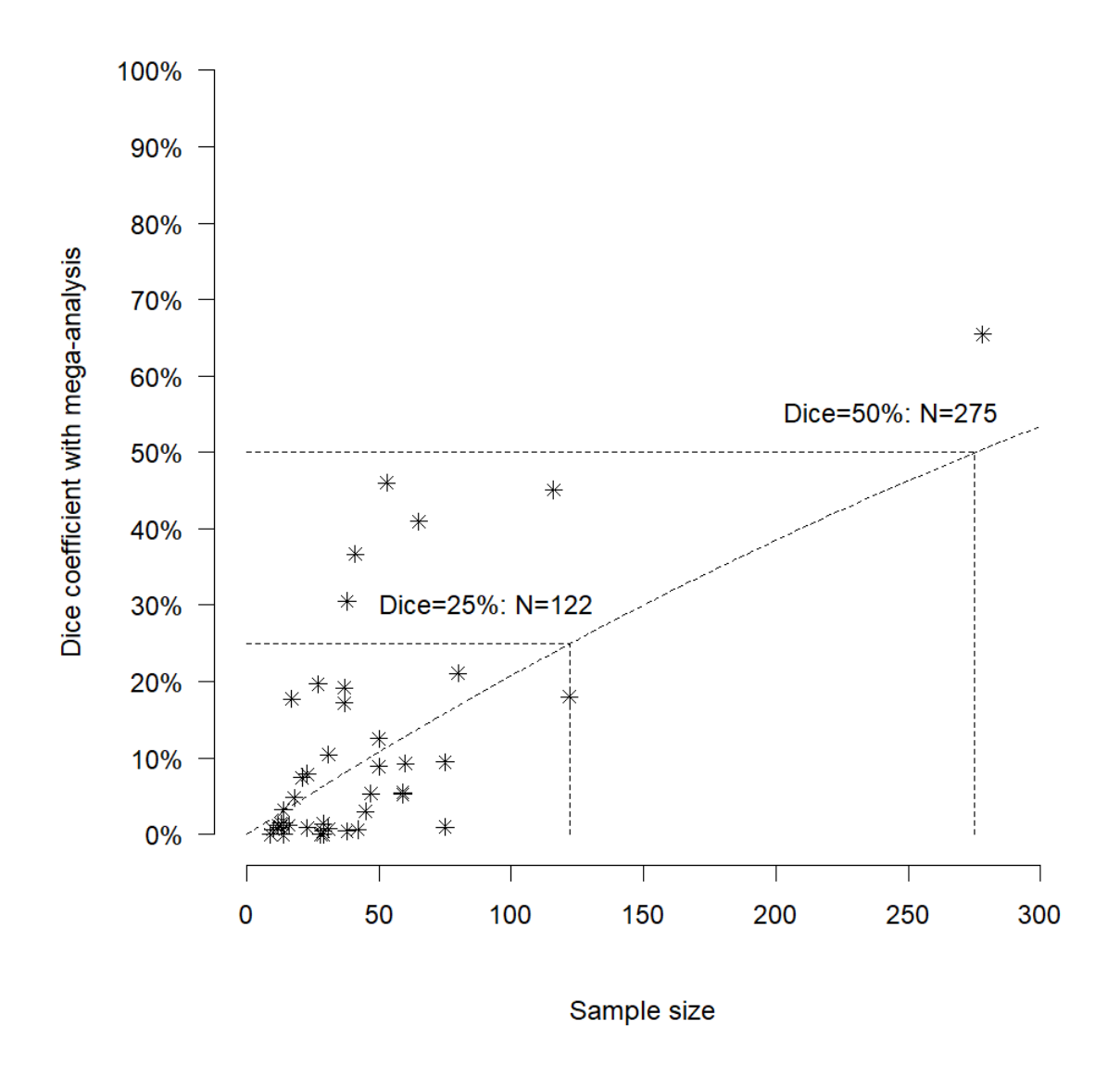
**Supplementary Figure S14.** Mean coefficient weights from multi-class support vector classifier, used to differentiate whole-brain unthresholded deviation maps between patient groups. Yellow indicates voxels that had a mean coefficient weight > 0.001 in all cross-folds (i.e. were frequently used to inform classification).



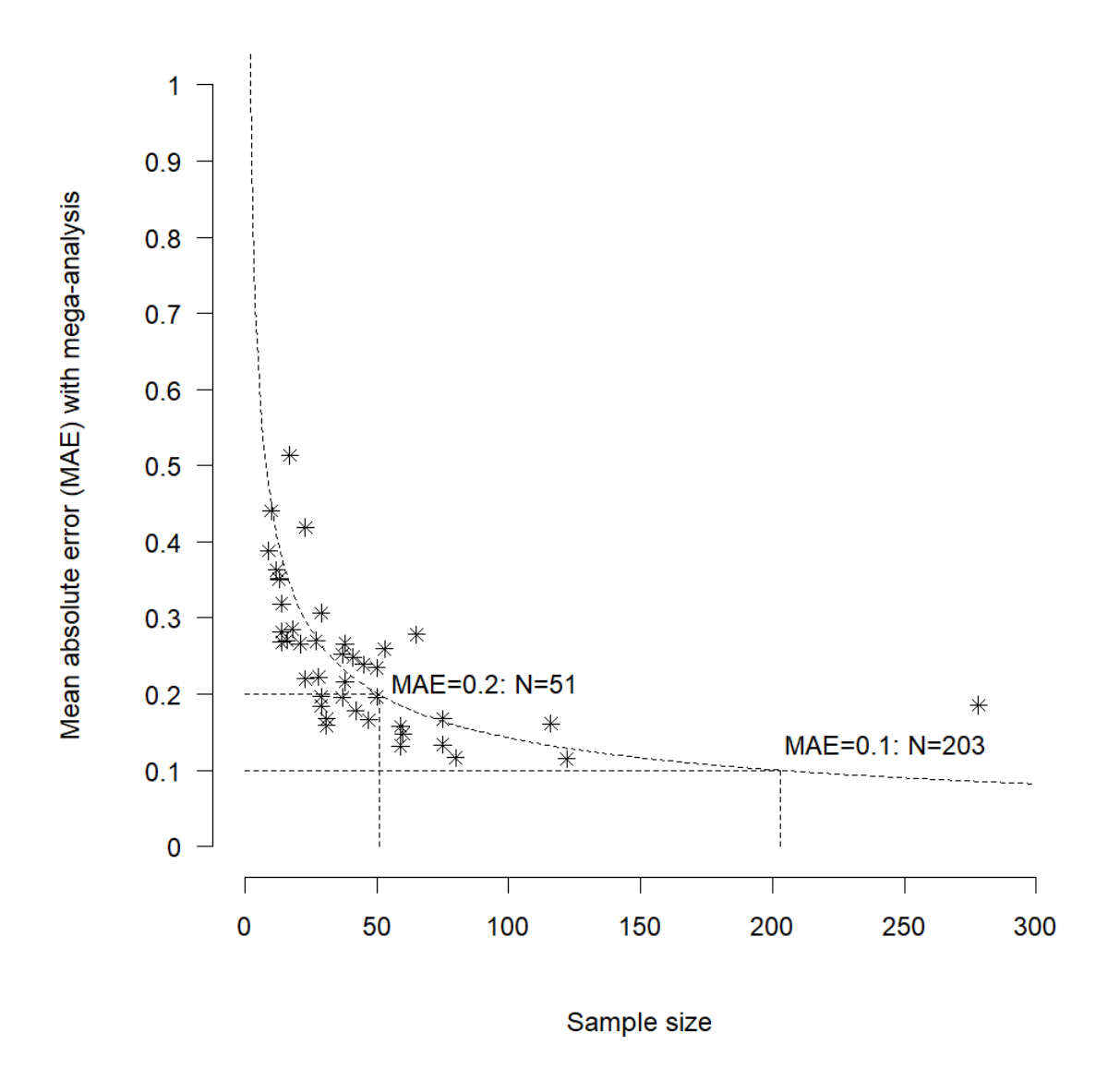
**Supplementary Figure S15**. Sample size analyses. Percentage of (de)activated brain regions detected in the mega-analysis according to sample size.



**Supplementary Figure S16**. (Fisher-transformed) correlation between the study and the mega-analysis. Sample sizes of 33 and 132 were required to achieve correlations of 0.5 and 0.8, respectively.



**Supplementary Figure S17**. (Arcsine-transformed) Dice coefficient between the study and the mega-analysis. Sample sizes of 122 and 275 were required to attain Dice coefficients of 25% and 50%, respectively.



**Supplementary Figure S18**. Sample size analyses. Mean absolute error (MAE) between the study and the mega-analysis. Sample sizes of 51 and 203 were required to achieve MAE values of 0.2 and 0.1, respectively.

# **Early conditioning** -3 Late conditioning -3 Early versus late conditioning

**Supplementary Figure S19**. Significant brain activation in response to CS+ versus CS- during early (n=679) and late (N=634) phases of conditioning, and brain regions showing significant differential activation between early and late conditioning in healthy controls (n = 634). Samples included in the analysis are reported in Supplementary Table S8

-16

# **Supplementary Tables**

**Supplementary Table S1.** Descriptive statistics for STAI-T and BDI across samples.

Sample	STAI-T (n)	STAI-T M (SD)	STAI-T range	BDI (n)	BDI M (SD)	BDI range
Amsterdam_Visser_sample_1	18	35.33 (10.39)	22 - 59	NA	NA	NA
Amsterdam_Visser_sample_2	41	34.66 (8.84)	22 - 53	NA	NA	NA
Amsterdam_Visser_sample_3	12	32.67 (5.82)	23 - 44	NA	NA	NA
Amsterdam_Visser_sample_4	10	35.3 (5.38)	29 - 46	NA	NA	NA
Amsterdam_Visser_sample_5	13	37.46 (9.47)	26 - 60	NA	NA	NA
Amsterdam_Visser_sample_6	14	35.29 (9.71)	21 - 58	NA	NA	NA
Amsterdam_Visser_sample_7	16	33.5 (6.04)	25 - 46	NA	NA	NA
Amsterdam_Visser_sample_8	9	36.44 (8.14)	27 - 52	NA	NA	NA
Amsterdam_Visser_sample_9	38	35.03 (8.63)	20 - 52	NA	NA	NA
Austin_Cisler	NA	NA	NA	61	22.57 (12.51)	0 - 55
Barcelona_Cardoner*	71	25.49 (13.49)	1 - 53	71	14 (11.87)	0 - 46
Barcelona_Soriano_sample_2*	147	20.47 (10.73)	1 - 52	NA	NA	NA
Bielefeld_Lonsdorf_sample_1	116	34.86 (7.36)	24 - 55	NA	NA	NA
Bielefeld_Lonsdorf_sample_2	80	35.37 (10)	20 - 59	NA	NA	NA
Bielefeld_Lonsdorf_sample_3	28	35.93 (6.96)	24 - 52	NA	NA	NA
Bochum_Elsenbruch	29	33.03 (6.51)	21 - 44	NA	NA	NA
Bochum_Merz_sample_5	31	33.32 (6.82)	20 - 52	NA	NA	NA
Bochum_Merz_sample_6	60	36.2 (6.88)	23 - 52	NA	NA	NA
Duke_LaBar_sample_1	38	32.39 (7.86)	21 - 53	NA	NA	NA
Duke_LaBar_sample_2	37	33.28 (6.55)	20 - 48	NA	NA	NA
Manitoba_Greening_sample_1	13	38.92 (9.3)	29 - 59	NA	NA	NA
Manitoba_Greening_sample_2	31	35.27 (10.45)	21 - 57	NA	NA	NA
Melbourne_Harrison	112	38.97 (13.05)	21 - 73	NA	NA	NA
Munster_Moeck_sample_1	42	34.19 (7.3)	22 - 50	42	3.62 (4.36)	0 - 16
Reading_Reekum_sample_1	21	41.62 (8.66)	27 - 59	NA	NA	NA
Reading_Reekum_sample_2	50	42.92 (9.82)	26 - 75	NA	NA	NA
Royal_Tuominen_sample_1	28	35.57 (13.83)	20 - 67	28	5.68 (7.98)	0 - 27

Royal_Tuominen_sample_2	71	34.97 (10.33)	20 - 68	71	5.15 (6.48)	0 - 23
USP_Diniz	NA	NA	NA	25	20.4 (11.47)	0 - 44
Texas_Dunsmoor	NA	NA	NA	45	15.68 (10.89)	0 - 41
Ulm_Abler	50	33.38 (6.13)	23 - 52	NA	NA	NA
Uppshala_Ahs	278	36.27 (11.44)	20 - 67	NA	NA	NA
Vanderbilt_Kaczkurkin	82	43.38 (12.14)	21 - 70	82	12.38 (8.62)	0 - 31
TOTAL	1586	34.45 (11.56)	1 - 75	425	12.41 (11.48)	0 - 55

BDI: Beck Depression Inventory; NA: Not available: STAI-T: State Trait Anxiety Inventory-Trait version. \*These samples used the Spanish version of the STAI-T (scores range from 0 to 60)

# Supplementary Table S2. Pairwise Pearson correlation between sociodemographic, individual differences and task variables.

Sex	0.03																		
Anxiety score	0.11	0.02																	
Depression score	0.12	0.19	0.73																
Instructions given about contingency prior to the task	0.06	0.08	0	0.33															
Number of trials in preconditioning	0.07	0.24	0.16	0.07	0.2														
Paradigm with multiple CS plus	0.03	0.12	0	0	0.23	0.16		_											
Paradigm with multiple CS minus	0.02	0.07	0.05		0.17	0.16	0.37												
Type of CS	0.33	0.05	0.14	0.41	0.3	0.31	0.27	0.16											
Number of CS plus during conditioning	0.06	0.09	0.02	0.11	0.26	0.18	0.26	0.03	0.07										
Number of CS minus during conditioning	0.23	0.02	0.05	0.1	0.09	0.58	0.08	0.38	0.08	0.42									
Average ITI	0.2	0.04	0.12	0.25	0.12	0.49	0.02	0.06	0.21	0.43	0.59								
Average ISI	0.26	0.04	0.14	0.14	0.11	0.07	0.16	0	0.26	0.2	0.15	0.13							
Pairing rate	0.34	0.17	0.13	0.44	0.71	0.26	0.68	0.18	0.46	0.36	0.53	0.3	0.62						
Type of US used	0.43	0.06	0.17	0.12	0.08	0.02	0.33	0.22	0.23	0.04	0.1	0.06	0.66	0.45					
Potential US confounding	0.41	0.04	0.12	0.15	0.13	0.09	0.18	0.03	0.39	0.25	0.18	0.05	0.44	0.6	0.38				
Number of CS plus included in the fMRI contrast	0.29	0.03	0.06	0.03	0.05	0.09	0.11	0.07	0.33	0.39	0.54	0.28	0.03	0.42	0.24	0.52			
Number of CS minus included in the fMRI contrast	0.22	0.03	0.03	0.07	0.02	0.43	0.2	0.17	0.11	0.4	0.79	0.4	0.11	0.36	0.17	0.17	0.7		_
Contingency awareness	0.1	0.01	0.04	0.06	0.01	0.04	0.01	0.1	0.23	0.06	0.09	0.07	0.21	0.19	0.18	0.03	0.14	0.09	Ì
Diagnosis of anxiety related disorder (PTSD,GAD,)	0.49	0.06	0.38	0.16	0.31	0.4	0.58	0.35		0.6	0.62	0.87	0.66	0.78	0.78	0.72	0.42	0.65	0.18
Patient versus controls	0.16	0.05	0.47	0.65	0.07	0.15	0.06	0.06	0.2	0.04	0.12	0.25	0.16	0.23	0.05	0.04	0.01	0.09	0.16
	Age	Sex	Anxiety score	Depression score	Instructions given about	Number of trials in	Paradigm with multiple CS	Paradigm with multiple CS	Type of CS	Number of CS plus during	Number of CS minus during	Average ITI	Average ISI	Pairing rate	Type of US used	Potential US confounding	Number of CS plus included	Number of CS minus included	Contingency awareness

## Supplementary Table S3. Pairwise variance inflation factor (VIF) between sociodemographic, individual differences and task variables\*

Sex	1.0																		
Anxiety score	1.0	1.0																	
Depression score	1.0	1.0	1.6																
Instructions given about contingency prior to the task	1.0	1.0	1.0	1.0															
Number of trials in preconditioning	1.0	1.0	1.0	1.1	1.1		_												
Paradigm with multiple CS plus	1.0	1.0	1.0	1.0	1.0	1.0													
Paradigm with multiple CS minus	1.0	1.0	1.0		1.0	1.0	1.2												
Type of CS	1.2	1.0	1.0	1.2	1.1	1.1	1.1	1.0											
Number of CS plus during conditioning	1.0	1.0	1.0	1.0	1.1	1.0	1.1	1.0	1.0										
Number of CS minus during conditioning	1.0	1.0	1.0	1.1	1.0	1.4	1.0	1.2	1.0	1.2									
Average ITI	1.0	1.0	1.0	1.2	1.0	1.3	1.0	1.0	1.1	1.2	1.3								
Average ISI	1.1	1.0	1.0	1.0	1.0	1.0	1.0	1.0	1.1	1.1	1.0	1.0							
Pairing rate	1.1	1.0	1.0	1.4	2.2	1.0	1.9	1.0	2.1	1.2	1.4	1.1	1.8						
Type of US used	1.2	1.0	1.0	1.0	1.0	1.0	1.1	1.0	1.1	1.0	1.0	1.0	2.0	1.2					
Potential US confounding	1.2	1.0	1.0	1.0	1.1	1.0	1.1	1.0	1.2	1.1	1.0	1.0	1.2	1.8	1.1				
Number of CS plus included in the fMRI contrast	1.1	1.0	1.0	1.1	1.0	1.0	1.1	1.0	1.2	1.2	1.4	1.1	1.0	1.4	1.0	1.3			
Number of CS minus included in the fMRI contrast	1.0	1.0	1.0	1.1	1.0	1.1	1.0	1.0	1.0	1.2	2.5	1.1	1.0	1.2	1.0	1.0	1.9		
Contingency awareness	1.0	1.0	1.0	1.0	1.0	1.0	1.0	1.0	1.1	1.0	1.0	1.0	1.1	1.0	1.1	1.0	1.0	1.0	
Diagnosis of anxiety related disorder (PTSD,GAD,)	1.3	1.0	1.2	1.0	1.1	1.2	1.5	1.1		1.6	1.6	4.0	1.8	7.8	2.5	2.1	1.2	1.7	1.0
Patient versus controls	1.0	1.0	1.3	1.7	1.0	1.0	1.0	1.0	1.0	1.0	1.0	1.1	1.0	1.1	1.0	1.0	1.0	1.0	1.0
	Age	Sex	Anxiety score	Depression score	Instructions given about	Number of trials in	Paradigm with multiple CS plus	Paradigm with multiple CS	Type of CS	Number of CS plus during	Number of CS minus during	4verage ITI	Average ISI	airing rate	Type of US used	Potential US confounding	Number of CS plus included in	Number of CS minus included	Contingency awareness

<sup>\*</sup> The VIF analysis revealed no collinearity concerns (VIF > 5), except for the pair of variables highlighted in red. However, their activation maps did not show any overlap.

## **Supplementary Table S4.** Task variables showing high (>0.5) inter-correlations.

Variable 1	Variable 2	n	r	VIF	Overlap
Number of CS minus during conditioning	Number of CS minus included in the fMRI contrast	1884	0.774975	2.503673	NO
Instructions given about contingency prior to the task	Pairing rate	1506	0.736404	2.184792	NO
Average ISI	Type of US used	1805	0.698958	1.955196	NO
Number of CS plus included in the fMRI contrast	Number of CS minus included in the fMRI contrast	1884	0.695982	1.939456	NO
Paradigm with multiple CS plus	Pairing rate	1506	0.680728	1.863555	NO
Pairing rate	Potential US confound	1506	0.675691	1.840122	YES*
Average ISI	Pairing rate	1506	0.658202	1.764384	NO
Anxiety score	Depression score	189	0.625581	1.642984	NO
Pairing rate	Number of CS plus included in the fMRI contrast	1506	0.538111	1.407584	NO
Number of CS minus during conditioning	Pairing rate	1506	0.536643	1.404466	NO
Type of CS	Pairing rate	1446	0.533694	2.135761	YES**
Number of CS minus during conditioning	Number of CS plus included in the fMRI contrast	1884	0.525154	1.38081	NO
Number of trials in preconditioning	Number of CS minus during conditioning	1251	0.523602	1.377713	NO
Depression score	Pairing rate	160	0.519464	1.369569	NO

<sup>\*(</sup>see main text)

<sup>\*\*</sup> Pairing rate and CS type shared two small clusters. In one cluster, both variables remained statistically significant when included in the same model. In the other cluster, located in the left orbitofrontal cortex, only the pairing rate remained significant. With no collinearity concerns (VIF = 2.1), this suggests that activation in this region is modulated by the pairing rate rather than CS type.

# **Supplementary Table S5.** Task and clinical variables showing high (>0.5) intercorrelations.

Variable 1	Variable 2	n	r	VIF	Overlap
Average ITI	Diagnosis of anxiety related disorder	288	0.866338	4.008687	NO
Pairing rate	Diagnosis of anxiety related disorder	228	0.784478	7.796471	NO
Type of US used	Diagnosis of anxiety related disorder	288	0.775372	2.507536	NO
Potential US confound	Diagnosis of anxiety related disorder	288	0.717325	2.059966	NO
Average ISI	Diagnosis of anxiety related disorder	288	0.656201	1.756235	NO
Depression score	Patient versus controls	375	0.652073	1.739734	NO
Number of CS minus included in the fMRI contrast	Diagnosis of anxiety related disorder	288	0.648278	1.724925	NO
Number of CS minus during conditioning	Diagnosis of anxiety related disorder	288	0.622024	1.631092	NO
Number of CS plus during conditioning	Diagnosis of anxiety related disorder	288	0.597379	1.554877	NO
Paradigm with multiple CS plus	Diagnosis of anxiety related disorder	288	0.580814	1.509081	NO

# **Supplementary Table S6.** Patient's medications.

Sample	Medicated (n)	SSRI or SNRI (n)	BZD (n)	Other* (n)
Austin_Cisler	36	2	0	34
Barcelona_Cardoner	1	0	1	0
Barcelona_Soriano_sample_1	16	10	0	6
Munich_Koch	12	7	0	5
Vanderbilt_Kaczkurkin	1	1	0	0
TOTAL	66	20	1	45

SSRI: Selective Serotonin Reuptake Inhibitors; SNRI: Selective Noradrenaline Reuptake Inhibitors; BZD: Benzodiazepines. \*Includes other medications or combinations of medications.

# Supplementary Table S7. Participants excluded after quality control (QC)

0	N U ( I	N excluded	N excluded	N included
Sample	N collected	after	after manual QC	in analysis
Ametordam Viscor sample 1	19	HALFpipe QC		18
Amsterdam_Visser_sample_1 Amsterdam_Visser_sample_2	41	0	1 0	41
Amsterdam_Visser_sample_3	12	0	0	12
Amsterdam_Visser_sample_4	11	1	0	10
Amsterdam_Visser_sample_5	13	0	0	13
	14	0	0	14
Amsterdam_Visser_sample_6 Amsterdam_Visser_sample_7	16	0	0	16
Amsterdam_Visser_sample_8	10	1	0	9
Amsterdam_Visser_sample_9	38	0	0	38
Austin_Cisler	 88	27	0	61
Barcelona_Cardoner	90	16	3	71
Barcelona_Soriano_sample_1	37	2	0	35
Barcelona_Soriano_sample_2	191	44	0	147
Bielefeld_Lonsdorf_sample_1	120	44	0	116
Bielefeld_Lonsdorf_sample_2	83	<u> </u>	2	80
Bielefeld_Lonsdorf_sample_3	32	4	0	28
Bochum Elsenbruch	30	1	0	29
Bochum_Merz_sample_1	60	1	0	59
Bochum_Merz_sample_2	60	1	0	59
Bochum_Merz_sample_3	48	1	0	47
Bochum_Merz_sample_4	33	4	0	29
	33	1	0	31
Bochum_Merz_sample_5				
Bochum_Merz_sample_6	64	4	0	60
Columbia_Neria	114	15	4	95
Duke_LaBar_sample_1	40	2	0	38
Duke_LaBar_sample_2	40	3	0	37
Florida_Keil	15	0	1	14
Harvard_McLaughlin	95	6	0	89
Manitoba_Greening_sample_1	13	0	0	13
Manitoba_Greening_sample_2	31	0	0	31
Melbourne_Harrison	154	40	2	112
Munich_Koch	52	4	3	45
Munster_Moeck_sample_1	44	2	0	42
Munster_Moeck_sample_2	31	2	0	29
Reading_Reekum_sample_1	22	1	0	21
Reading_Reekum_sample_2	52	2	0	50
Royal_Tuominen_sample_1	17	0	3	14
Royal_Tuominen_sample_2	37	0	0	37
Texas_Dunsmoor	48	3	0	45
			<b>~</b>	

Ulm_Abler	51	1	0	50
Uppsala_Ahs	306	28	0	278
USP_Diniz	56	1	0	55
Vanderbilt_Kaczkurkin	88	6	1	81
TOTAL	2448	229	20	2199

## Supplementary Table S8. Samples included in the early versus late analyses

Sample	n	CS+ trials included in early/late analysis (n/n)	CS- trials included in early/late analysis (n/n)	Pairing rate (%)	US confound in early/late analysis
Barcelona_Cardoner*	45	8/-	16/-	50	no
Barcelona_Soriano_datas et_2	122	5/5	5/5	33	no
Bochum_Elsenbruch	29	4/4	4/4	100	yes
Bochum_Merz_dataset_1	56	8/8	4/4	62.5	yes
Bochum_Merz_dataset_2	58	8/8	4/4	62.5	yes
Bochum_Merz_dataset_3	47	10/10	10/10	100	yes
Bochum_Merz_dataset_4	28	8/8	4/4	62.5	yes
Bochum_Merz_dataset_5	31	8/8	4/4	62.5	yes
Bochum_Merz_dataset_6	60	8/8	4/4	62.5	yes
Duke_LaBar_dataset_1	38	5/5	5/5	50	yes
Duke_LaBar_dataset_2	37	8/8	8/8	31	yes
Harvard_McLaughlin	75	4/4	2/2	40	yes
Vanderbilt_Kaczkurkin	53	7/7	15/15	80	yes

CS, conditioned stimulus; CS+, CS followed by unconditioned stimulus; CS -, CS not followed by unconditioned stimulus; CS+/CS-, US=Unconditioned stimulus.

All samples used visual conditioned stimuli. All samples used an electric shock as US except Barcelona\_Cardoner and Harvard\_McLaughlin, which used an auditory stimulus.

\*Only early trials were available.

## **Supplementary Methods**

#### Changes with respect to pre-registration

As noted in the main text, both the mega-analysis (<a href="https://osf.io/7n953">https://osf.io/7n953</a>) and normative modeling analysis (<a href="https://osf.io/w74bt">https://osf.io/w74bt</a>) were pre-registered. The following changes were made after pre-registration:

- 1. At the time of pre-registration, we had collected data from 43 samples. We excluded one sample (n=22) because it employed a "multi-CS" conditioning paradigm (36 CS+, 18 CS-) which is difficult to compare with the other experiments included.
- 2. For the mega-analysis, we used pre-scaling instead of Combat to reduce site-related heterogeneity (see "Pre-scaling" in page 5).

The normative modelling analysis plan was updated to best complement the metaanalysis approach and thus the following changes were made after pre-registration:

- 1. Sample size. The participants included were a subset of the final sample used in the meta-analysis, for whom all required data were available.
- 2. Variables included. The variables used were matched to those included in the mega-analysis study to facilitate a better comparison between the results of these complementary methods
- 3. Analysis plan. Research question 1A. We chose not to create models for separate ROIs. Research question 1C. We did not perform whole-brain sparse canonical correlation analysis to determine how deviations in task activation predicted outcome measures, rather, we chose statistical approaches more appropriate to the type of data. Research question 2B. Again, we did not perform whole-brain sparse canonical correlation analysis, for the same reasons as mentioned above. We did not perform analyses on transdiagnostic scales with insufficient sample sizes (e.g., Beck Anxiety Inventory, Hamilton-Anxiety, Hamilton-Depression) and similarly excluded small diagnostic groups from relevant analyses. We did not use a clustering method.

#### Variables collected and not included in analyses

The following variables were collected but not included in the analyses because the data collected were insufficient, or too heterogeneous to be aggregated: IQ, comorbidity, ethnicity, years of education, use of a concurrent task during conditioning, and US aversiveness. We excluded the variable "use of preconditioning"

phase" from the analyses because we already accounted for it by including "number of trials during preconditioning". Descriptive data on years of education and comorbidity for the samples with available data are reported in Tables 1 and 3 of the main manuscript.

## Non-imaging data

Harmonization of trait anxiety scores

As noted in the main text, we conducted the analysis of the State-Trait Anxiety Inventory-Trait version (STAI-T) scores using both raw and harmonized scores. To harmonize the STAI-T scores, we took the following steps, we first assessed the potential variability of STAI-T scores across versions, languages, or countries, by conducting a meta-analysis of the mean STAI-T scores reported in the normative studies<sup>1-11</sup> as well as a meta-analysis of the reported standard deviations. In both analyses, substantial heterogeneity between studies was observed (f statistic for the mean: 99%; f statistic for the standard deviation: 95%, Q test p<0.001 in both cases). This heterogeneity indicates significant differences in the reported means and standard deviations between studies. We then examined potential moderators of this heterogeneity, including the version of the STAI-T (X or Y), language, and country. The results revealed statistically significant differences in the mean and standard deviation across countries (p=0.014 and 0.001, respectively) and in the mean across languages (p=0.012) but not on the version of the STAI-T.

		Mean		Log SD		
		Estimate (95%CI)	Р	Estimate (95%CI)	Р	
Version	X	41.2 (36.9-45.4)	n.s.	2.36 (2.31-2.41)	n.s.	
	Υ	39.2 (36.4-42.0)		2.22 (2.09-2.35)		
Language	Dutch	35.2 (33.0-37.5)	0.012	2.23 (1.97-2.48)	0.353	
	English	38.0 (35.7-40.4)		2.17 (2.01-2.32)		
	French	41.9 (40.7-43.1)		2.15 (2.05-2.25)		
	German	43.0 (41.0-44.9)		2.39 (2.36-2.42)		
	Japanese	46.8 (44.6-49.1)		2.43 (2.29-2.57)		
	Spanish	46.2 (37.5-55.0)		2.32 (2.25-2.39)		
Country	America	36.5 (33.9-39.1)	0.014	2.13 (1.88-2.39)	0.001	
	Australia	36.4 (35.8-37.0)		2.41 (2.37-2.45)		
	England	41.1 (36.1-46.2)		2.02 (1.79-2.25)		
	France	41.9 (40.7-43.1)		2.15 (2.05-2.25)		
	Germany	43.0 (41.0-44.9)		2.39 (2.36-2.42)		
	Japan	46.8 (44.6-49.1)		2.43 (2.29-2.57)		
	Netherlands	35.2 (33.0-37.5)		2.23 (1.97-2.48)		
	Spain	46.2 (37.5-55.0)		2.32 (2.25-2.39)		

These findings suggest that the observed heterogeneity in STAI-T scores is partly explained by country (or language) differences in the included studies. We could not separate the effects of "country" and "language" because each language corresponded to one country, except for English (which corresponded to America, Australia, and England). However, given that "country" better explained the heterogeneity and that we expected cultural differences among English-speaking countries, we decided to harmonize STAI-T scores based on country (rather than language). The harmonization was conducted with ComBat for ENIGMA<sup>12</sup> (see expanded code in the figshare repository):

### Quality control

Three investigators (EV, HS, MAF) independently performed quality control of the non-imaging data and contacted the sites for additional information when necessary.

## **Neuroimaging data**

Quality control

Data were collected from 2448 participants. In addition to quality control using HALFpipe, which excluded 229 individuals (**Supplementary Table S7**, two investigators (EV, HS) independently reviewed all neuroimaging data, which excluded 20 additional participants. Two of the included samples (Manitoba\_Greening\_sample\_1 and Manitoba\_Greening\_sample\_2) were analyzed in different runs. For these samples, we used the average of all runs to obtain the main contrast. One sample (Harvard\_McLaughlin) was analyzed using blocks; due to the short interval-stimulus-interval (ISI), individual events could not be reliably obtained.

#### Statistical analyses. Mega-analyses

Pre-scaling

As noted in the main text, after processing with HALFpipe, we observed differences in the BOLD response between sites. Such variability exceeded the expected small normally distributed differences typically addressed by site-harmonizing mixed-effects models such as ComBat<sup>12</sup>. To remove these differences, we performed a prescaling step that consisted of dividing the BOLD response of individuals from each site by their standard deviation. The use of such standardized scores is common in many areas of psychology and neuroscience. Specifically, for each voxel with brain

coverage across all sites, we estimated the standard deviation using linear models with appropriate covariates (see below). We then calculated the median of the standard deviations across these voxels and divided all images in the sample by this standard deviation. We have included this step in the "combat.enigma" package<sup>12</sup> in R for use by other groups. Following recommendations for between-site harmonization (see below), we estimated the standard deviations exclusively using data from healthy controls.

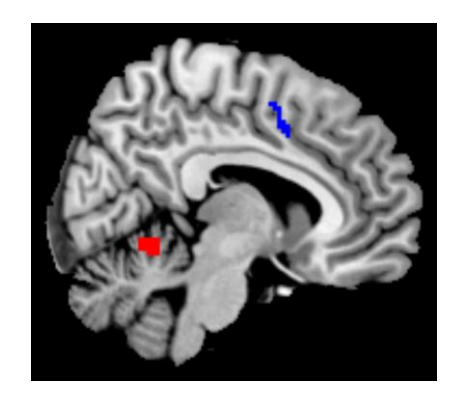
A note about the use of z-statistics in mega-analyses

HALFpipe generates "z-statistic images", and one may (wrongly) assume that these z-statistic images are equivalent to z-scores. However, z-statistic images are calculated by dividing each participant's mean BOLD response (to different trials) by its standard error rather than by the standard deviation across participants. Thus, critically, these z-statistic images mix the task-related BOLD response with its standard error. This is not inherently wrong, but it means that differences in z-statistics between cases and controls may be due not only to differences in the task-related BOLD response but also to differences in its standard error.

These differences in standard error could be unrelated to the task, for example, due to differences in the amplitude of BOLD signal fluctuations. In the following R code, we simulated a study comparing the task-related BOLD response between cases and controls, with no actual differences in the task-related BOLD response but differences in its standard error. As expected, the t-tests comparing the groups show no differences in the task-related BOLD response. However, they do show statistically significant differences in within-subject z-scores.

```
# Create a task time-series design matrix
design = rep(c(rep(0:1, 20), 0), each = 8)
dat = NULL
# For each group
for (group in c("patient", "control")) {
 # For each individual in the group
 for (i in 1:30) {
  # Simulate the BOLD signal with the same BOLD response but more noise
  # in patients
  ts = rnorm(length(design), design, ifelse(group == "patient", 1.2, 1))
  # Simplified analysis to estimate the task-related BOLD response
  m = summary(lm(ts ~ design))$coefficients[2,]
  # Save the individual task-related BOLD response and z-statistic
  dat = rbind(dat, data, frame(
    group,
   bold_response = m[1],
    z_{statistic} = m[1] / m[2]
# Conduct t-tests to compare patients and controls
t.test(dat$bold response ~ dat$group)
t.test(dat$z statistic ~ dat$group)
```

In other words, we do not know whether differences in z-statistics are related to differences in the task-related BOLD response or to differences in other aspects of the BOLD signal that may be unrelated to the task. Indeed, we examined whether cases (individuals with anxiety-related and depressive disorders) and controls in this study might have different standard errors of the fear conditioning-related BOLD response and found that they might. For each sample containing cases and controls, we calculated the standardized mean difference (Cohen's d) in standard error and then averaged d across the samples. At a descriptive level, using a threshold of d≥0.2, cases showed larger standard errors in the cerebellum, but smaller in the midcingulum (see figure).



Linear mixed-effects models

To fit the models, we created a new function that, for each voxel, performs the following steps:

- 1) Assesses which participants and sites have information, taking into account the specific brain coverage of each individual fMRI scan;
- 2) Detects and discards collinear or constant covariates, which can vary depending on the participants with information in that voxel;
- 3) Fits a linear mixed-effects model using the "lme" function from the "nlme" R package<sup>13</sup>:

```
m = Ime(y \sim x, random = \sim 1 | sample)
```

or a simple linear model if the participants are from only one sample:

$$m = Im(y \sim x)$$

Where "m" is the model, "y" is the voxel value, "x" is a matrix with the variables of interest and covariates, and "site" is a random intercept.

4) Tests the linear hypothesis if specified (e.g., for ANOVAs):

linearHypothesis(m, hypothesis)

where "m" is the model, and "hypothesis" is the hypothesis matrix.

5) Saves the results, including maps of sigma (the standard deviation estimated in the model), the model coefficients, and z-statistics. We have included this function in the "combat.enigma" R package.

We used cluster-based inference to correct for multiple testing. Specifically, we created clusters of voxels with Z≥3.1 and converted cluster sizes to cluster-wise p-values using the Gaussian Random Field (GRF) theory, using the FSL utilities smoothest and cluster.

#### Normative modelling: Thresholding

We follow existing work in the field and apply a threshold equal to or greater than 2.6 (Z±2.6) to determine 'large' deviation scores. With the normative modelling approach, we are not performing a group-level hypothesis test as would be done

using a statistical parameteric mapping framework, rather we are aiming to statistically detect differences in individual subjects with respect to the common reference model. For this type of analysis, it is not clear that how spatial comparisons, and multiple comparison correction ought to be done, nor that doing so is even appropriate because multiple comparisons correction obscures the degree of inter-individual differences that are detected. In prior work<sup>14</sup>, a subject level FDR method was evaluated where the results did not differ from the conclusions made when using the original un-corrected input data. The interpretation of the single subject FDR correction method is not straightforward as a different threshold is estimated for every subject. In other words, an individual with widespread decreased or increased BOLD activation during the task (as quantified using a contrast zstatistic) may appear to have 'normal' findings using an FDR threshold as the overall distribution of their voxel intensities is shifted. Therefore, in this work we elected to use a single fixed threshold (Z±2.6) to determine the significance of a deviation. which simplifies the comparison across individuals and is in line with other work on normative models<sup>14-16</sup>.

# Sample size analyses

Leveraging data from the 43 samples included in the study, we conducted a series of sample size analyses to inform the design of future studies. Specifically, we treated the mega-analytic primary activation map as the ground truth and examined how activation patterns at varying sample sizes compared to this reference. To ensure harmonization across datasets, all analyses were re-run using the Imm\_fit function and corrected for multiple comparisons using Gaussian random field theory. The primary objective was to examine how study sample size relates to the proportion of brain regions showing activation or deactivation in the mega-analysis. To this end, we parcellated the brain using the AAL atlas<sup>17</sup>, and defined a region as activated (or deactivated) if it contained at least 10 statistically significant activating (or deactivating) voxels. For each study, we then calculated the percentage of AAL regions identified as activated (or deactivated) in the mega-analysis that were also detected in the individual study. The relationship between the arcsine-

transformed percentage of detected regions and the square root of the study's sample size was subsequently assessed.

For completeness, we also computed the average false positive rate—defined as the percentage of regions not activated or deactivated in the mega-analysis but incorrectly identified as such in the individual studies. All analyses were conducted separately for activations and deactivations. Secondary analyses examined how the square root of the study's sample size related to several additional metrics:

- a) the Fisher-transformed correlation between the study and mega-analytic maps;
- b) the mean absolute error between the two; and
- c) the arcsine-transformed Dice coefficient<sup>18</sup> quantifying their spatial overlap.

## **Supplementary Discussion**

In the main text, we highlighted those individual differences or task variables with more robust effects. Here we discuss the remaining significant associations.

#### Sociodemographic variables

Older age was significantly associated with greater activation in the ventromedial prefrontal cortex and medial temporal gyrus, as well as significantly less activation in the anterior insula, pre-supplementary motor area extending to the dorsal anterior cingulate, dorsal caudate and bilateral supramarginal gyrus extending to the posterior insula. Female participants (n=973) showed greater activation across the visual cortex, and left medial/superior temporal gyrus than males (n=915). Regression coefficients from the normative models indicated a minimal effect of age on the predicted BOLD signal, but unthresholded effects largely replicated the findings of the mega-analysis. Structure coefficients from the normative models showed minimal relation between sex and predicted BOLD signal, with only a very small cluster in the mid-anterior cerebellum predicted to show heightened activation in females. These results are presented in **Sup. Figure S5**.

#### Task variables

The following task variables showed significant albeit small/weak associations with brain activation during conditioning (see **Sup. Figure S8** for the mega-analysis

results and **Sup. Figure S9** for the structure coefficients of the normative modeling results). Normative modelling regression coefficient maps are also shown in **Sup. Figure S9** for completeness but are not discussed below.

The <u>number of trials during preconditioning</u> showed a significant positive association with activation in the inferior cerebellum in the mega-analysis. Structure coefficients did not show a relationship between the number of trials during preconditioning and predicted BOLD signal.

In the mega-analysis, the type of CS (categorized as humanoid, affective pictures, and neutral faces) revealed significant effects. See full results at https://figshare.com/s/d44cc1390711bad3c147.In normative modeling analyses, the use of a humanoid CS was predictive of increased activation in the cingulate cortex, extending to the dorsomedial prefrontal cortex and pre-supplementary motor area, secondary somatosensory cortex (SII), dorsal precuneus, dorsolateral prefrontal cortex, the bilateral insula, the bilateral temporoparietal junction, the thalamus, the caudate and the left anterior cerebellum, as well as decreased activation (i.e. more deactivation) in the anterior ventromedial prefrontal cortex and posterior cinqulate cortex. Moreover, the use of neutral pictures as CS predicted more activation (i.e. less deactivation) in the anterior ventromedial prefrontal cortex and posterior cingulate cortex, and less activation within the cingulate cortex, extending to the dorsomedial prefrontal cortex and pre-supplementary motor area, dorsal precuneus, SII, the bilateral insula, the bilateral temporoparietal junction, the thalamus, the caudate and left anterior cerebellum Finally, the use of neutral faces as CS predicted more activation within the subgenual anterior cingulate cortex, and less activation within the bilateral fusiform face area and SII. The use of other types of CS (affective faces and pictures, a gabor patch, a neutral male avatar, images of animals or tools, or of snakes and spiders) did not have an influence on predicted BOLD signal.

Average intertrial-interval (ITI) length demonstrated a significant positive association with activation within the bilateral primary visual cortex and a significant negative association with the bilateral posterior parietal cortex, and superior frontal gyri extending to the supplementary motor area in the mega-analysis. Structure coefficients showed that increased average ITI was predictive of increased activation within the primary visual cortex, dorsomedial prefrontal cortex, extending to the pre SMA, the bilateral thalamus, caudate and putamen, the brainstem, and the anterior

and medial cerebellum. Conversely, a longer ITI predicted less activation (i.e., more deactivation) within an expanse of the ventromedial prefrontal cortex, within the dorsolateral prefrontal cortex, primary somatosensory cortex (SI) the precuneus, the lingual gyrus and fusiform face area extending into bilateral middle gyri of the temporal lobe, and bilateral hippocampus.

In the mega-analysis, the <u>number of CS+ included in the fMRI</u>

<u>contrast</u> showed a significant positive association with activation in the left primary visual cortex, right orbitofrontal cortex, right precuneus, right superior parietal lobule, and right dorsolateral prefrontal cortex. Moreover, the <u>number of CS- included in the fMRI contrast</u> showed a significant positive association with activation in the left superior parietal lobule and the right dorsolateral prefrontal cortex.

Being unaware of the relationship between CS and US (i.e., contingency unawareness; n=72) showed a positive association with activation in the ventral posterior cingulate extending to the dorsal anterior cingulate/precuneus compared with being aware (n=1260). As contingency awareness was not available for all participants this variable was not included in the construction of the normative models, and therefore their relationship to predicted task (de)activation cannot be assessed using structure coefficients. Rather, for participants in the two test samples (controls + individuals with an anxiety or mood-related disorder) with these data available (n = 703) we used a support vector classifier and found whole-brain deviation score could not be used to predict whether a participant was contingency aware or not (mean accuracy = 50% +/- 16%; p = 0.426; 10-fold cross validation; 1000 permutations).

For the main results on type of US, please refer to the main text. In addition to these main results, in normative modeling analyses, the use of a thermal stimuli as US was predictive of decreased activation within the bilateral amygdala, the mid-cingulate cortex extending to the pre-supplementary motor area, the dorsomedial prefrontal cortex, a posterior region of the ventromedial prefrontal cortex, the cuneus, and (i.e., more deactivation) in the angular gyrus. The use of a visceral stimuli as US had no influence on predicted BOLD signal during CS+>CS-. These two variables were not investigated separately using linear models.

The following task variables were not significant in the mega-analysis nor in normative modelling analyses: number of CS+ trials during conditioning; number of CS- trials during conditioning; and average ISI (inter-stimulus interval, i.e., between the CS+ and the US).

#### **Supplementary References**

- Crawford, J., Cayley, C., Lovibond, P. F., Wilson, P. H. & Hartley, C. Percentile norms and accompanying interval estimates from an Australian general adult population sample for self-report mood scales (BAI, BDI, CRSD, CES-D, DASS, DASS-21, STAI-X, STAI-Y, SRDS, and SRAS). *Aust. Psychol.* 46, 3–14 (2011).
- 2. Guillén-Riquelme, A. & Buela-Casal, G. Psychometric revision and differential item functioning in the State Trait Anxiety Inventory (STAI). *Psicothema* **23**, 510–515 (2011).
- Sandin, B., Chorot, P. & McNally, R. J. Anxiety sensitivity index: normative data and its differentiation from trait anxiety. *Behav. Res. Ther.* 39, 213–219 (2001).
- 4. Spielberger, C. D. Manual for the State-Trait Anxiety Inventory (self-evaluation questionnaire). (1970).
- 5. Caci, H., Baylé, F. J., Dossios, C., Robert, P. & Boyer, P. The Spielberger trait anxiety inventory measures more than anxiety. *Eur. Psychiatry* **18**, 394–400 (2003).
- 6. Kennedy, B. L., Schwab, J. J., Morris, R. L. & Beldia, G. Assessment of state and trait anxiety in subjects with anxiety and depressive disorders. *Psychiatr. Q.* **72**, 263–276 (2001).
- 7. Marteau, T. M. & Bekker, H. The development of a six-item short-form of the state scale of the Spielberger State-Trait Anxiety Inventory (STAI). *Br. J. Clin. Psychol.* **31**, 301–306 (1992).
- 8. Iwata, N. & Higuchi, H. R. Responses of Japanese and American university students to the STAI items that assess the presence or absence of anxiety. *J. Pers. Assess.* **74**, 48–62 (2000).
- 9. Bieling, P. J., Antony, M. M. & Swinson, R. P. The State-Trait Anxiety Inventory, Trait version: structure and content re-examined. *Behav. Res. Ther.* **36**, 777–788 (1998).
- 10. Brand, S. *et al.* A multi-site German validation of the Interoceptive Accuracy Scale and its relation to psychopathological symptom burden. *Commun. Psychol.* **1**, 14 (2023).
- 11. Ryckewaert, R. Aandachtsbias voor doodsgerelateerde informatie bij ouderen versus jongeren. *Thesis*, Universiteit Gent (2008).
- 12. Radua, J. *et al.* Increased power by harmonizing structural MRI site differences with the ComBat batch adjustment method in ENIGMA. *Neuroimage* **218**, 116956 (2020).
- 13. Pinheiro, J., Bates, D. & R Core Team. *nlme: Linear and Nonlinear Mixed Effects Models* (2024).
- 14. Wolfers, T. *et al.* Mapping the heterogeneous phenotype of schizophrenia and bipolar disorder using normative models. *JAMA Psychiatry* **75**, 1146–1155 (2018).
- 15. Holz, N. E. *et al.* A stable and replicable neural signature of lifespan adversity in the adult brain. *Nat. Neurosci.* **26**, 1603–1612 (2023).
- 16. Floris, D. L. *et al.* Atypical brain asymmetry in autism—a candidate for clinically meaningful stratification. *Biol. Psychiatry Cogn. Neurosci. Neuroimaging* **6**, 802–812 (2021).

- 17. Tzourio-Mazoyer, N. *et al.* Automated anatomical labeling of activations in SPM using a macroscopic anatomical parcellation of the MNI MRI single-subject brain. *Neuroimage* **15**, 273–289 (2002).
- 18. Zou, K. H. *et al.* Statistical validation of image segmentation quality based on a spatial overlap index: Scientific reports. *Acad. Radiol.* **11**, 178–189 (2004).